# Utah Lake Water Quality Study—Analysis Update

# FINAL

October 28, 2021

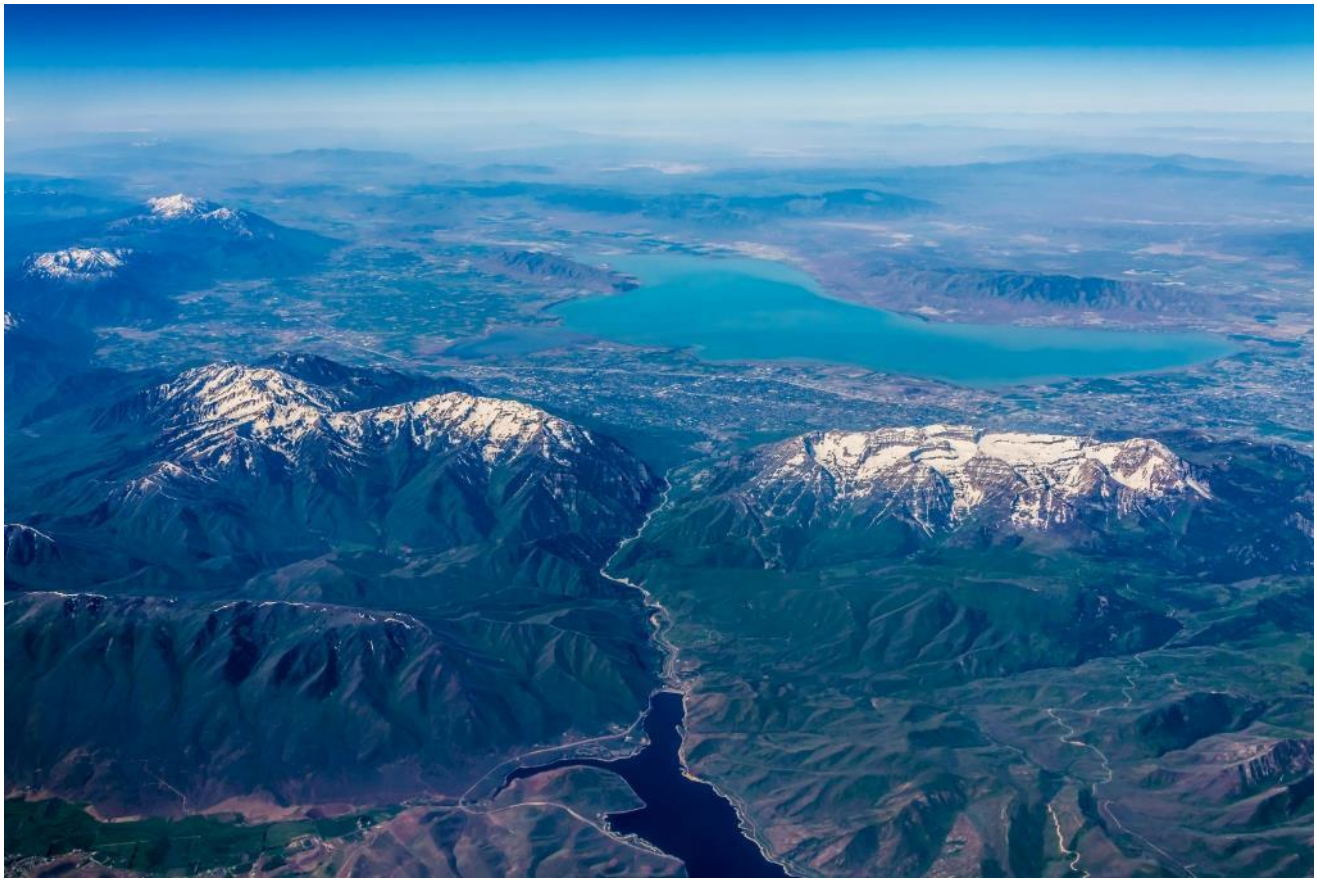

## PRESENTED TO

**Utah Department of Environmental Quality**
PO Box 144870
Salt Lake City, UT 84114

## PREPARED BY

**Tetra Tech**
1468 West Ninth Street, Suite 620
Cleveland, OH 44113

**Cover image**: Aerial View of Provo Utah with River Valley and Utah Lake, by Aqua Mechanical. Source file available at https://www.flickr.com/photos/aquamech-utah/24776739750/in/photostream/


## Acknowledgements

Prepared by Kateri Salk and Michael Paul, with analysis support by Mark Fernandez

Data provided by Scott Daly, Input from Mitch Hogsett, Nicholas von Stackelberg

# TABLE OF CONTENTS

# ABBREVIATIONS

| Abbreviation | Definition |
|---|---|
| AIC | Akaike information criterion |
| ANCOVA | Analysis of Covariance |
| BGA | Blue-green algae |
| CCA | Canonical Correspondence Analysis |
| CDOM | Colored dissolved organic matter |
| DO | Dissolved oxygen |
| DOC | Dissolved organic carbon |
| HAB | Harmful algal bloom |
| k | Light attenuation coefficient |
| LMICM | Lake Macrophyte Intercalibration Metric |
| N | Nitrogen |
| $NH_4^+$ | Ammonium |
| NMDS | Non-metric Multidimensional Scaling |
| NTU | Nephelometric turbidity units |
| OTU | Operational taxonomic unit |
| PAR | Photosynthetically active radiation |
| POTW | Publicly Owned Treatment Works |
| P | Phosphorus |
| RFU | Relative fluorescence units |
| SD | Standard deviation |
| SRP | Soluble reactive phosphorus |
| SP | Science Panel |
| TN | Total nitrogen |
| TP | Total phosphorus |
| TSI | Trophic state index |
| TSS | Total suspended solids |
| UDWQ | Utah Department of Water Quality |
| ULWQS | Utah Lake Water Quality Study |
| VSS | Volatile suspended solids |

# 1.0 BACKGROUND

This report is a second mid-project update on analyses in preparation for Science Panel consideration. This second interim report provides a summary of data, methods and results of various analyses being pursued to support the Science Panel response to charge questions from the Steering Committee related to Utah Lake. These details can be elaborated upon in future Science Panel meetings.

# 2.0 ANALYSES AND APPROACHES

The following analyses are based on the Phase 2 Purpose and Initial Charge to Science Panel from Steering Committee document (September, 6 2018), initial charge questions working content document (October 2, 2018 version), Attachment A ULWQS Science Panel Ideas for Studies, Experiments, and Literature Reviews (August 24, 2018), and feedback from the Science Panel during an analysis planning session on workshop 3 (February 8, 2019) and subsequent Science Panel discussions.

## 2.1 CARP EXCRETION

**Proposed**

Question: What contribution do carp make to the total nutrient budget of the lake via excretion rates and bioturbation? How much nutrient cycling can be attributed to carp? (Charge question 2.1.i)

Objective: Estimate potential nutrient excretion rates of carp.

Approach: Using fish excretion data provided by R. King from two sources and estimates of lake fish densities, estimate fish nutrient excretion loads. Calculate standard measures of statistical uncertainty (means and standard deviations). Compare these to existing annual external load estimates as a percentage of load moving through fish.

**Actual**

***Data and Methods***

Carp excretion data were provided by R. King (2019-02-18; Aquatic_animal_excretion_variable_descriptions.csv and Vanni_aquatic_animal_excretion_2017.csv). Excretion data included individual carp excretion rates, in µg phosphorus (P) $ind^{-1}$ $h^{-1}$, and dry mass (n = 84). Carp size data were derived from Gaeta and Landom (2016), and fish wet:dry weight ratios (5) were obtained from Cresson et al. (2017). Current carp biomass estimates are 14 million kg wet weight (Gaeta et al. 2019). Carp P and nitrogen (N) excretion rates were compared with P and N loading estimates (Brett, Pers. Comm., Psomas and SWCA 2007, Merritt and Miller 2016).

***Results***

Average adult carp wet mass was estimated at 2.9 kg (Gaeta and Landom 2016), corresponding to a dry mass of 0.58 kg. The carp biomass estimate for Utah Lake is 14 million kg wet weight (95% credible interval: 10-23 million kg), corresponding to 2.8 million kg dry weight (95% credible interval: 2.0-4.6 million kg). These mass estimates are equivalent to 4.8 million individuals (95% credible interval: 3.4-7.9 million). Logged individual excretion rates of nutrients were positively correlated with logged dry mass, and this relationship was weaker for total P (TP; Figure 2.1.1) than for soluble reactive P (SRP; Figure 2.1.2), total N (TN; Figure 2.1.3), and ammonium ($NH_4^+$; Figure 2.1.4)

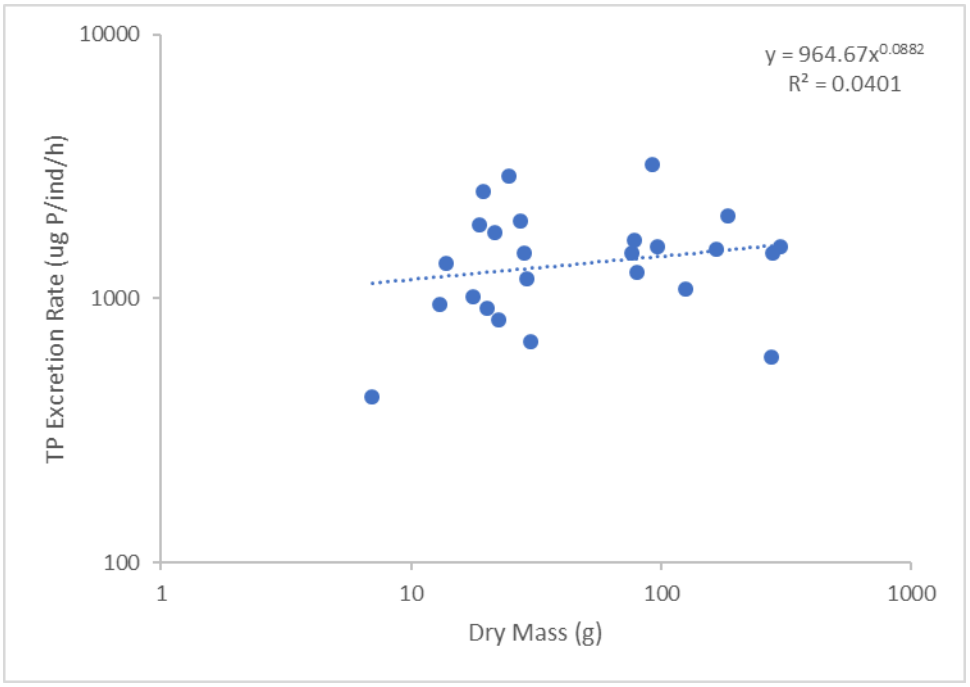


**Figure 2.1.1.** TP individual excretion rate per hour as a function of individual dry mass.

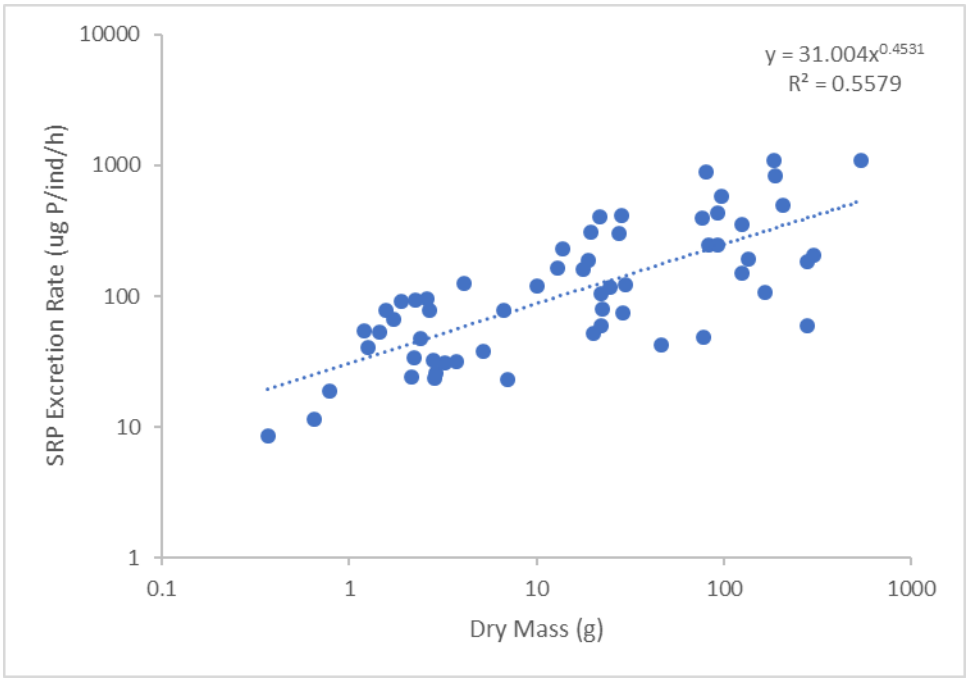


**Figure 2.1.2**. SRP individual excretion rate per hour as a function of individual dry mass.

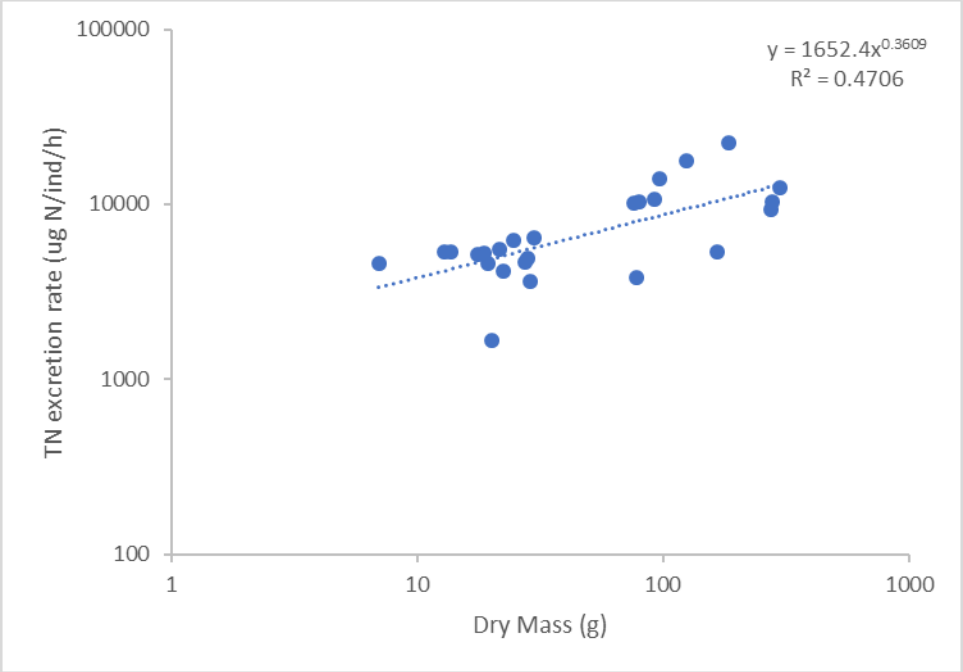


**Figure 2.1.3.** TN individual excretion rate per hour as a function of individual dry mass.

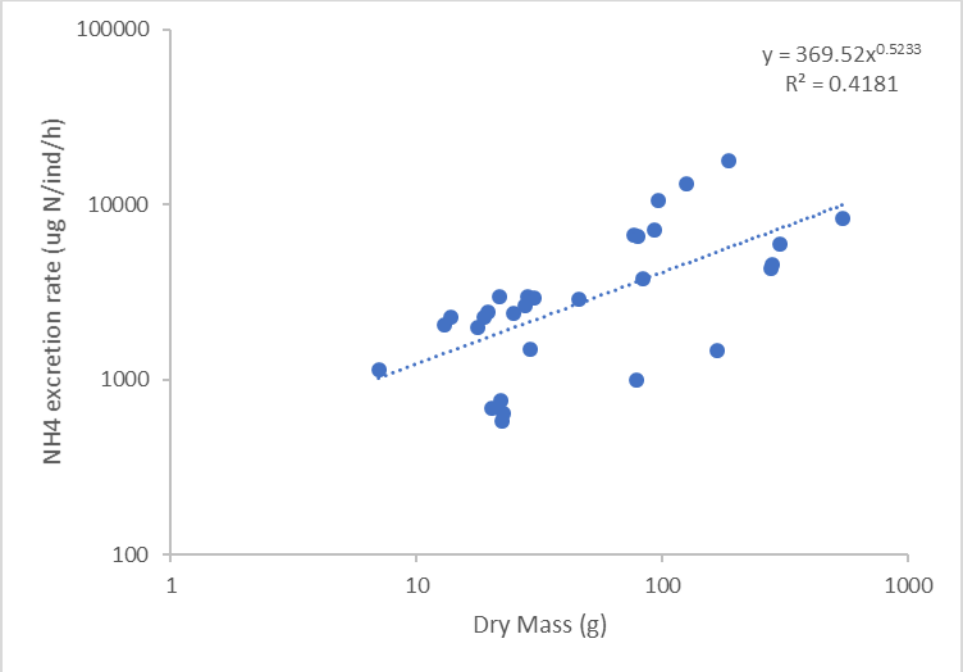


**Figure 2.1.4.** NH4 individual excretion rate per hour as a function of individual dry mass.

Lakewide carp excretion estimates based on individual size, density, and regression (mean and 95 % credible interval) were 71,500 kg TP $y^{-1}$ (51,100-117,000), 23,400 kg SRP $y^{-1}$ (16,700-38,500), 694,000 kg TN $y^{-1}$ (496,000-1,140,000), and 436,000 kg $NH_4^+$ $y^{-1}$ (312,000-717,000). These estimates were compared to external nutrient loads and retention, with “low” and “high” representing the 95 % credible interval (tables 2.1.1, 2.1.2,

2.1.3, 2.1.4). Across ranges and loading estimates, TP recycling by carp excretion based on 2018 population estimates represented 19-85 % of external P loads and 23-60 % of P net retention. TN recycling by carp excretion represented 27-62 % of external N loads.

**Table 2.1.1.** Carp TP excretion compared to Utah Lake P inputs and retention.

| | | | TP Excretion as Percent of Lake Inputs/Retained | | | Load Source |
|---|---|---|---|---|---|---|
| **Load Measure** | **Tons P /y** | **kg P/y** | **Low** | **Mean** | **High** | |
| Total Inputs | 152.4 | 138,255 | 37% | 52% | 85% | M. Brett, Pers. Comm |
| Total Inputs | 272 | 246,754 | 21% | 29% | 48% | Merritt, L.B. and A. W. Miller. 2016. |
| Net retained | 246 | 223,167 | 23% | 32% | 53% | Merritt, L.B. and A. W. Miller. 2016. |
| Total Inputs | 297.6 | 269,978 | 19% | 26% | 44% | Psomas and SWCA. 2007. |
| Net retained | 214.1 | 194,228 | 26% | 37% | 60% | Psomas and SWCA. 2007. |

**Table 2.1.2.** Carp SRP excretion compared to Utah Lake P inputs and retention.

| | | | SRP Excretion as Percent of Lake Inputs/Retained | | | Load Source |
|---|---|---|---|---|---|---|
| **Load Measure** | **Tons P /y** | **kg P/y** | **Low** | **Mean** | **High** | |
| Total Inputs | 152.4 | 138,255 | 12% | 17% | 28% | M. Brett, Pers. Comm |
| Total Inputs | 272 | 246,754 | 7% | 9% | 16% | Merritt, L.B. and A. W. Miller. 2016. |
| Net retained | 246 | 223,167 | 7% | 10% | 17% | Merritt, L.B. and A. W. Miller. 2016. |
| Total Inputs | 297.6 | 269,978 | 6% | 9% | 14% | Psomas and SWCA. 2007. |
| Net retained | 214.1 | 194,228 | 9% | 12% | 20% | Psomas and SWCA. 2007. |

**Table 2.1.3.** Carp TN excretion compared to Utah Lake N inputs.

| | | | TN Excretion as Percent of Lake Inputs/Retained | | | Load Source |
|---|---|---|---|---|---|---|
| **Load Measure** | **Tons N /y** | **kg N/y** | **Low** | **Mean** | **High** | |
| Total Inputs | 2,022 | 1,834,328 | 27% | 38% | 62% | M. Brett, Pers. Comm |

**Table 2.1.4.** Carp $NH_4^+$ excretion compared to Utah Lake N inputs.

| | | | $NH_4^+$ Excretion as Percent of Lake Inputs/Retained | | | Load Source |
|---|---|---|---|---|---|---|
| **Load Measure** | **Tons N /y** | **kg N/y** | **Low** | **Mean** | **High** | |
| Total Inputs | 2,022 | 1,834,328 | 17% | 24% | 39% | M. Brett, Pers. Comm |

### Outstanding Questions

This analysis generates an estimate of the contribution to N and P budgets via excretion; do estimates of N and P consumed and bound in carp standing stock need to be addressed?

How should the question of bioturbation impacts be addressed?

Note: The C, N, P mass balance RFP will both evaluate and incorporate the load and excretion estimates presented in this section.

## 2.2 ALGAL CELL COUNT AND PIGMENT RELATIONSHIPS

**Proposed**

Question: What is the relationship between cell count, biovolume, and pigment concentration data? (Question raised in workshop 3)

Objective: Estimate relationships between cell count, biovolume, and pigment concentrations.

Approach: Using Phase I and II monitoring data which includes cell count, biovolume and chlorophyll a data, construct simple general linear models relating pigment concentrations to cell counts and biovolumes from paired samples. Calculate mean relationships and measures of uncertainty (confidence and prediction intervals).

**Actual**

***Data and Methods***

UDWQ Phase I and Phase II Utah Lake surface water quality data were provided by UDWQ (https://deq.utah.gov/division-water-quality) via the Water Quality Portal. Chlorophyll data included data corrected for pheophytin (Chla-C) and uncorrected for pheophytin (Chla). Data were split into grab (site-date), annual (site-year), and long-term averaged observations (i.e., one observation per site-variable combination, averaged across the period of record).

***Results***

Phytoplankton indicators from grab samples were positively correlated with one another. Chlorophyll concentrations (corrected and uncorrected) explained 30-38 % of the variance in phytoplankton cell counts and cell volumes on a log-log scale (Figure 2.2.1). Annual data displayed similar positive correlations, with 20-36 % of variance in logged phytoplankton cell counts and cell volumes explained by logged chlorophyll concentrations (Figure 2.2.2).

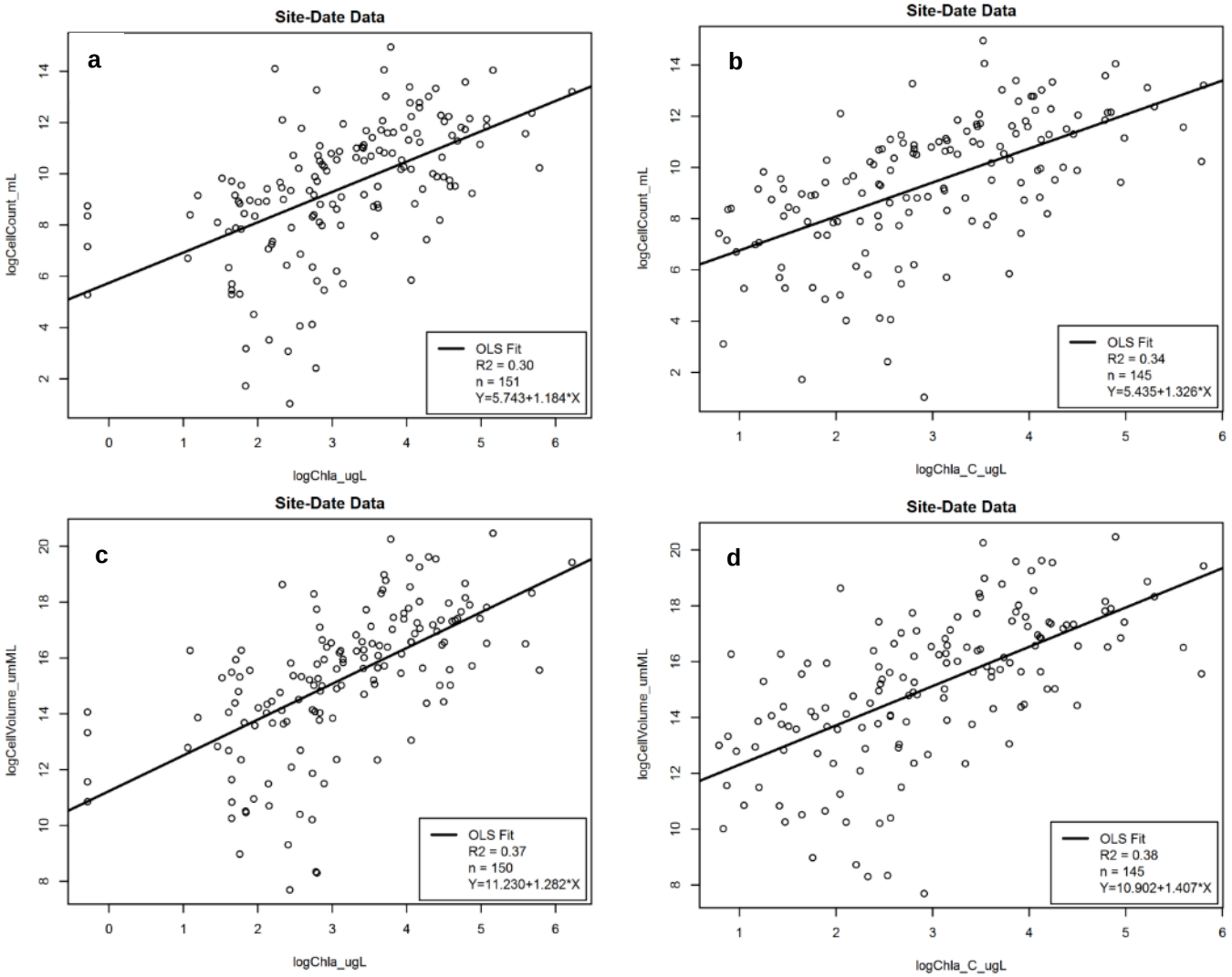


**Figure 2.2.1.** Relationship between (a) chlorophyll concentration and phytoplankton cell count, (b) corrected chlorophyll concentration and phytoplankton cell count, (c) chlorophyll concentration and phytoplankton cell volume, and (d) corrected chlorophyll concentration and phytoplankton cell volume. Points represent measurements made at sites on specific dates.

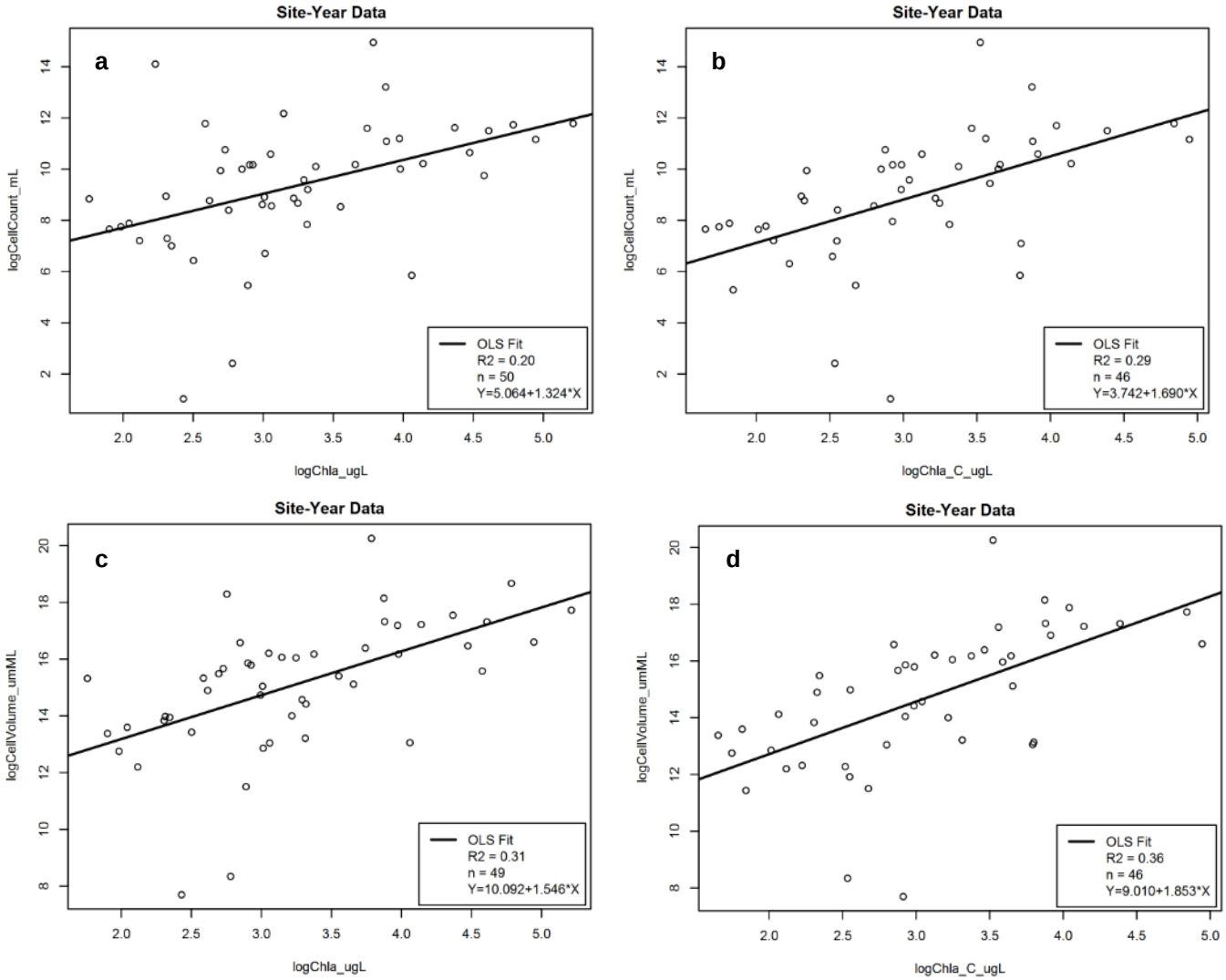


**Figure 2.2.2.** Relationship between (a) chlorophyll concentration and phytoplankton cell count, (b) corrected chlorophyll concentration and phytoplankton cell count, (c) chlorophyll concentration and phytoplankton cell volume, and (d) corrected chlorophyll concentration and phytoplankton cell volume. Points represent measurements made at sites averaged by year.

## 2.3 SONDE DATA ANALYSIS

**Proposed**

Question: Can sonde data be teased apart? (Question raised in workshop 3)

Objective: Extract sonde data and examine relationships among sonde variables. Run descriptive statistics on sonde data.

Approach: Using Phase I and II continuous sonde data, examine relationships among sonde variables using standard correlation and regression analyses. Calculate mean relationships and measures of uncertainty (confidence and prediction intervals). Examine any differences in sonde location using, potentially, location as a random effect in regression models.

**Actual**

***Data and Methods***

UDWQ Phase I and Phase II Utah Lake Sonde Water Quality Data were provided by UDWQ (https://deq.utah.gov/division-water-quality) via the Water Quality Portal. Variables measured by buoys included temperature, chlorophyll fluorescence, phycocyanin (blue-green algae; BGA) fluorescence, dissolved oxygen (DO) concentration, pH, and turbidity. Buoy data were sampled in 15-minute intervals, but for most analyses daily mean values were calculated. Buoy sites consisted of a northern site (North; 4917365), a middle site (State Park; 4917390), a Provo Bay site (Provo Bay; 4917446), and a southern site (South; 4917715). Buoy data were analyzed in relation to other variables, across sites, and with respect to corresponding grab sample data (noted as “surface” and/or a sampled depth of < 0.3 m). When sites were not sampled concurrently for grab and buoy data, nearby monitoring were compared with buoy sites, matched temporally by date and time of day.

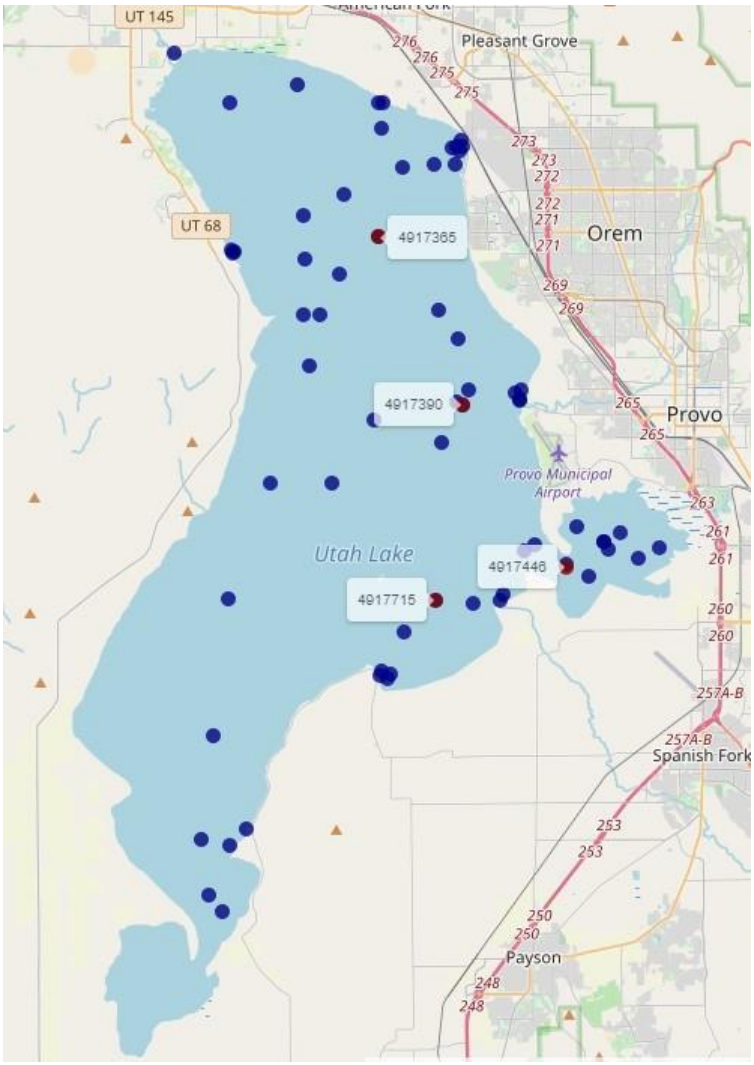


**Figure 2.3.1.** Sampling sites in Utah Lake. Blue symbols represent grab sampling sites and red symbols represent sonde sampling sites. Site codes are as follows: North = 4917365, State Park = 4917390, Provo Bay = 4917446, South = 4917715.

***Results***

Summary statistics for buoy sites are listed in tables 2.3.1, 2.3.2, 2.3.3, and 2.3.4.

**Table 2.3.1.** Summary statistics for measured variables at the North buoy site (site code = 4917365). P25 = 25th percentile, SD = standard deviation, P75 = 75th percentile, BGA = blue-green algae, RFU = relative fluorescence units, NTU = nephelometric turbidity units. Time periods of measurement are displayed in **figure 2.3.2**.

| Variable | Min | P25 | Median | Mean | SD | P75 | Max | units |
|---|---|---|---|---|---|---|---|---|
| Phycocyanin (BGA) | 0 | 0.4 | 0.8 | 1.0 | 1.1 | 1.2 | 32.6 | RFU |
| Chlorophyll Fluorescence | 0 | 1.1 | 1.8 | 2.4 | 2.2 | 3.2 | 147.1 | RFU |
| Dissolved Oxygen | 5.2 | 7.2 | 8.1 | 8.2 | 1.3 | 9.1 | 16.2 | mg/L |
| Dissolved Oxygen Saturation | 62.6 | 78.0 | 83.2 | 85.6 | 12.5 | 90.4 | 209.3 | % |
| pH | 8.2 | 8.5 | 8.6 | 8.6 | 0.2 | 8.7 | 9.2 | |
| Specific Conductance | 1327 | 1805 | 1907 | 2062 | 402 | 2119 | 3341 | µS/cm |
| Temperature | 3.1 | 12.8 | 18.1 | 17.5 | 5.8 | 22.6 | 28.6 | ºC |
| Turbidity | 0.6 | 22.8 | 39.0 | 56.3 | 66.5 | 65.3 | 2283.9 | NTU |

**Table 2.3.2.** Summary statistics for measured variables at the State Park buoy site (site code = 4917390). P25 = 25th percentile, SD = standard deviation, P75 = 75th percentile, BGA = blue-green algae, RFU = relative fluorescence units, NTU = nephelometric turbidity units. Time periods of measurement are displayed in **figure 2.3.2.**

| Variable | Min | P25 | Median | Mean | SD | P75 | Max | units |
|---|---|---|---|---|---|---|---|---|
| Phycocyanin (BGA) | 0 | 0.4 | 0.8 | 1.1 | 1.1 | 1.3 | 22.9 | RFU |
| Chlorophyll Fluorescence | 0 | 1.6 | 2.6 | 3.4 | 3.0 | 4.4 | 82.5 | RFU |
| Dissolved Oxygen | 3.0 | 7.5 | 8.5 | 8.5 | 1.6 | 9.4 | 25.0 | mg/L |
| Dissolved Oxygen Saturation | 37.2 | 79.8 | 86.4 | 90.4 | 18.0 | 97.1 | 313.5 | % |
| pH | 8.1 | 8.4 | 8.6 | 8.6 | 0.3 | 8.8 | 10.1 | |
| Specific Conductance | 473 | 1753 | 1894 | 1959 | 332 | 2078 | 2947 | µS/cm |
| Temperature | 3.1 | 13.7 | 19.1 | 18.4 | 5.6 | 23.2 | 28.8 | ºC |
| Turbidity | 0 | 18.5 | 40.1 | 51.5 | 58.4 | 65.3 | 1248.9 | NTU |

**Table 2.3.3.** Summary statistics for measured variables at the Provo Bay buoy site (site code = 4917446). P25 = 25th percentile, SD = standard deviation, P75 = 75th percentile, BGA = blue-green algae, CDOM = colored dissolved organic matter, RFU = relative fluorescence units, NTU = nephelometric turbidity units. Time periods of measurement are displayed in **figure 2.3.2**.

| Variable | Min | P25 | Median | Mean | SD | P75 | Max | units |
|---|---|---|---|---|---|---|---|---|
| Phycocyanin (BGA) | 0.1 | 0.8 | 2.9 | 6.9 | 8.3 | 10.8 | 98.3 | RFU |
| Chlorophyll Fluorescence | 0 | 6.4 | 24.7 | 44.9 | 44.1 | 78.5 | 157.4 | RFU |
| CDOM | 0 | 12.7 | 13.8 | 14.2 | 2.3 | 15.4 | 32.3 | RFU |
| Dissolved Oxygen | 1.4 | 4.7 | 7.3 | 8.0 | 4.0 | 10.7 | 23.6 | mg/L |
| Dissolved Oxygen Saturation | 14.8 | 51.7 | 77.3 | 84.5 | 42.1 | 108.5 | 248.3 | % |
| pH | 8 | 8.5 | 8.7 | 8.7 | 0.2 | 8.8 | 9.7 | |
| Specific Conductance | 434 | 867 | 942 | 1005 | 231 | 1060 | 2044 | µS/cm |
| Temperature | 2.6 | 13.9 | 19.0 | 18.3 | 5.7 | 22.8 | 31.3 | ºC |
| Turbidity | 0 | 5.8 | 15.2 | 48.1 | 109.3 | 48.5 | 3158.8 | NTU |

**Table 2.3.4.** Summary statistics for measured variables at the South buoy site (site code = 4917715). P25 = 25th percentile, SD = standard deviation, P75 = 75th percentile, BGA = blue-green algae, RFU = relative fluorescence units, NTU = nephelometric turbidity units. Time periods of measurement are displayed in **figure 2.3.2**.

| Variable | Min | P25 | Median | Mean | SD | P75 | Max | units |
|---|---|---|---|---|---|---|---|---|
| Phycocyanin (BGA) | 0 | 0.4 | 0.7 | 1.0 | 1.2 | 1.3 | 52.4 | RFU |
| Chlorophyll Fluorescence | 0.1 | 1.3 | 2.2 | 2.8 | 2.1 | 3.5 | 49.8 | RFU |
| Dissolved Oxygen | 5.0 | 7.6 | 8.5 | 8.6 | 1.4 | 9.3 | 23.8 | mg/L |
| Dissolved Oxygen Saturation | 60.5 | 80.2 | 86.2 | 89.6 | 13.4 | 97.2 | 285.3 | % |
| pH | 8.2 | 8.4 | 8.6 | 8.6 | 0.2 | 8.6 | 9.4 | |
| Specific Conductance | 1144 | 1841 | 1999 | 2081 | 339 | 2165 | 3154 | µS/cm |
| Temperature | 3.1 | 13.1 | 18.7 | 17.9 | 5.8 | 23.0 | 28.2 | ºC |
| Turbidity | 0.1 | 20.9 | 37.3 | 52.8 | 62.9 | 61.2 | 1966.8 | NTU |

Temperatures were consistent across buoy sites, peaking in July-August of each year. Chlorophyll and BGA fluorescence values were generally < 10 RFU, with the exception of late summer samples in Provo Bay. Buoy data suggest a peak in phytoplankton growth during early spring and mid- to late-summer. Daily mean DO concentrations did not reach hypoxic levels, but lower concentrations were associated with or preceded by high chlorophyll fluorescence. The most noticeable swings in pH were observed in Provo Bay, where lower pH values were associated with high chlorophyll and BGA fluorescence, and high pH occurred following a decrease in chlorophyll and BGA fluorescence. Turbidity was variable across the measured time frame (Figure 2.3.2).

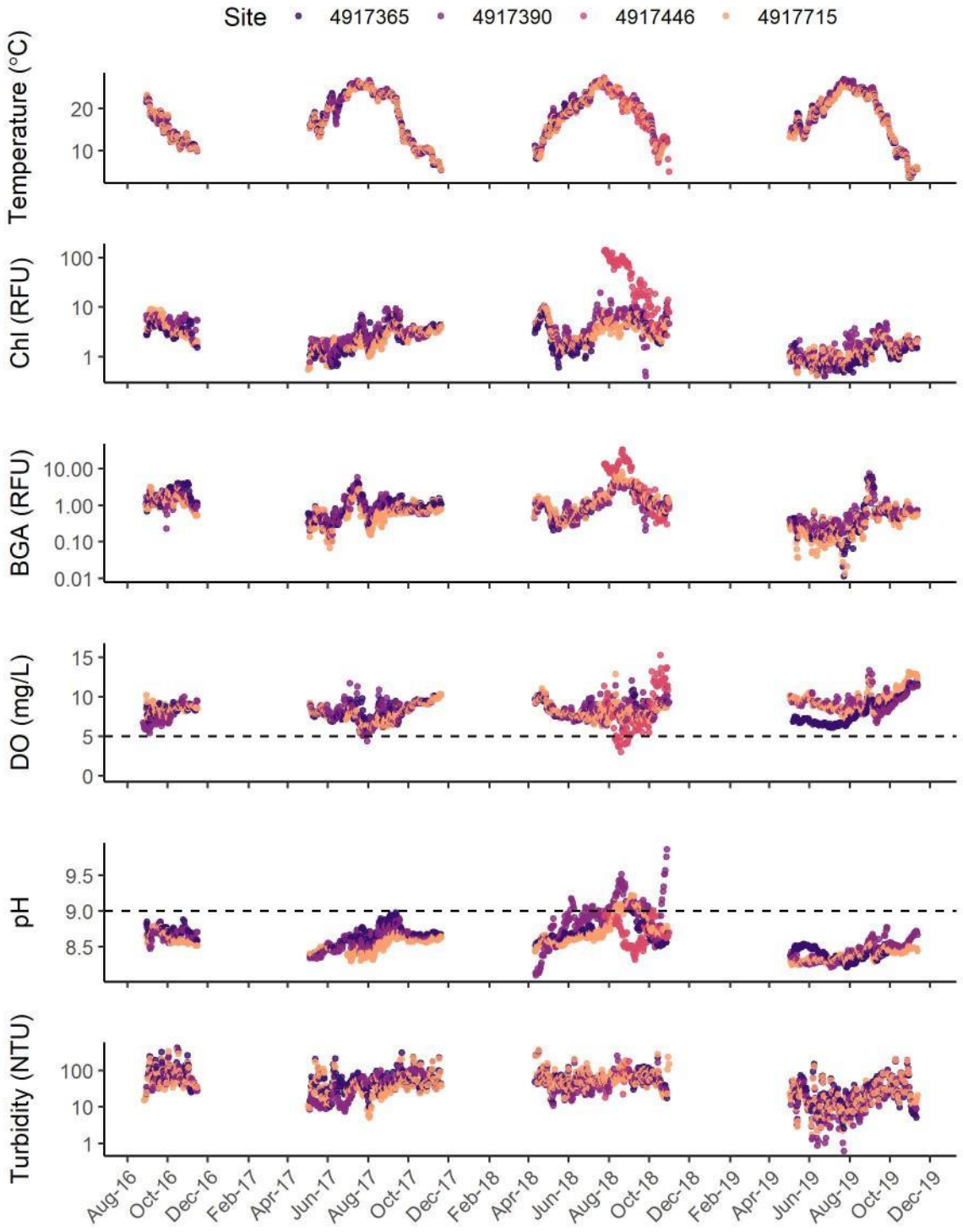


**Figure 2.3.2.** Time series of mean daily conditions at buoy sites. Site codes are as follows: North = 4917365, State Park = 4917390, Provo Bay = 4917446, South = 4917715. Chl = chlorophyll, RFU = relative fluorescence units, BGA = blue-green algae, DO = dissolved oxygen, NTU = nephelometric turbidity units. Horizontal dotted lines represent Utah aquatic life criteria for DO (5 mg/L) and pH (9).

Consistent with expectations based on diel shifts in photosynthesis and respiration, diel patterns in pH and DO were apparent (Figures 2.3.3, 2.3.4). For both pH and DO, daily minima were observed in nighttime as a function of respiration, and daily maxima were observed in daytime as a function of photosynthesis. pH maxima above the state criterion of 9 were observed 4.4, 19.8, 40.4, and 8.6% of measured days at the North (4917365), State Park (4917390), Provo Bay (4917446), and South (4917715) sites, respectively. DO minima below the state criterion of 5 mg/L for early life stages were observed 0, 3.3, 63.3, and 0% of measured days at the North (4917365), State Park (4917390), Provo Bay (4917446), and South (4917715) sites, respectively. DO minima below the state criterion of 5 mg/L for early life stages were observed 0, 0, 29, and 0% of measured days at the North (4917365), State Park (4917390), Provo Bay (4917446), and South (4917715) sites, respectively. The Provo Bay site experienced exceedances of the 7-day and 30-day average DO concentration criteria 1 and 19% of the time, respectively (further detail provided in ULWQS Steering Committee 2020).

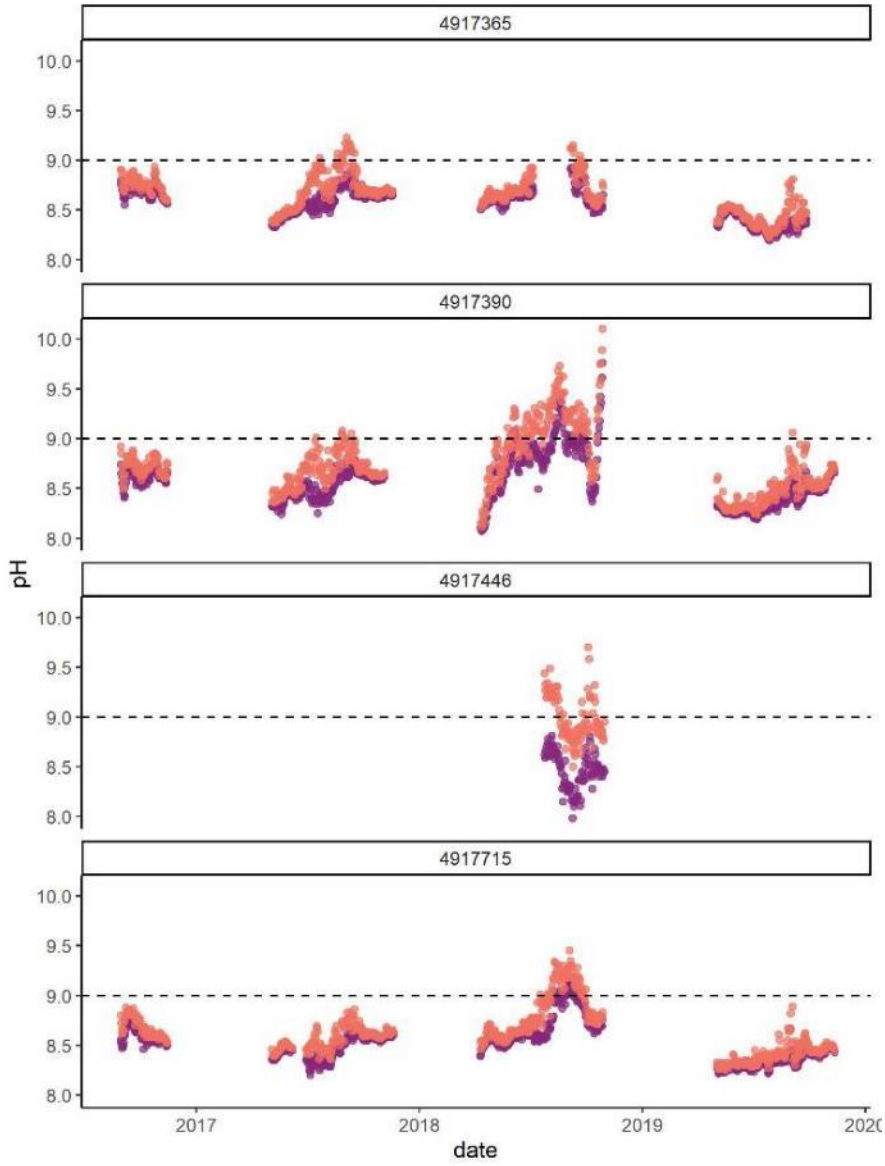


**Figure 2.3.3.** Time series of maximum (orange) and minimum (purple) daily pH conditions at buoy sites. Site codes are as follows: North = 4917365, State Park = 4917390, Provo Bay = 4917446, South = 4917715. Horizontal dotted lines represent Utah aquatic life criteria for pH (9).

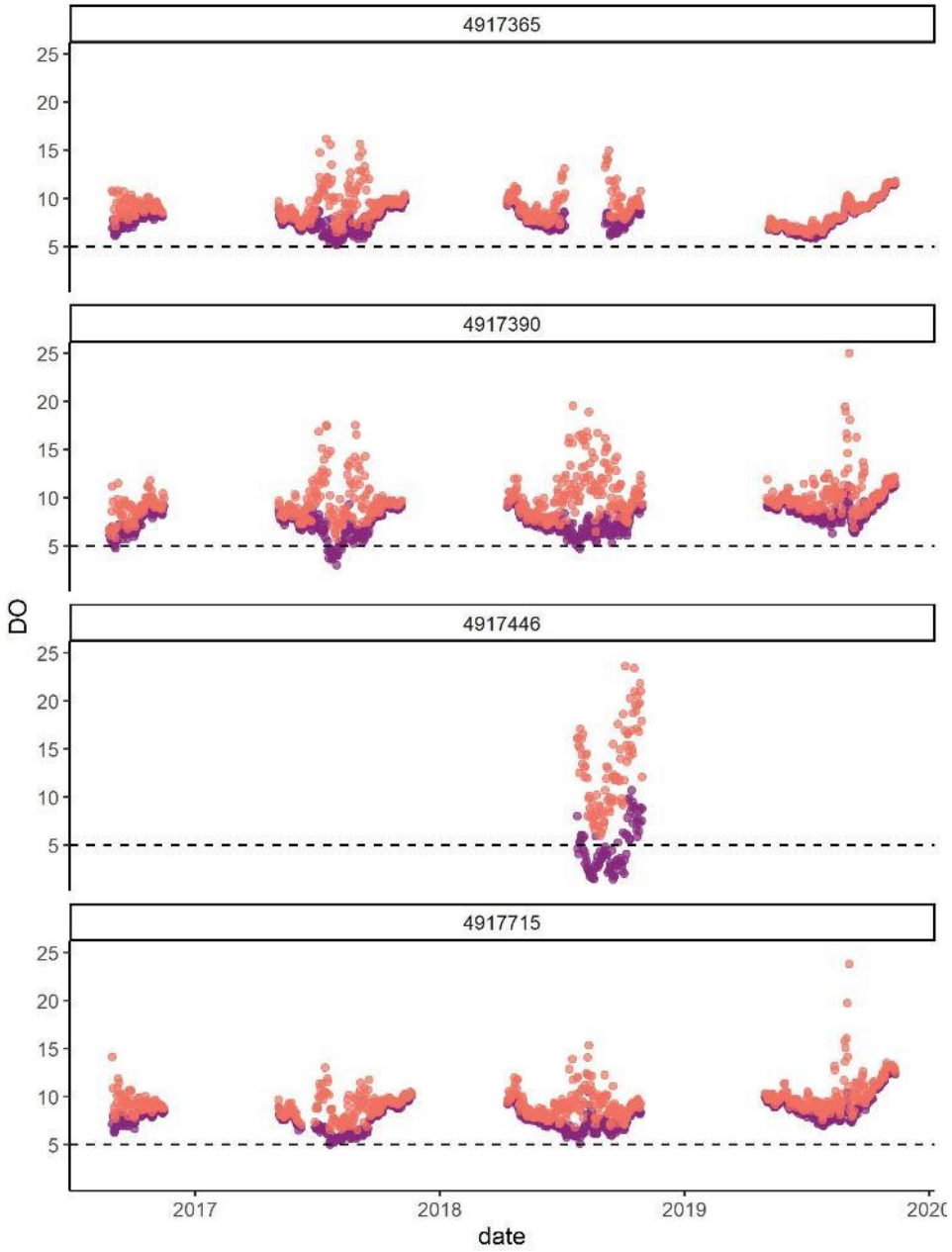


**Figure 2.3.4.** Time series of maximum (orange) and minimum (purple) daily dissolved oxygen (DO) conditions at buoy sites. Site codes are as follows: North = 4917365, State Park = 4917390, Provo Bay = 4917446, South = 4917715. Horizontal dotted lines represent Utah aquatic life criteria for DO for early life stages (5 mg/L).

Distributions of daily average chlorophyll varied significantly by site and month, with a significant interaction among site and month (two-way interaction effects ANOVA; $F_{17,1989} = 906$, $p < 0.0001$), with Provo Bay displaying significantly higher values in July, August, and September than other sites and months (Figure 2.3.5). Daily average DO concentrations also varied significantly by site and month (Figure 2.3.5; two-way interaction effects ANOVA; $F_{17,1983} = 23$, $p < 0.0001$). Provo Bay was also unique with respect to DO, displaying the highest concentrations in July and October and the lowest concentrations in August and September. Daily minimum DO concentrations were negatively correlated with chlorophyll (log-transformed), turbidity (log-transformed), and temperature (multiple regression, df = 1897, $R^2 = 0.59$, $p < 0.0001$). The explanatory variables for DO, in order of importance, were chlorophyll, turbidity, and temperature (backward model selection by AIC).

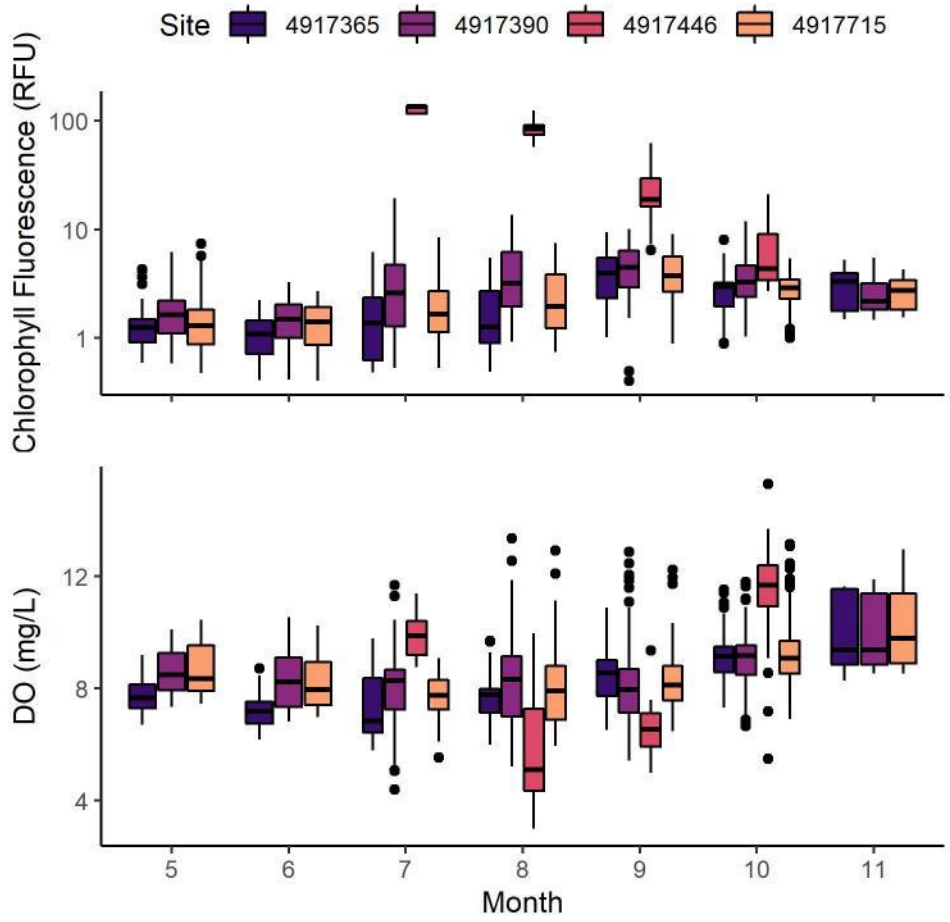


**Figure 2.3.5.** Monthly distributions of daily average chlorophyll fluorescence and dissolved oxygen (DO) concentrations at buoy sites. Site codes are as follows: North = 4917365, State Park = 4917390, Provo Bay = 4917446, South = 4917715. RFU = relative fluorescence units, DO = dissolved oxygen.

Turbidity was positively correlated with logged chlorophyll fluorescence for all three sites in main basin of the lake, although a substantial amount of variance was left unexplained (Figure 2.3.6; linear regression, df = 602-654, $R^2 = 0.17$-$0.24$, $p < 0.0001$). Provo Bay, conversely, displayed a negative correlation between turbidity and chlorophyll (linear regression, df = 11, $R^2 = 0.44$, $p < 0.01$).

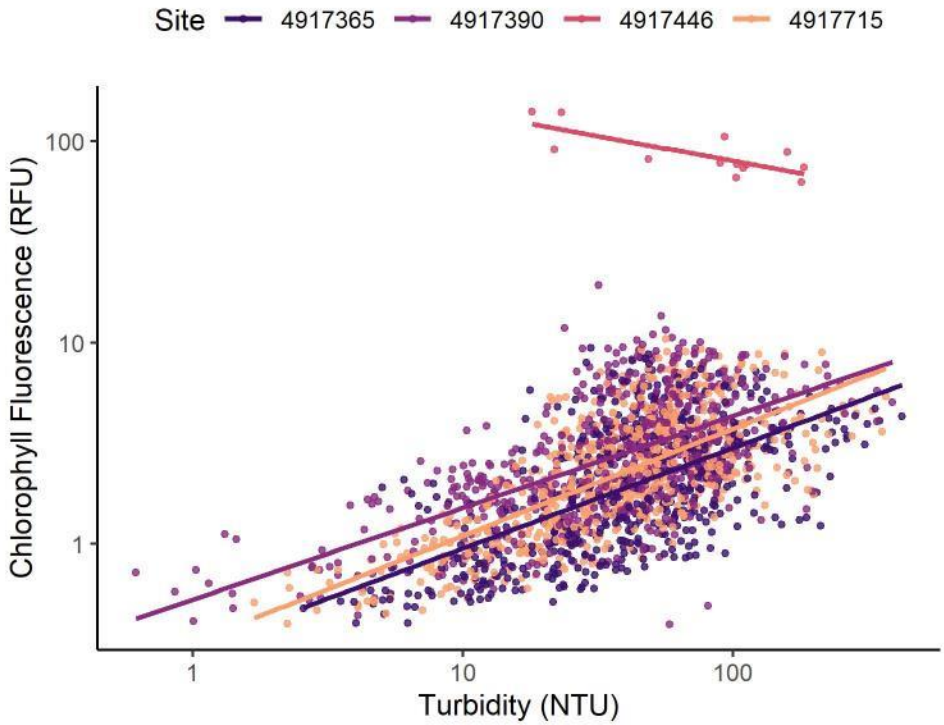


**Figure 2.3.6.** Correlation of turbidity and chlorophyll fluorescence at buoy sites. Site codes are as follows: North = 4917365, State Park = 4917390, Provo Bay = 4917446, South = 4917715. RFU = relative fluorescence units, NTU = nephelometric turbidity units.

Temperature, turbidity, DO, pH, and chlorophyll exhibited varying degrees of agreement between buoy measurements and grab samples. Temperature exhibited the closest agreement, with most values falling near but slightly below the 1:1 line (Figure 2.3.7). Turbidity values also fell near the 1:1 line, with direct site matches displaying a greater agreement than nearby sites (Figure 2.3.8). DO displayed similar results as turbidity, with the Provo Bay site displaying a poor fit on four data points (Figure 2.3.9). pH measurements generally fell above the 1:1 line (Figure 2.3.10). Chlorophyll values displayed the worst fit between buoy and grab samples, suggesting a discrepancy between fluorescence and measured concentrations (Figure 2.3.11). In general, comparisons of buoy and grab data with a direct location match fell closer to the 1:1 line than comparisons between nearby stations. It is unclear from this analysis whether the buoy or grab samples are more accurate (hence the avoidance of terms “overestimate” and “underestimate”), but the relationships among the sampling techniques point to the possibility of using correction factors to generate estimates in the instance of missing data for some parameters.

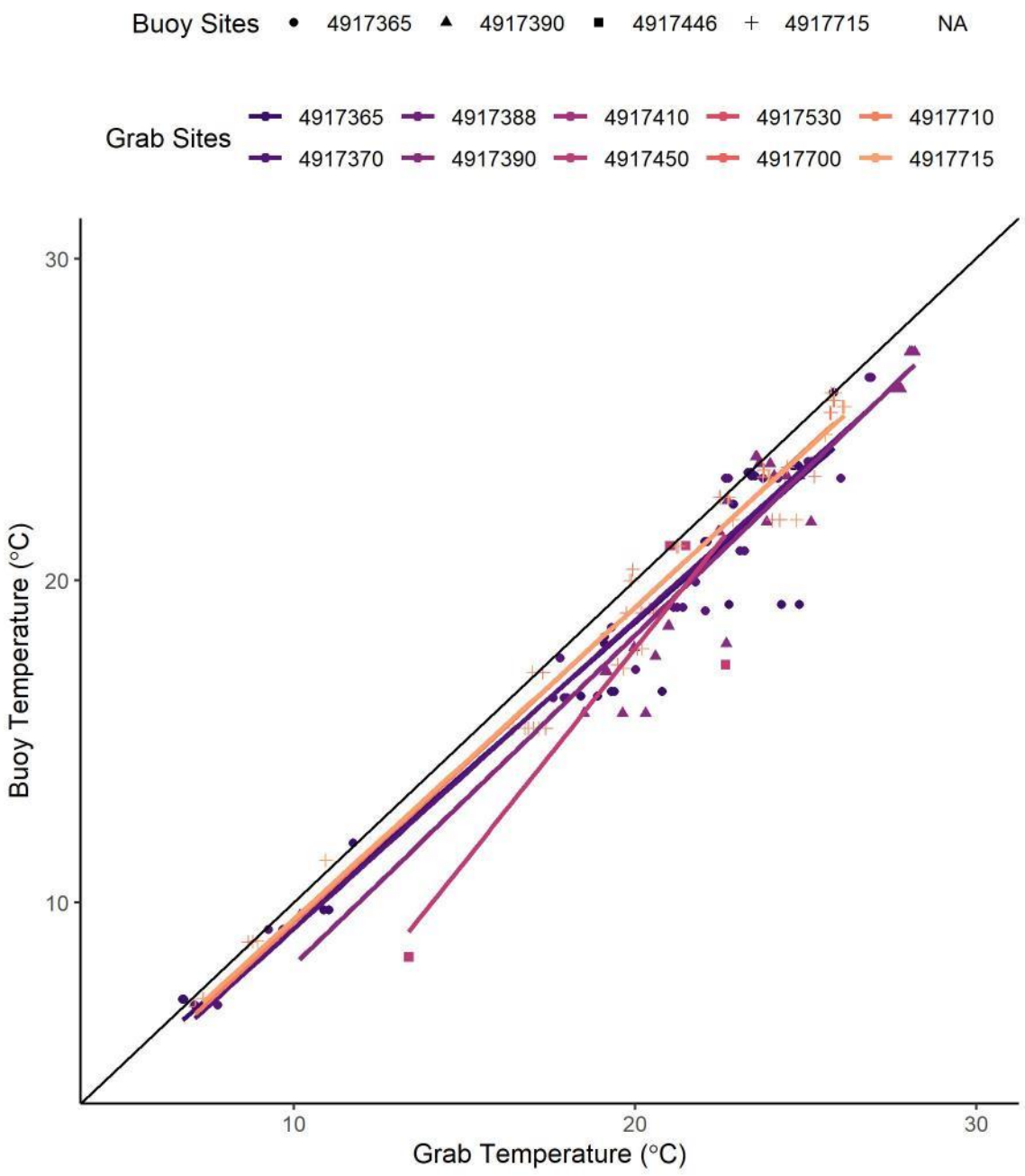


**Figure 2.3.7.** Comparisons of temperature measured at buoy and grab sampling sites. Grab sites correspond to sites near the buoy site, which did not necessarily have data available. A direct match in site code indicates grab and buoy samples were taken at the same location. The solid black line represents a 1:1 relationship.

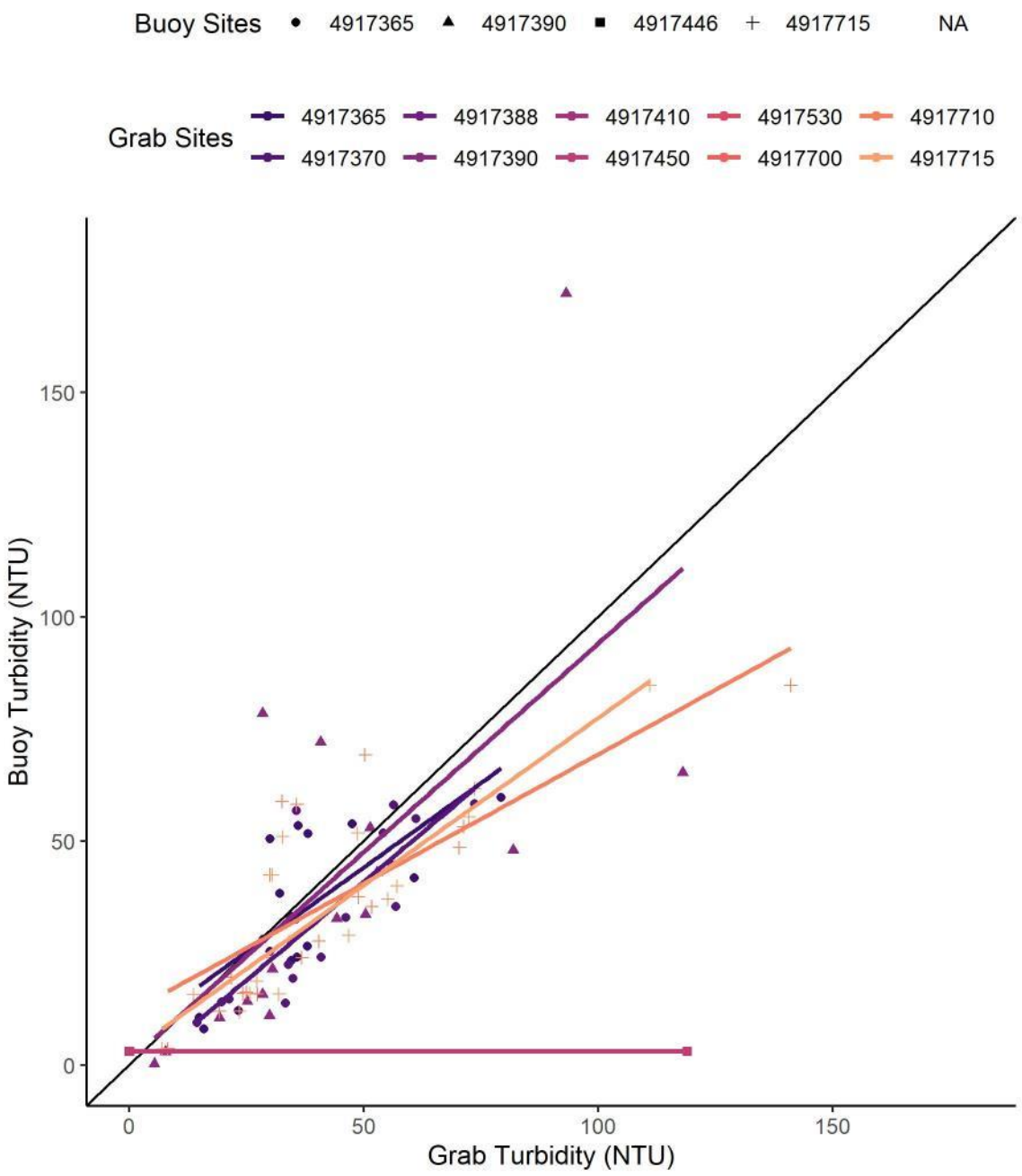


**Figure 2.3.8.** Comparisons of turbidity measured at buoy and grab sampling sites. Turbidity was not measured at the Provo Bay site (4917446). Grab sites correspond to sites near the buoy site, which did not necessarily have data available. A direct match in site code indicates grab and buoy samples were taken at the same location. NTU = nephelometric turbidity units. The solid black line represents a 1:1 relationship.

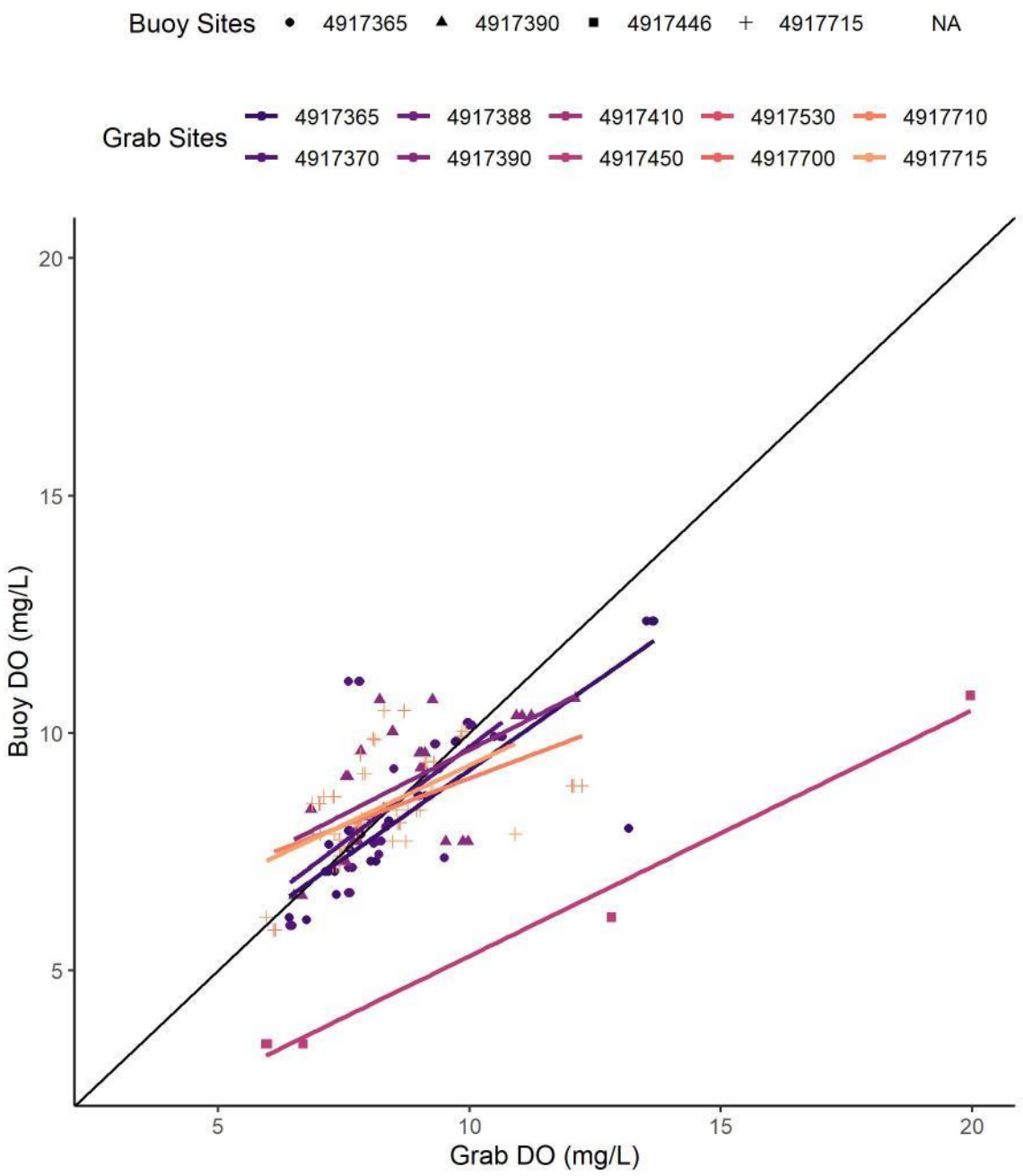


**Figure 2.3.9.** Comparisons of dissolved oxygen (DO) measured at buoy and grab sampling sites. Grab sites correspond to sites near the buoy site, which did not necessarily have data available. A direct match in site code indicates grab and buoy samples were taken at the same location. The solid black line represents a 1:1 relationship.

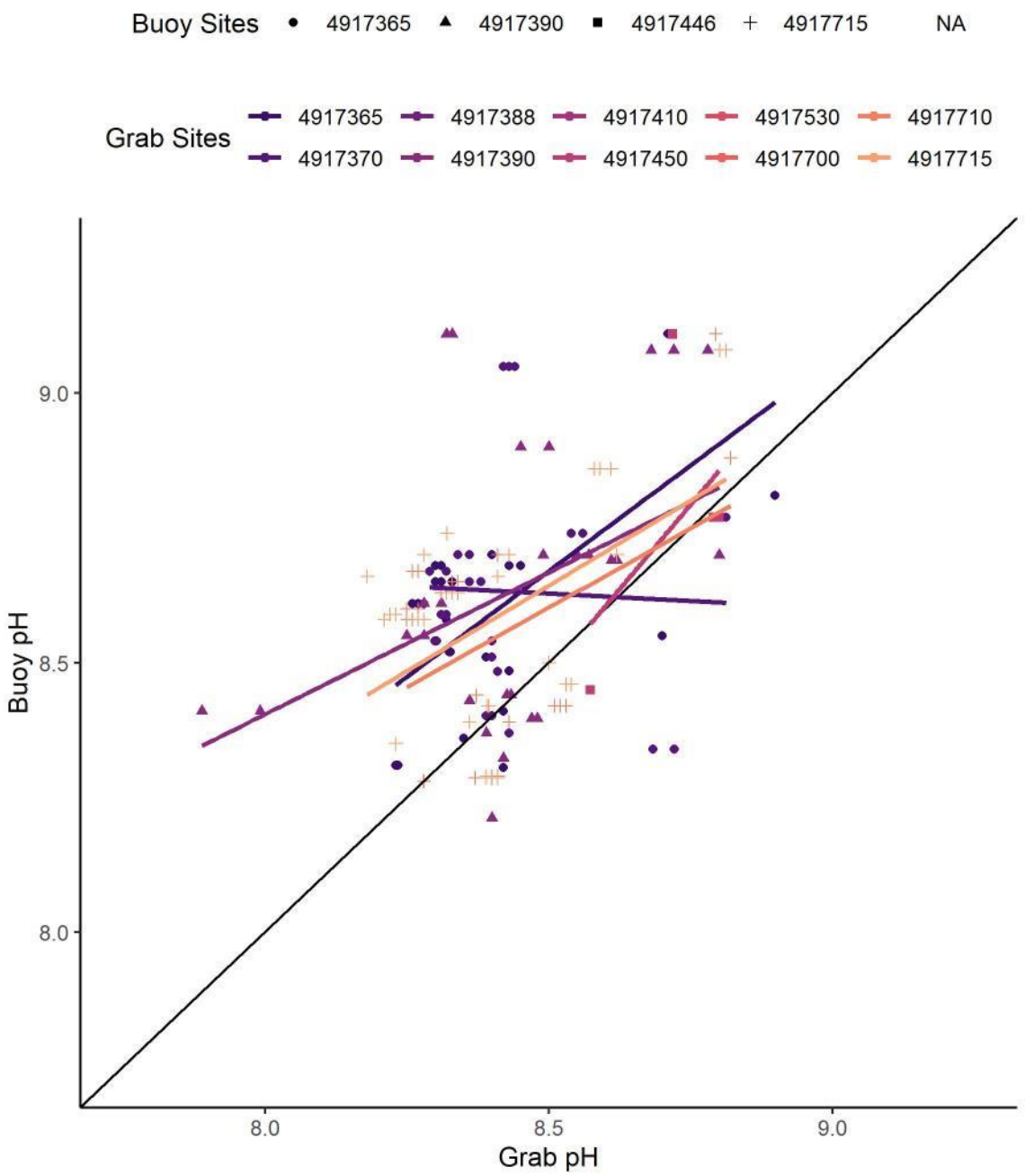


**Figure 2.3.10.** Comparisons of pH measured at buoy and grab sampling sites. Grab sites correspond to sites near the buoy site, which did not necessarily have data available. A direct match in site code indicates grab and buoy samples were taken at the same location. The solid black line represents a 1:1 relationship.

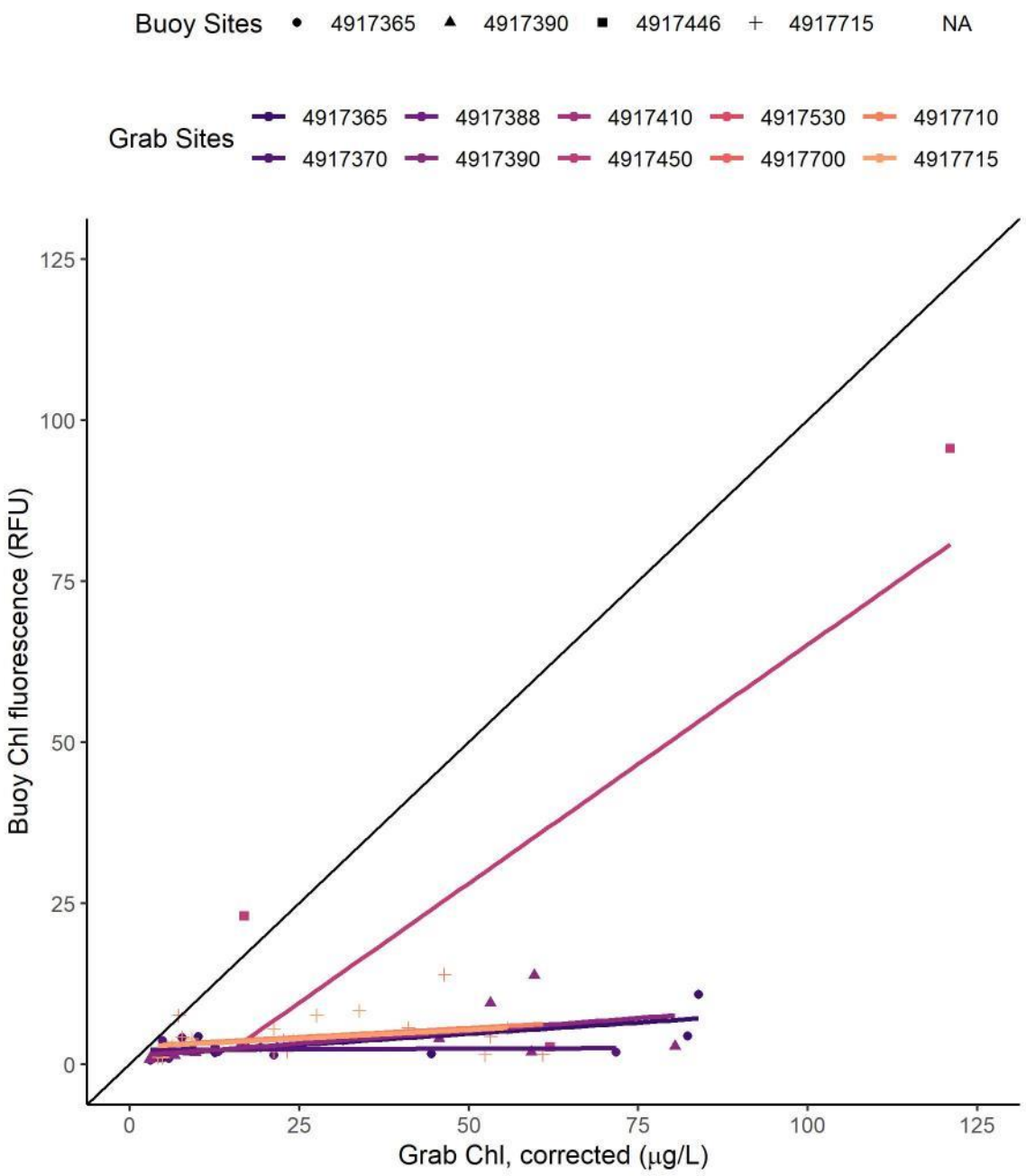


**Figure 2.3.11.** Comparisons of chlorophyll (chl) measured at buoy and grab sampling sites. Grab sites correspond to sites near the buoy site, which did not necessarily have data available. A direct match in site code indicates grab and buoy samples were taken at the same location. The solid black line represents a 1:1 relationship. RFU = relative fluorescence units.

## 2.4 PHYTOPLANKTON AND ZOOPLANKTON ANALYSIS

Phytoplankton and zooplankton spatial analysis are requests found in both the charge question working content as well as Attachment A ULWQS Science Panel Ideas for Studies, Experiments, and Literature Reviews documents. Here they are split into a number of sub-analyses.

### Phytoplankton and zooplankton temporal dynamics

**Proposed**

Question: When do HABs most frequently start/occur? (Charge question 2.3.i) What are the temporal patterns in phytoplankton and zooplankton? What is the seasonal succession of phytoplankton and zooplankton? What is the typical pattern of phytoplankton and zooplankton, how do they wax and wane? (Attachment A ULWQS Science Panel Ideas for Studies, Experiments, and Literature Reviews question).

Objective: Estimate temporal patterns in plankton, including HAB, assemblages.

Approach: The Utah Lake Data Explorer already has an analysis of gross temporal patterns of phytoplankton using Phase I data that has been updated with Phase II data and will have zooplankton data added, to the extent allowed by the data. Additional time series analyses will be conducted to test for specific patterns in plankton species/group composition using time as a predictor in multivariate models of phytoplankton assemblage structure. In addition, to the extent practicable with the data, UDWQ could use the Cyan[1] (satellite imagery) database and could calculate weekly cyanobacterial frequencies and using the available time series, evaluate the series for potential patterns using visual analysis or detrending algorithms. They could also calculate Julian day estimates for maximum bloom frequencies (with uncertainty estimates) for each resolvable Cyan lake pixel.

**Actual**

***Data and Methods***

UDWQ Phase I and Phase II Utah Lake surface water quality data were provided by UDWQ (https://deq.utah.gov/division-water-quality) via the Water Quality Portal. An operational taxonomic unit (OTU) reconciliation was run to resolve ambiguous taxa across samples. Temporal variation in phytoplankton taxa was analyzed for pooled sites. Cyanobacterial and total phytoplankton cell count and biovolume over time and with respect to basic spatial location (Provo Bay vs. main basin) were analyzed by two-way interaction effects ANOVA. Utah Lake zooplankton data were obtained from K. Landom (Pers.Comm., Landom et al. 2019a). Data were collected from 2002-2019, but only 2013-2019 were targeted for analysis due to a lack of systematic temporal and spatial sampling in other years. Zooplankton were divided into large-bodied taxa (calanoid copepods, *Daphnia*, *Diaphanosoma*, and *Leptodora*) and small-bodied taxa (*Bosmina*, *Ceriodaphnia*, cyclopoid copepods, nauplii, and rotifers) and pooled by month and year. Zooplankton data were not added to the Utah Lake Data Explorer in order to preserve data privacy for a forthcoming manuscript.

***Results***

Temporal variation in phytoplankton taxa for pooled sites revealed a common seasonal succession for eutrophic lakes (Tallberg et al. 1999). For both relative abundance and biovolume, diatoms (Bacillariophyta) are dominant from January to April, green algae (Chlorophyta) are most common from March to April and again in November, and cyanobacteria (Cyanophyta) are dominant from June to October (Figure 2.4.1). There were significant differences in cyanobacterial and total phytoplankton cell count and biovolume by month and location (Figure

[1] https://www.epa.gov/water-research/cyanobacteria-assessment-network-cyan

2.4.2). Cyanobacterial cell count was significantly higher from July-October than in other months, and cell counts in Provo Bay were higher than in the main basin of the lake (no significant interaction between month and location; two-way ANOVA, df = 1066, month F = 29.91, location F = 49.05, $p < 0.0001$). Results were similar for total phytoplankton cell counts as for cyanobacterial cell counts (no significant interaction between month and location; two-way ANOVA, df = 1066, month F = 19.96, location F = 114.66, $p < 0.0001$). There was a significant interaction between month and location for cyanobacterial and total phytoplankton biovolume, and although the statistical groupings were less distinct the general spatial and temporal dynamics were similar to those for cell counts (two-way interaction effects ANOVA; cyanobacteria: df = 827, F = 3.64, $p < 0.0001$; total phytoplankton: df = 827, F = 3.46, $p < 0.001$).

Of the large-bodied zooplankton, calanoid copepods and *Daphnia* tended to be most common across seasons (Figure 2.4.2). The predatory zooplankton, *Leptodora*, tended to have uniformly low counts of individuals across months and years but due to large body size tended to have the highest biomass among large-bodied taxa. Fluctuations in interannual large-bodied zooplankton abundance (Figure 2.4.3) have been attributed to carp removal efforts (Landom and Walsworth 2020). Of the small-bodied zooplankton, nauplii and rotifers tended to have high counts of individuals but uniformly low biomass across seasons (Figure 2.4.4). Other small-bodied taxa had variable abundance across seasons. Small-bodied taxa exhibited more interannual variability than large-bodied taxa (Figure 2.4.5), attributed to changes in lake level and carp removal (Landom and Walsworth 2020) Overall, temporal trends depended on whether the metric of interest was counts of individuals or biomass.

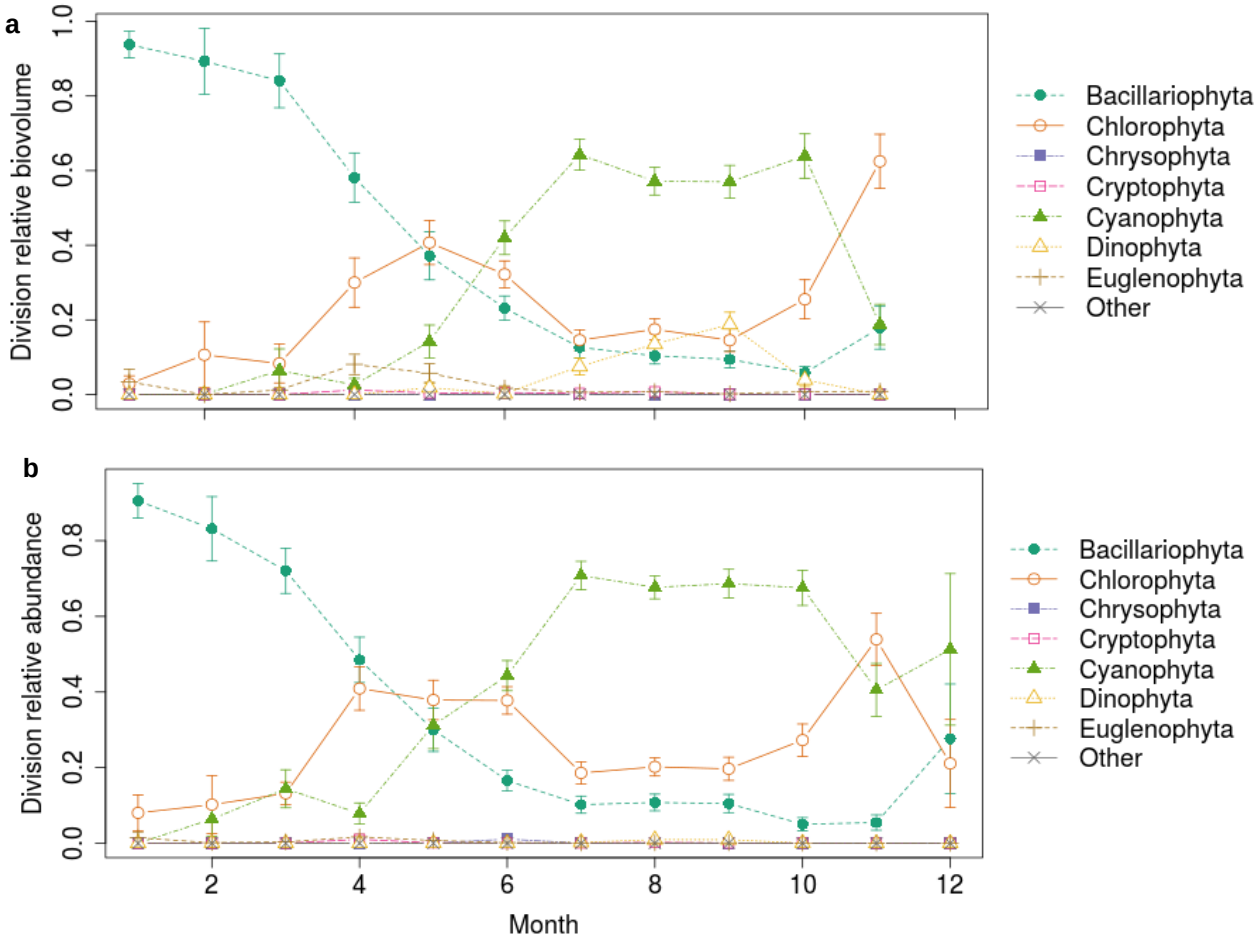


**Figure 2.4.1.** Seasonal succession in the (a) relative biovolume and (b) relative abundance of phytoplankton taxa in Utah Lake.

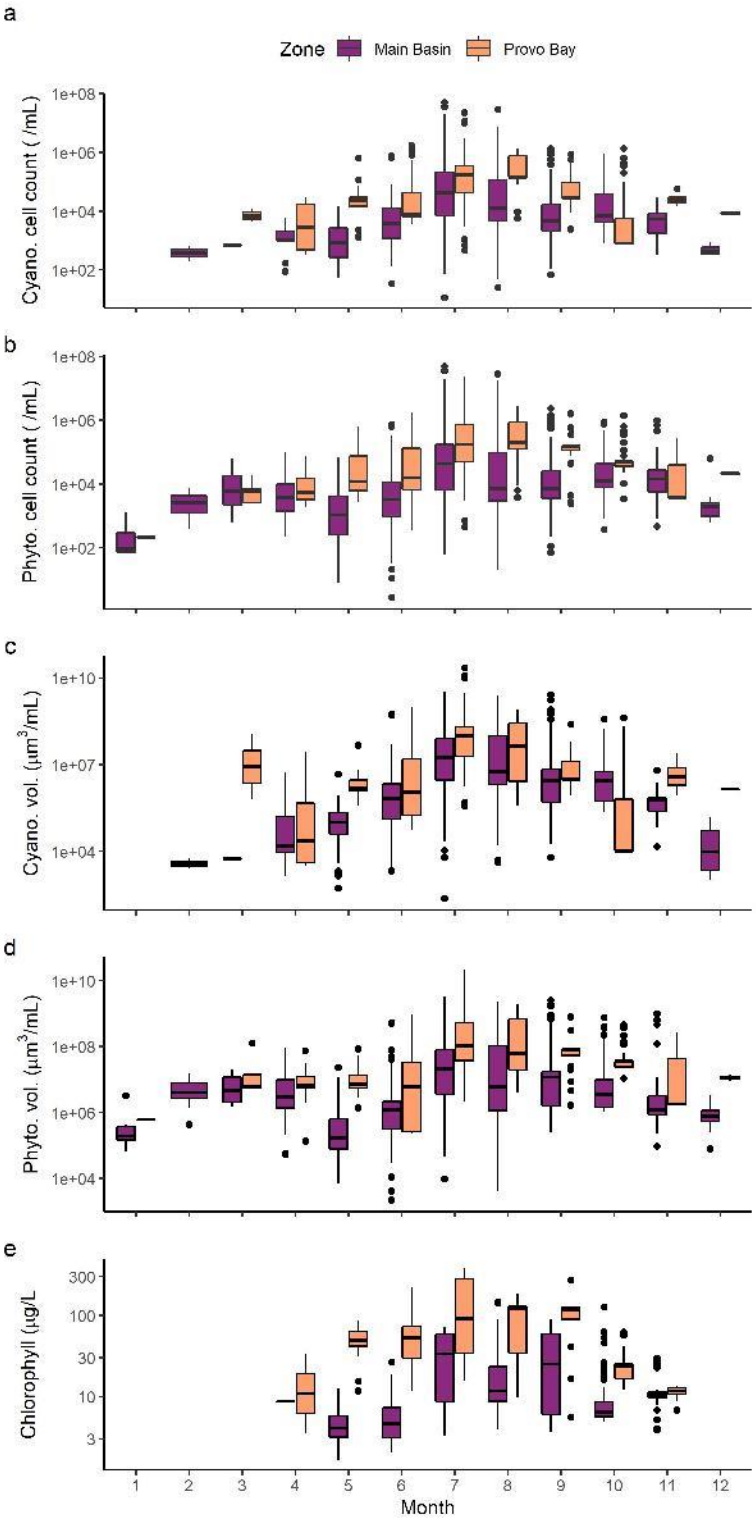


**Figure 2.4.2.** Relationships of (a) cyanobacteria cell count, (b) total phytoplankton cell count, (c) cyanobacteria biovolume, (d) total phytoplankton volume, and (e) chlorophyll concentration by month and location (Provo Bay = orange, main basin = purple).

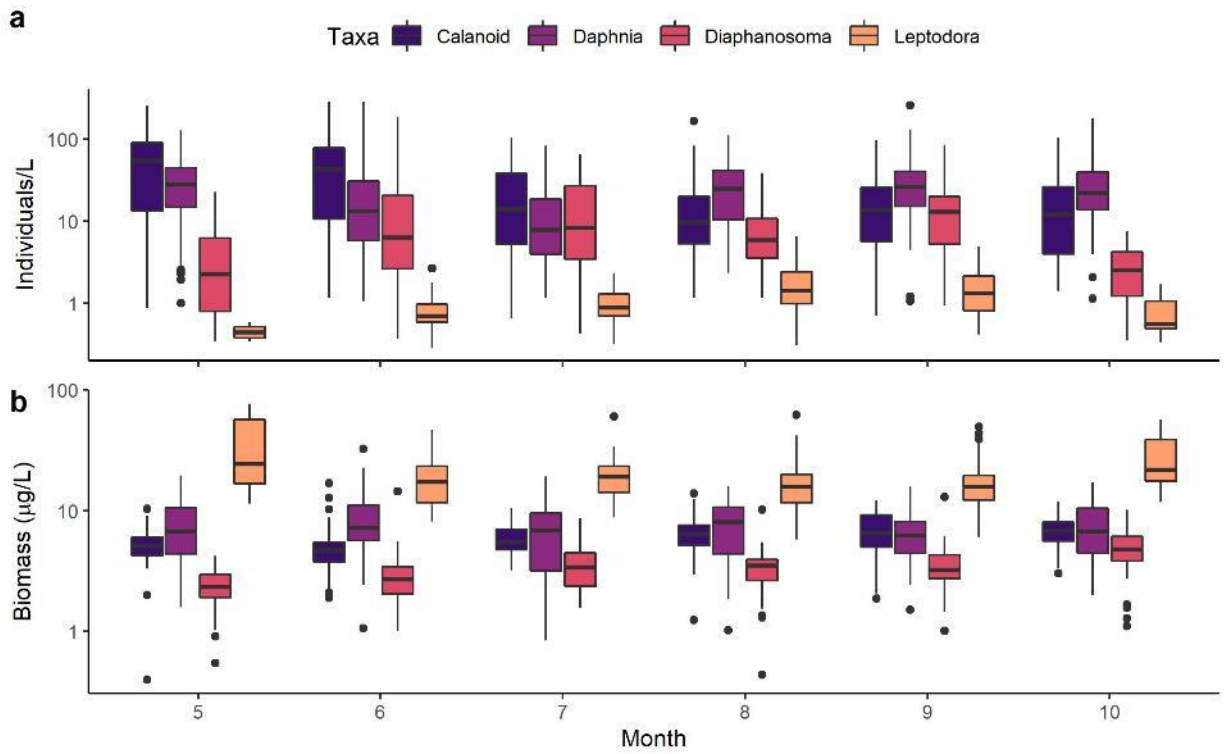


**Figure 2.4.3.** Monthly distributions of large-bodied zooplankton taxa for (a) individuals and (b) biomass.

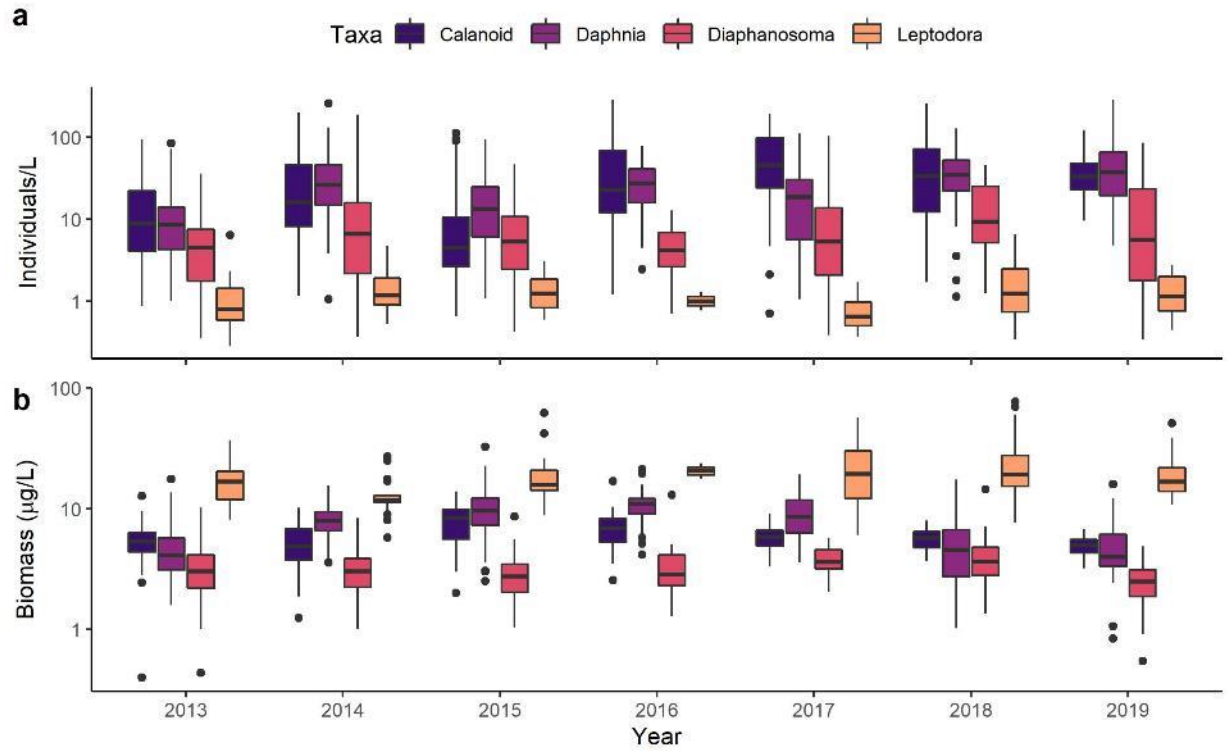


**Figure 2.4.4.** Annual distributions of large-bodied zooplankton taxa for (a) individuals and (b) biomass.

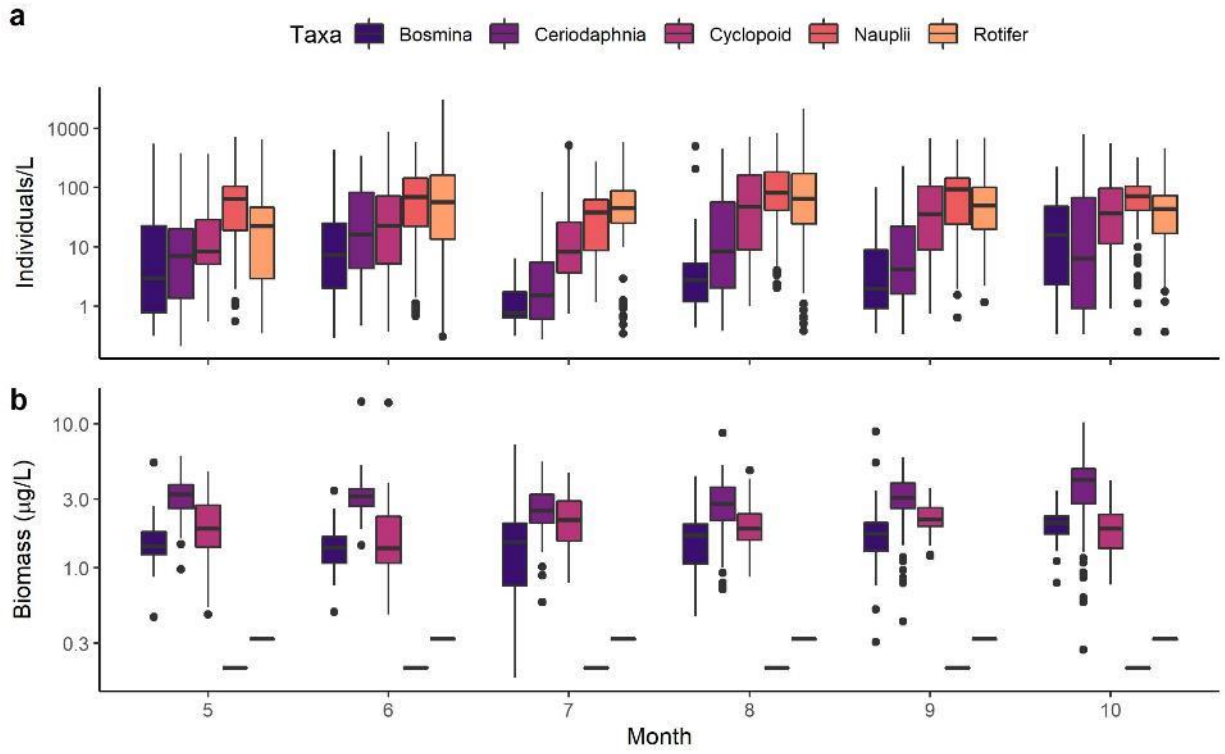


**Figure 2.4.5.** Monthly distributions of small-bodied zooplankton taxa for (a) individuals and (b) biomass.

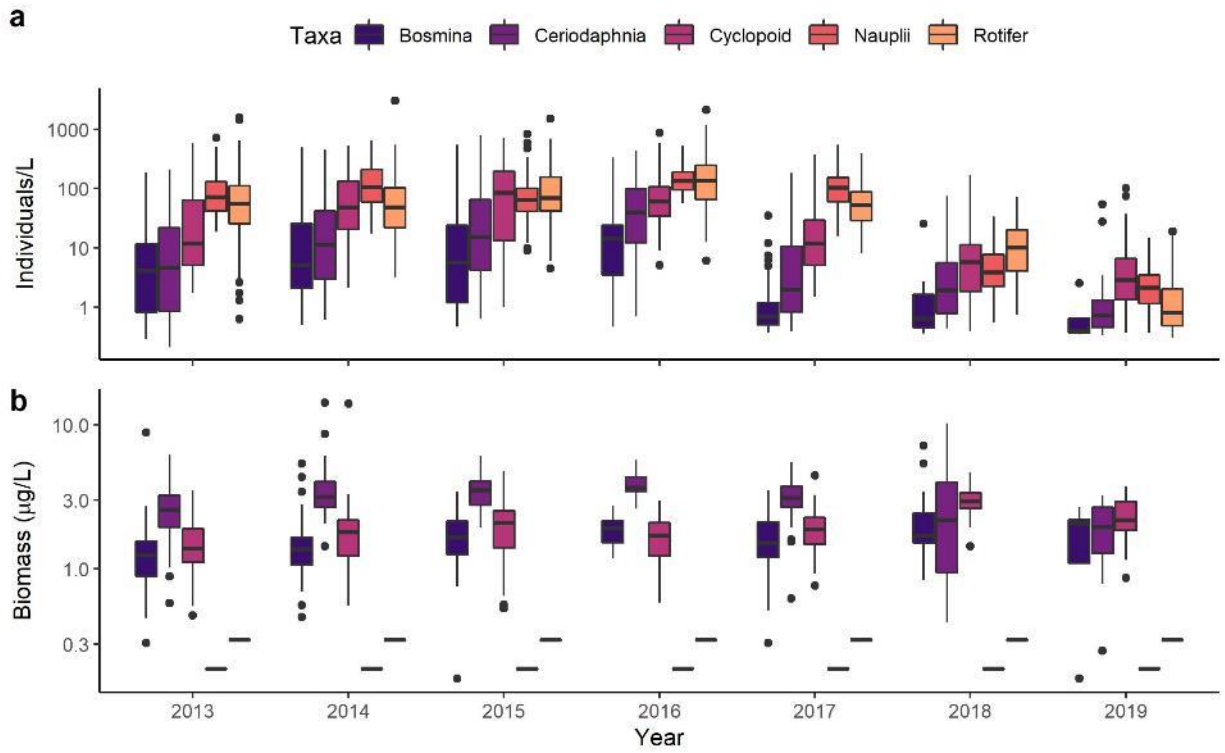


**Figure 2.4.6.** Annual distributions of small-bodied zooplankton taxa for (a) individuals and (b) biomass.

## Phytoplankton and zooplankton spatial dynamics

### Proposed

Question: Are there hotspots and do they tend to occur near major nutrient sources? (Charge question 2.3.i) Do HABs generally begin near Publicly Owned Treatment Works (POTW) outfalls? (Attachment A ULWQS Science Panel Ideas for Studies, Experiments, and Literature Reviews question).

Objective: Estimate spatial patterns in plankton, including HAB, assemblages.

Approach: Explorer already has an analysis of gross spatial patterns of phytoplankton using Phase I data that will be updated with Phase II data and will have zooplankton data added, to the extent allowed by the data. To the extent allowed by the data, additional spatial analyses will be conducted to test for specific patterns in plankton species/group composition using location as a predictor in multivariate models of phytoplankton assemblage structure. Environmental variables will be overlaid on the spatial patterns in biota to examine congruence in environmental and biological structure. Distance to POTW will be calculated and included as a predictor in nested multivariate models of plankton structure and environmental predictors. Indicator species analysis may also be used to identify specific taxa driving any spatial patterns in plankton assemblage structure.

In addition, again using the Cyan database and weekly cyanobacterial frequency data for resolvable pixels, evaluate the time series for potential spatial patterns using visual analysis or testing for differences among pixels in Cyan index dynamics. Test for spatial differences using some frequency analysis, like chi-squared test for the number or pixels assuming random distribution.

### Actual

#### *Data and Methods*

UDWQ Phase I and Phase II Utah Lake Surface Water Quality Data were provided by UDWQ (https://deq.utah.gov/division-water-quality) via the Water Quality Portal. Phytoplankton data were paired with chemical data from the same site and date. An operational taxonomic unit (OTU) reconciliation was run to resolve ambiguous taxa across samples, and maps were created for cyanobacterial taxa. Utah Lake zooplankton data were obtained from K. Landom (Pers.Comm., Landom et al. 2019a). Data were pooled by month and location for nine zooplankton taxa and visualized over space.

#### *Results*

There is a clear spatial structure to the phytoplankton dataset, with hotspots of high taxon biomass occurring in Provo Bay and in some cases in other locations (Figure 2.4.7). The cyanobacterial community contains several taxa capable of producing toxins (see https://epa.ohio.gov/Portals/28/documents/habs/toxin_producing_cyanobacteria.pdf). Cyanobacteria hot spots included Provo Bay and the northern bay near Lindon Marina, with individual taxa displaying similar spatial patterns.

For distributions of individual zooplankton taxa by month, regions in the main basin had largely similar distributions of individual counts and biomass, whereas Provo Bay tended to have higher or lower taxon abundance (Figures 2.4.8, 2.4.9). When mean biomass was computed for each sampling location, taxa appeared to be distributed variably across the lake with few apparent hotspots (Figure 2.4.10).

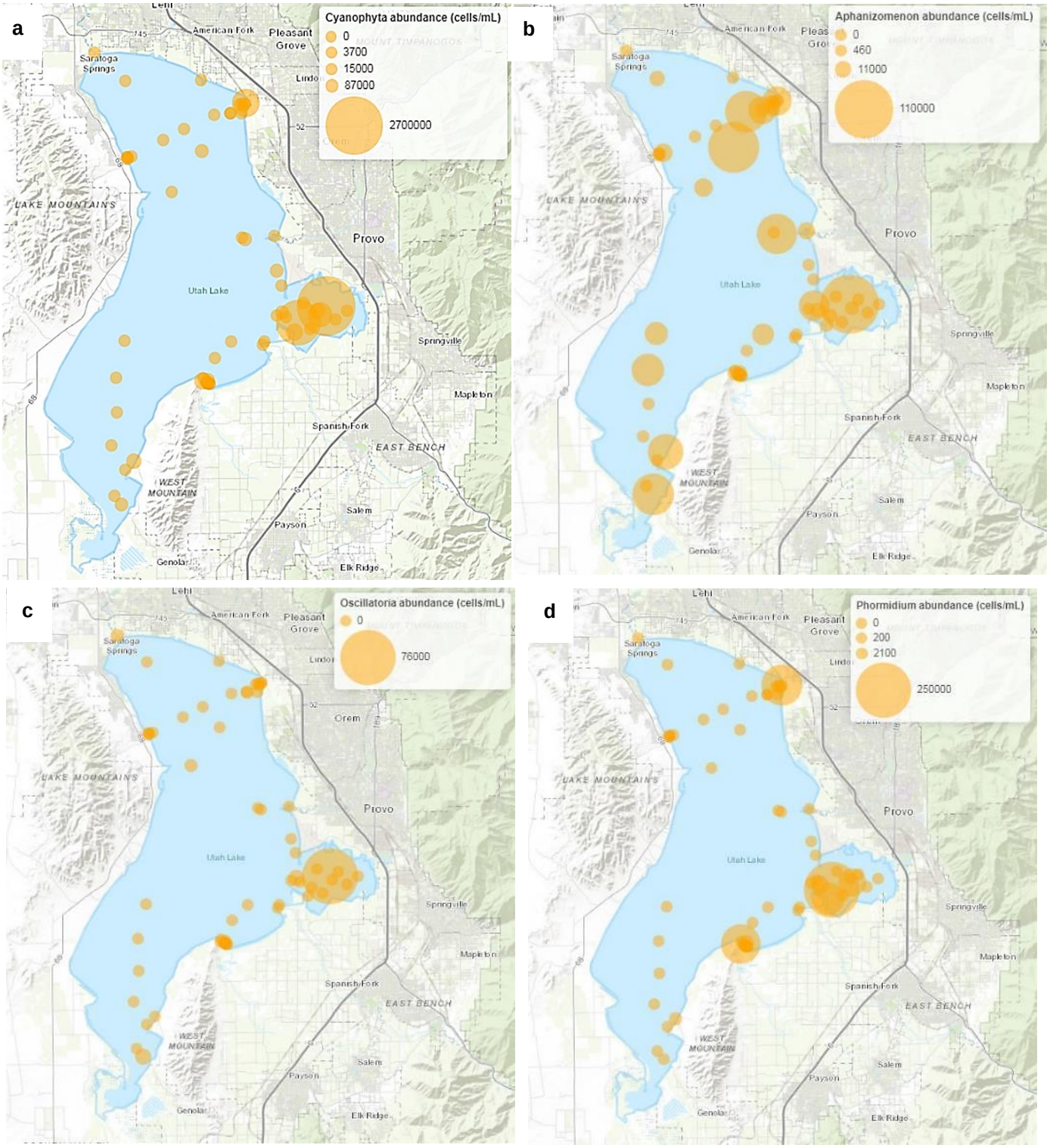
a
Cyanophyta abundance (cells/mL)
0
3700
15000
87000
2700000
b
Aphanizomenon abundance (cells/mL)
0
460
11000
110000
c
Oscillatoria abundance (cells/mL)
0
76000
d
Phormidium abundance (cells/mL)
0
200
2100
250000
Lehi
American Fork
Pleasant Grove
Saratoga Springs
Lindon
Orem
Provo
Utah Lake
LAKE MOUNTAINS
Springville
Mapleton
Spanish Fork
EAST BENCH
WEST MOUNTAIN
Salem
Payson
Genola
Elk Ridge

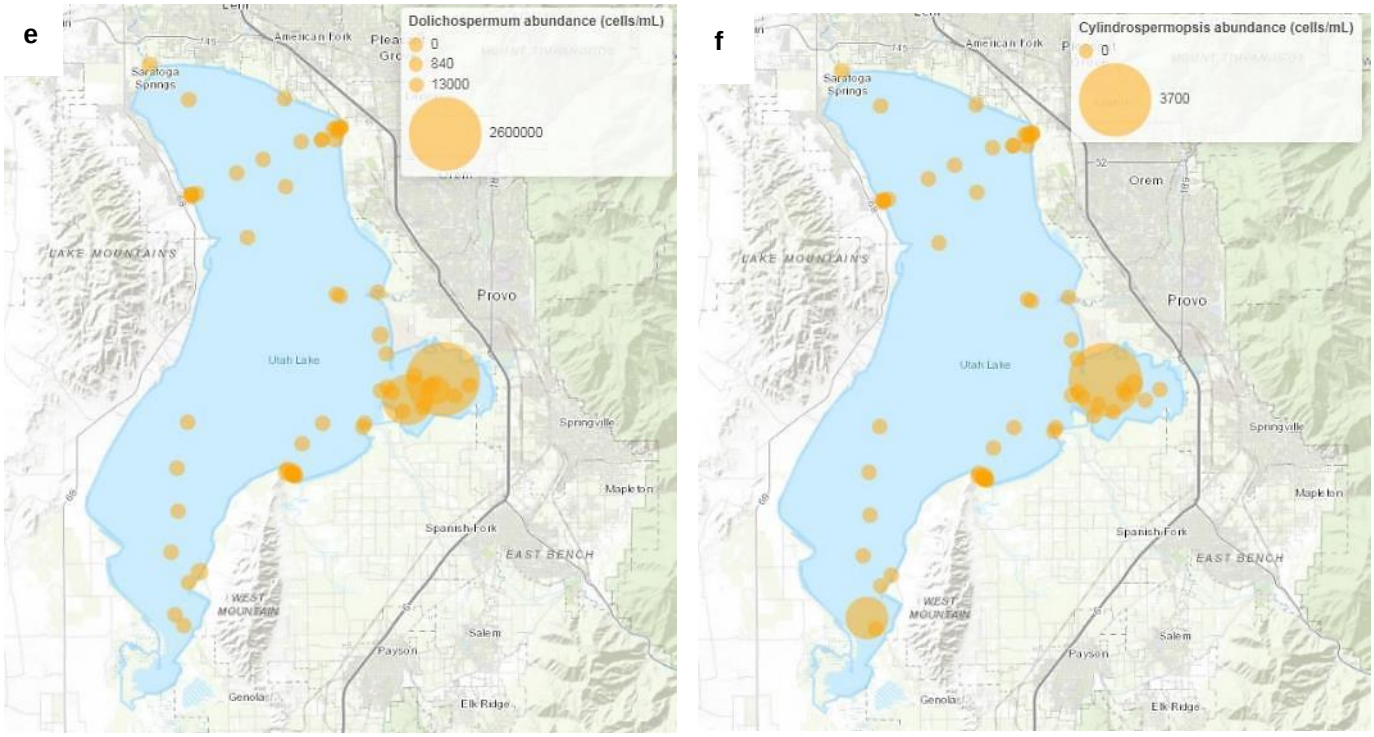


**Figure 2.4.7.** Cellular densities of cyanobacterial groups in Utah Lake: (a) cyanophyta (cyanobacteria), (b) *Aphanizomenon* spp., (c) *Oscillatoria* spp., (d) *Phormidium* spp., (e) *Dolichospermum* (née *Anabaena*) spp., (f) *Cylindrospermopsis* spp.

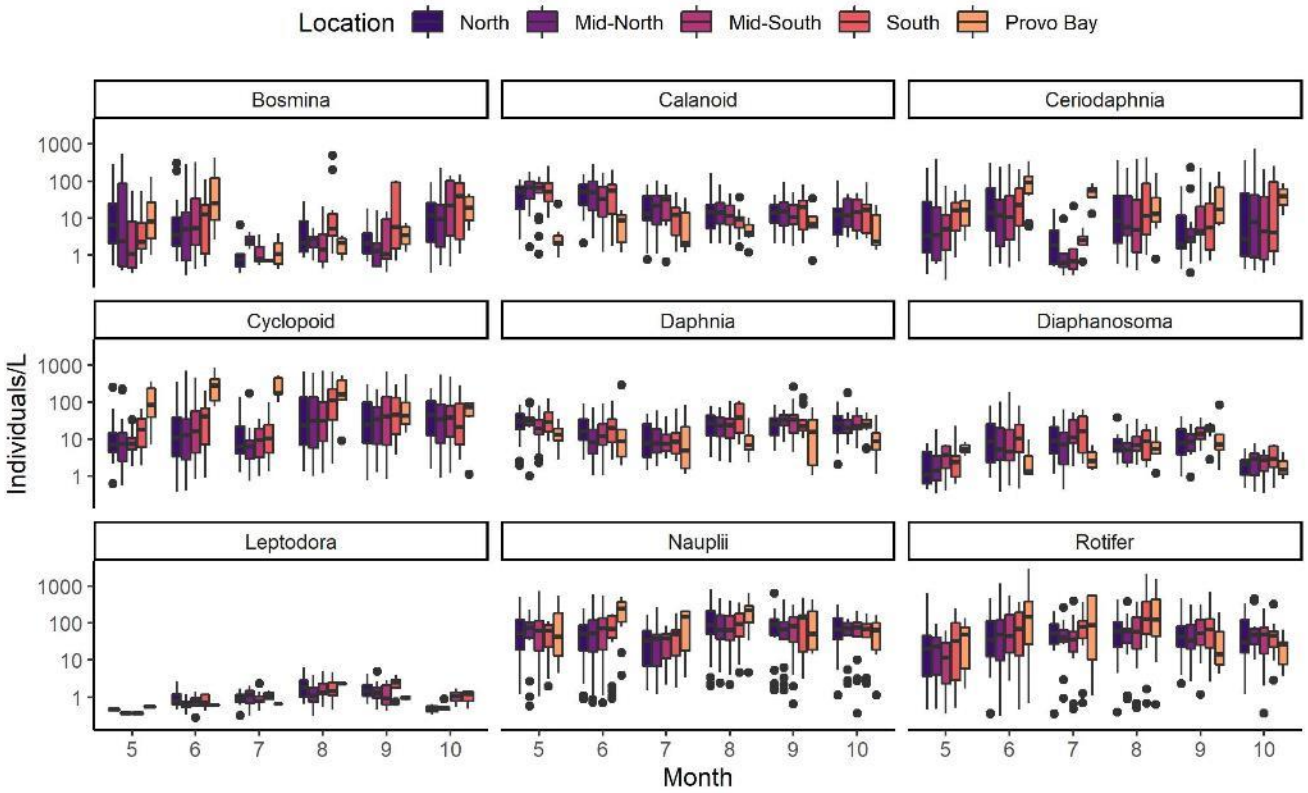


**Figure 2.4.8.** Seasonal distributions of zooplankton taxa individuals by location. Utah Lake was divided into four vertical quadrants (north, mid-north, mid-south, and south) plus Provo Bay.

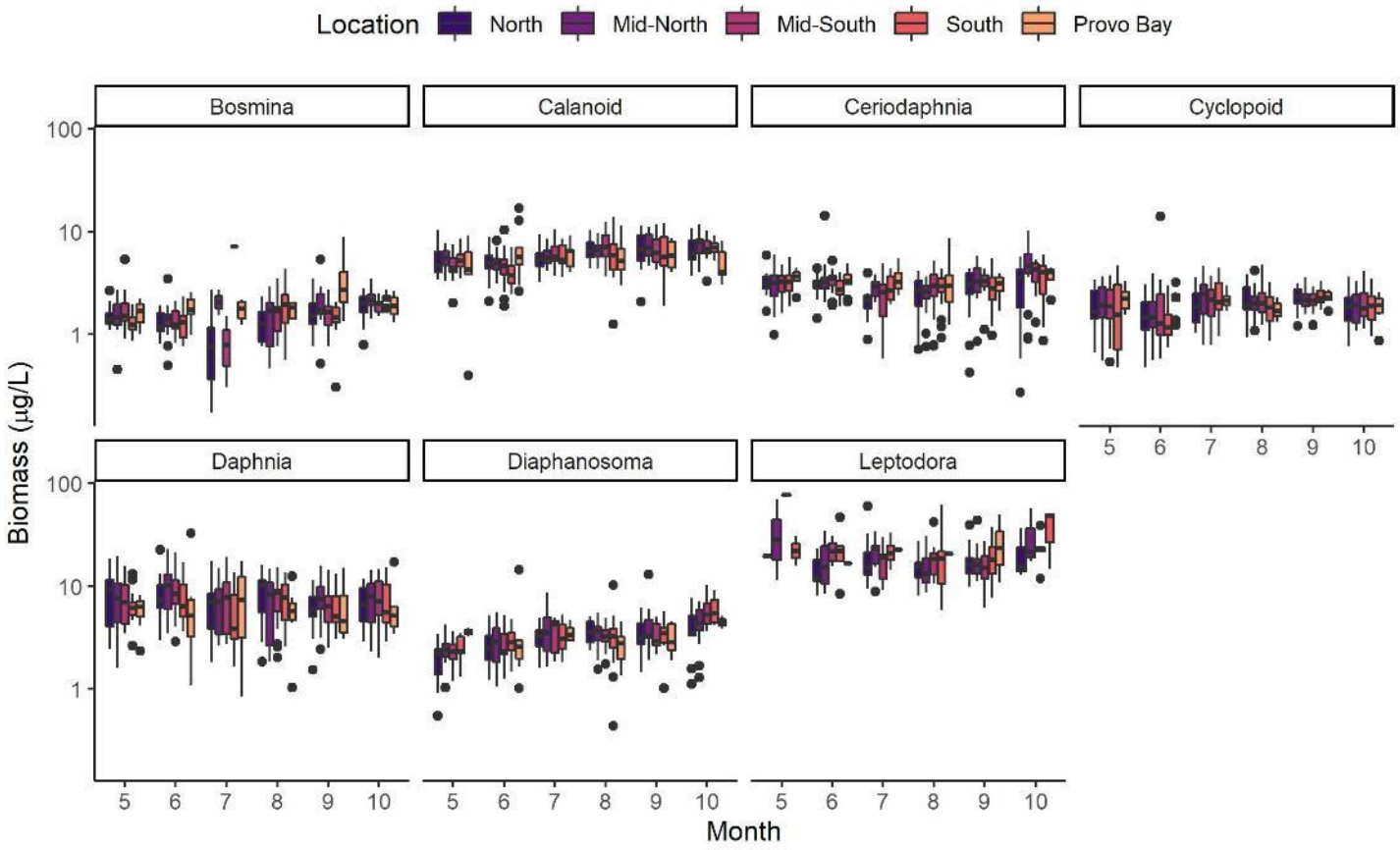


**Figure 2.4.9.** Seasonal distributions of zooplankton taxa biomass by location. Utah Lake was divided into four vertical quadrants (north, mid-north, mid-south, and south) plus Provo Bay.

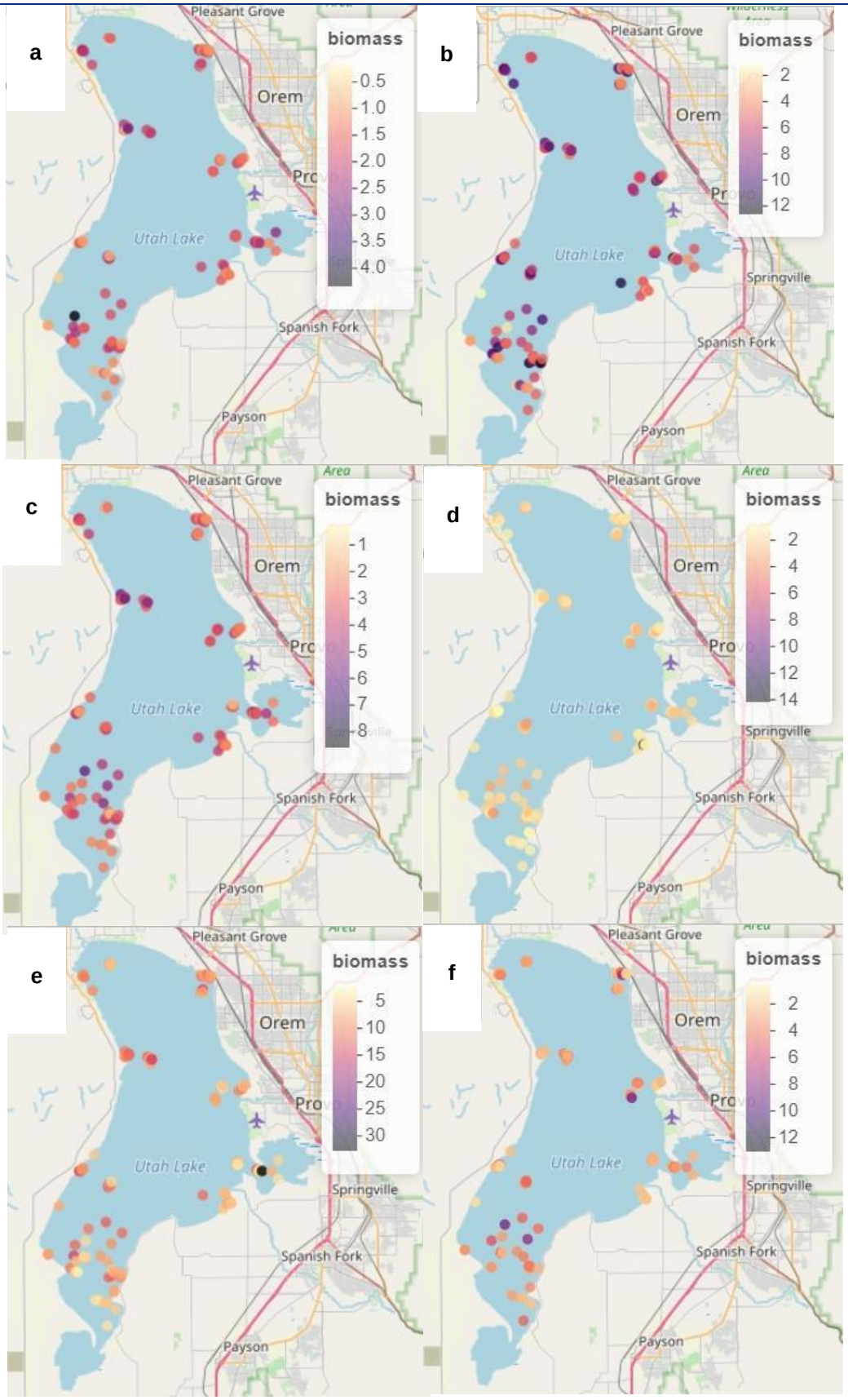


**Figure 2.4.10**. Mean annual maximum biomass (µg/L) of (a) *Bosmina*, (b) calanoid copepods, (c) *Ceriodaphnia*, (d) cyclopoid copepods, (e) *Daphnia*, and (f) *Diaphanosoma* in Utah Lake.

**Ongoing Questions**

Is an analysis of phytoplankton data in relation to the publicly owned treatment works locations desired?

## Dynamics in phytoplankton related to nutrients

**Proposed**

Question: Which nutrients are actually controlling primary production and HABs and when? (Charge question 2.3.ii) If there are linkages between changes in nutrient regime and HABs?? (Charge question 2.3.iii)

Objective: Test for a relationship between nutrient concentrations and HAB abundances.

Approach: Using the spatial analyses conducted in previous sub-analyses, test for relationships between nutrient concentration and HAB abundances. Using exploratory analyses like non-metric multidimensional scaling (NMDS) and canonical correspondence analysis (CCA), first explore potential relationships between nutrient concentrations and HAB abundances. Test for statistical relationships between nutrient concentration and HAB abundances at specific locations, using adjustments for repeated measures as necessary. Location may be treated as a random effect in ANCOVA like models where nutrients are continuous predictors of HAB abundance. Uncertainty will be quantified and reported.

*Note: analyses for this item (nutrients) have been combined with the following two items (lake level and other factors) as one "Actual" section.*

## Dynamics in phytoplankton related to lake level

**Proposed**

Question: If there are linkages between changes in nutrient regime and HABs, what role if any does lake elevation change play? (Charge question 2.3.iii)

Objective: Test for a relationship between lake level and HAB abundances.

Approach: Using the spatial analyses conducted in previous sub-analyses, test for relationships between lake level and HAB abundance. Using Phase I and II data, Cyan data (as allowed by availability), and lake level records, estimate the relationship between lake level and plankton (including HAB) abundance. This extends the plankton spatial analysis to add lake level as a predictor in multivariate models of plankton structure. We will also extend the ANCOVA like models of the previous sub-analysis of dynamics in plankton pattern related to nutrients to add lake level as a predictor and test for an effect on nutrient-plankton response relationships.

*Note: analyses for this item (lake level) have been combined with the other two items (nutrients and other factors) as one "Actual" section.*

## Dynamics in phytoplankton related to other factors

**Proposed**

Question: How do other factors affect HAB formation in Utah Lake (e.g., climate change; temperature; lake stratification; changes in zooplankton and benthic grazers and transparency)? (Charge question 2.3.iv)

Objective: Test for a relationship between temperature, stratification and HAB abundances.

Approach: Using the spatial analyses conducted in previous sub-analyses, test for relationships between temperature or stratification and HAB abundance. Using Phase I and II data, Cyan data (as allowed by availability), and temperature records (both average and vertical profile), estimate the relationship between temperature, lake water column stability (as measured by Schmidt stability and plankton (including HAB) abundance. This extends the plankton spatial analysis to add temperature and water column stratification as predictors in multivariate models of plankton structure. We will also extend the ANCOVA like models of the

previous sub-analysis of dynamics in plankton pattern related to nutrients to add temperature and water column stability as predictors and test for effects on nutrient-plankton response relationships.

We understand that empirical data suggest Utah Lake rarely stratifies and given the average depths and area, physical models suggest it is unlikely that the lake consistent stratifies, however small summer temperature gradients in this lake can set up strong thermal stability and it is worth investigating how strong even small thermal gradients may be, how resistant they may be to mixing (i.e., what wind force would be needed to mix them), and what the relationship to some algal response measures may be.

*Note: analyses for this item (other factors) have been combined with the preceding two items (nutrients and lake level) as one "Actual" section.*

**Actual**

***Data and Methods***

UDWQ Phase I and Phase II Utah Lake Surface Water Quality Data were provided by UDWQ (https://deq.utah.gov/division-water-quality) via the Water Quality Portal. Phytoplankton data were paired with chemical data from the same site and date. An operational taxonomic unit (OTU) reconciliation was run to resolve ambiguous taxa across samples. Phytoplankton data were then run through an NMDS analysis to determine spatial patterns across multidimensional space. First, univariate relationships between chlorophyll, total and cyanobacterial cell count, and total and cyanobacterial biovolume vs. TP and TN concentrations were tested using quantile regression. Next, from the results of the NMDS analysis, the following variables were chosen to run in multiple regression: TP, TN, turbidity, lake elevation, and month. The variables were then fed into a hierarchical (mixed effects) model with the variable subset as fixed effects and site as a random effect. The proportion variance explained by fixed effects (marginal $R^2$) was compared to the proportion of variance explained when the random site effect was added (conditional $R^2$).

Several potential distributions were tested to determine which were most appropriate to characterize total and cyanobacterial cell count. A Poisson or negative binomial distribution is often used for count data, with the latter common in zero-inflated datasets. A log-transformed normal distribution was also tested. Model fit was best for the log-transformed normal distribution, as indicated by q-q plots and residuals vs. fitted diagrams (Figure 2.4.11).

Stratification was considered as a possible variable of interest. Using the rLakeAnalyzer package, thermoclines were analyzed for available sites and dates. Thermal stratification was detected at several site-date combinations (Table 2.4.1), but stratification was not included in the analysis due to (1) several detected thermoclines were detected at < 1 m depth, which may indicate transient conditions and (2) the absence of oxygen gradients that result in hypoxia at depth (also tested as part of the stratification analysis). We recommend more frequent sampling of temperature profiles at a finer depth resolution to better quantify the role of thermal stratification in Utah Lake.

**a. Poisson distribution**

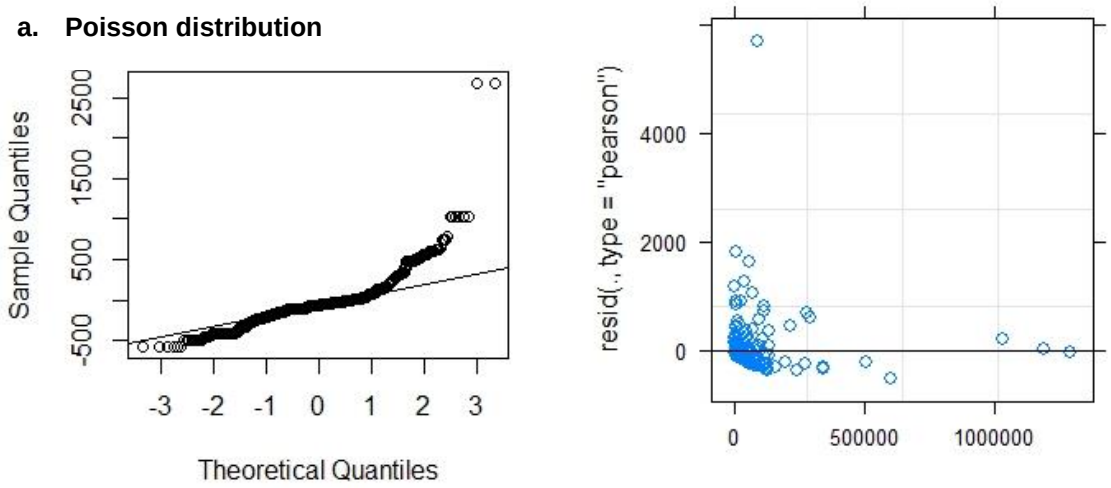


**b. Negative binomial distribution**

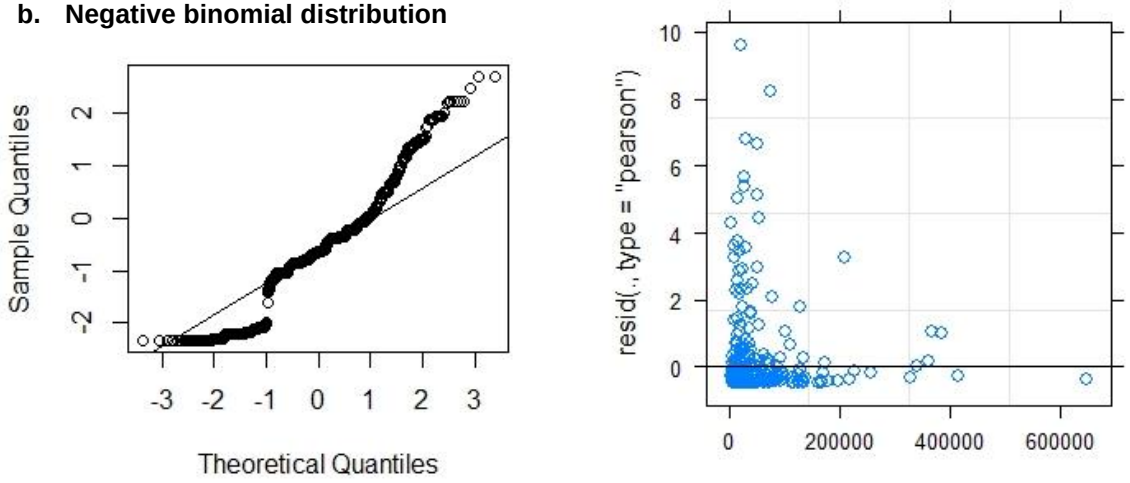


**c. Normal distribution (log-transformed)**

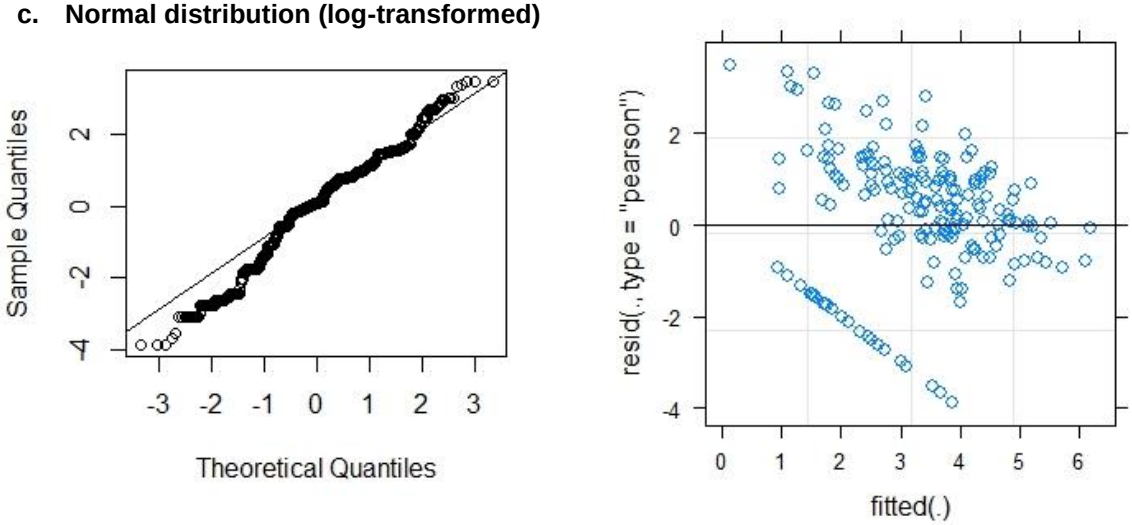


**Figure 2.4.11.** Cyanobacteria cell count hierarchical model fit for (a) Poisson, (b) negative binomial, and (c) normal distributions. The left panels are q-q plots of theoretical and sample quantiles, where points indicating a good model fit would fall along the solid 1:1 line. The right panels are plots of fitted values and their residuals, where a good model fit would be indicated by even spacing of positive and negative residuals across the range of fitted values.

**Table 2.4.1.** Preliminary analysis of temperature profiles and detected thermoclines in Utah Lake.

| Site | # of temperature profiles | # of profiles with detected thermocline | # of thermoclines < 1 m depth |
|---|---|---|---|
| 4917310 | 17 | 8 | 3 |
| 4917390 (North) | 17 | 10 | 7 |
| 4917500 | 17 | 5 | 2 |
| 4917520 | 17 | 6 | 4 |

***Results***

NMDS plots show relationships among individual samples and environmental variables (Figure 2.4.12). Day of year, chlorophyll, and TN loaded strongly onto the first NMDS axis, whereas TN, lake elevation, latitude, and longitude loaded strongly onto the second NMDS axis. Specific cyanobacterial taxa are plotted with their loadings in multivariate space, indicating their relationships with the environmental variables in multivariate space. Some taxa clustered together, whereas *Pseudoanabaena* sp. loaded into a separate quadrant as other taxa.

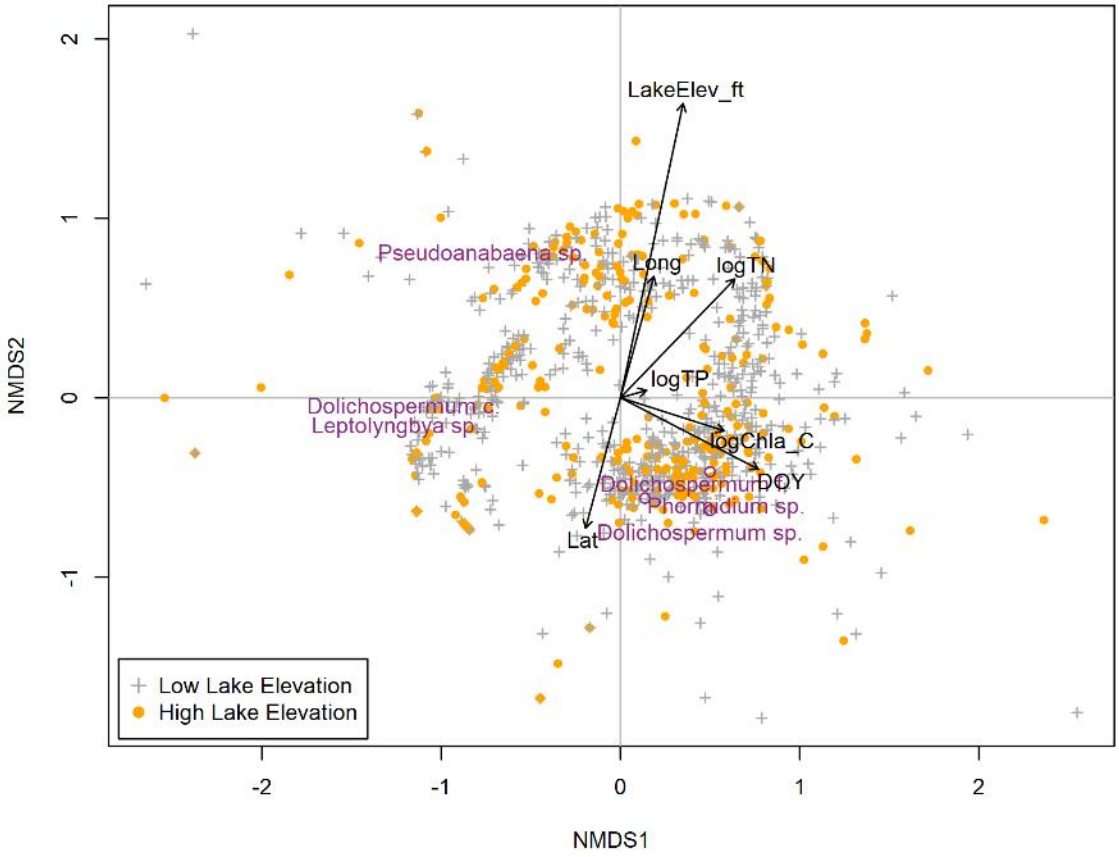


**Figure 2.4.12.** Non-metric multidimensional scaling (NMDS) relationships of individual samples (points; noted as either high or low lake elevation) and phytoplankton taxa (purple labels) as they relate to environmental variables (black vectors and labels). DOY = day of year, Long = longitude, Lat = latitude.

Quantile regression showed that TP had a consistently positive relationship with all phytoplankton metrics (chlorophyll, cyanobacterial and total cell count and biovolume) across quantiles. TN had a modest positive relationship with phytoplankton metrics at the median quantile, but the relationship was not consistently positive across quantiles (Figures 2.4.13, 2.4.14, 2.4.15).

For the TP hierarchical model, TP was positively related to phytoplankton metrics, and turbidity and lake elevation were negatively correlated to phytoplankton metrics. Turbidity was a significant predictor for cell count but not biovolume, and lake elevation was a significant predictor for all phytoplankton metrics except cyanobacterial biovolume. For the TN hierarchical model, TN and lake elevation were negatively related to phytoplankton metrics, and turbidity was not a significant predictor. Month was a significant predictor for both models, with July being the most consistently significant positive predictor (Table 2.4.2). The conditional $R^2$ was higher than the marginal $R^2$ for all metrics, indicating that incorporating spatial variability as a random effect explained more variability in the dataset than with fixed effects alone.

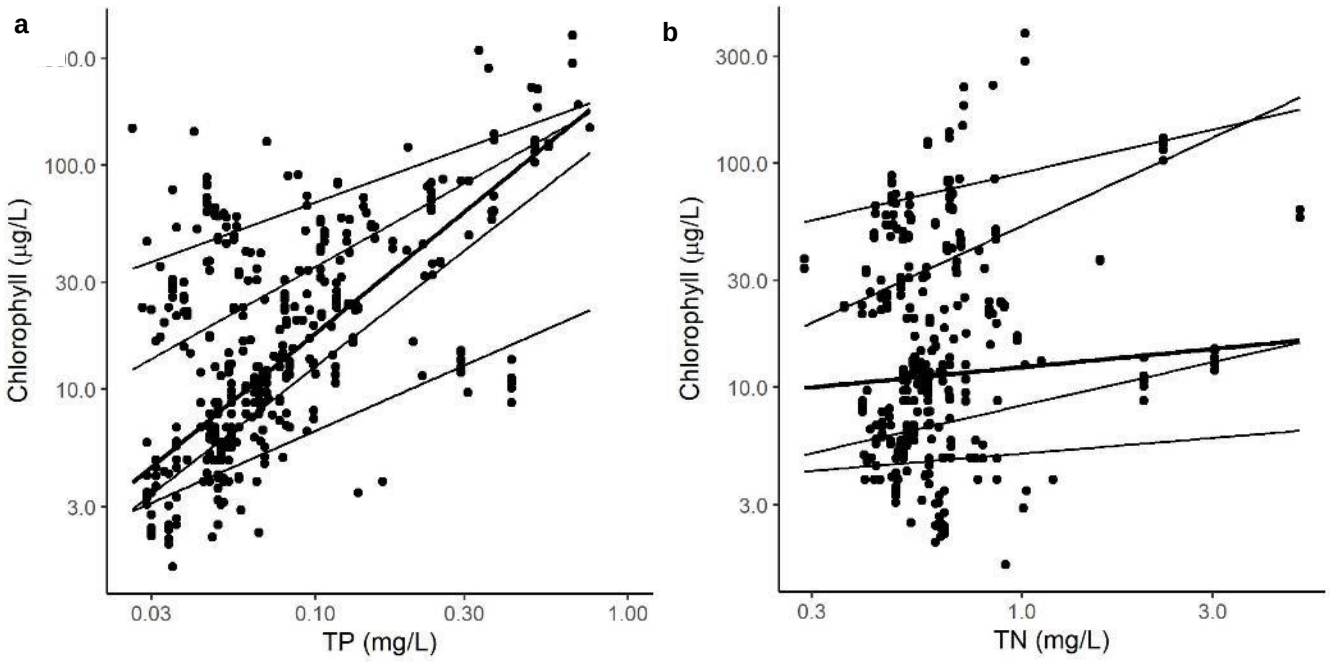


**Figure 2.4.13.** Chlorophyll relationship with (a) TP and (b) TN. Lines represent a quantile regression with the 10th, 25th, 50th (bold), 75th, and 90th quantiles of the data. Note the logged axes for all variables.

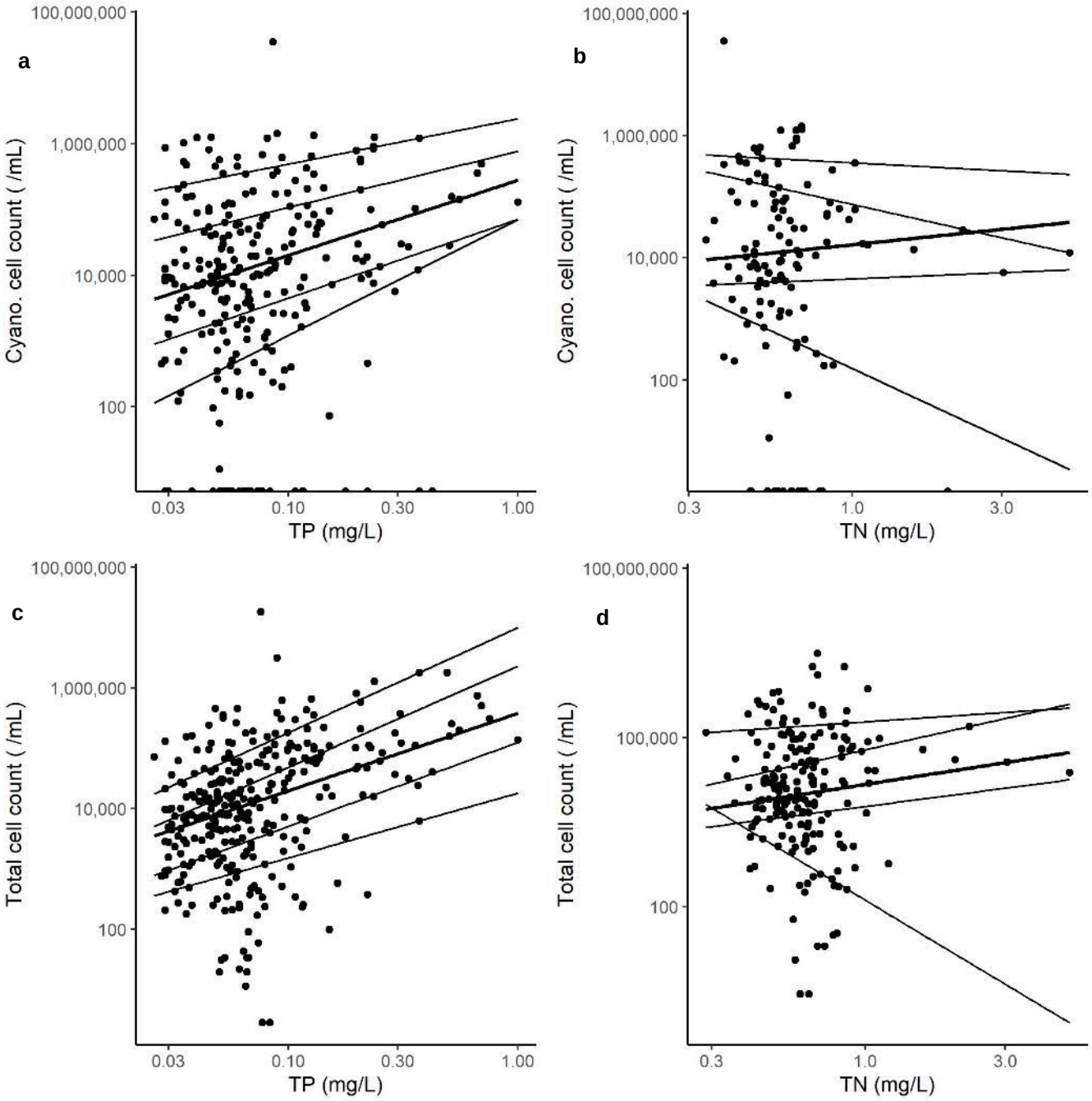


**Figure 2.4.14.** Relationship of (a) cyanobacterial cell count with TP, (b) cyanobacterial cell count with TN, (c) total phytoplankton cell count with TP, and (d) total phytoplankton cell count with TN. Lines represent a quantile regression with the 10th, 25th, 50th (bold), 75th, and 90th quantiles of the data. Note the logged axes for all variables.

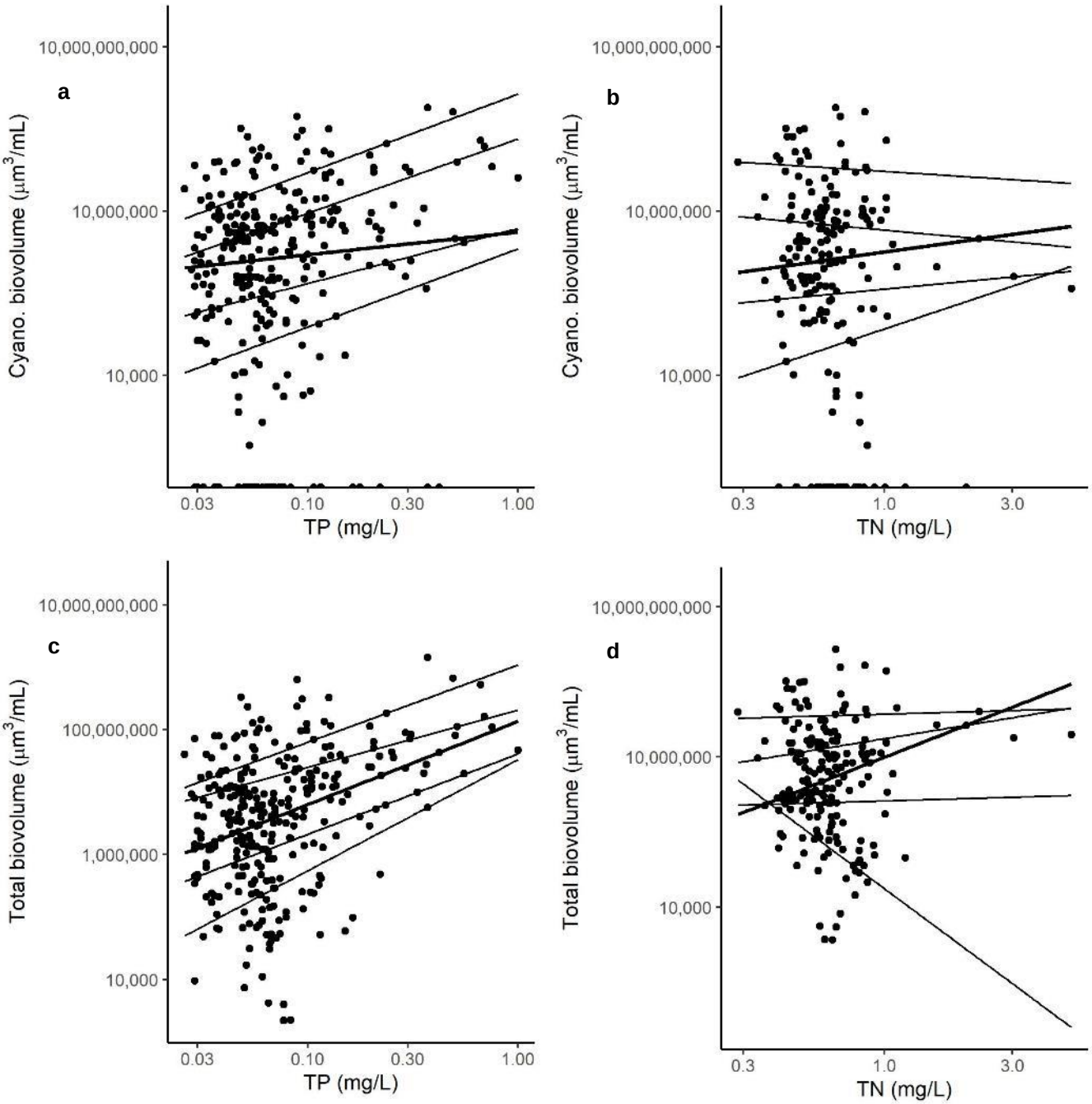


**Figure 2.4.15.** Relationship of (a) cyanobacterial biovolume with TP, (b) cyanobacterial biovolume with TN, (c) total phytoplankton biovolume with TP, and (d) total phytoplankton biovolume with TN. Lines represent a quantile regression with the 10th, 25th, 50th (bold), 75th, and 90th quantiles of the data. Note the logged axes for all variables.

**Table 2.4.2.** Coefficients and model fit of hierarchical models to predict phytoplankton metrics from TP (top panel), TN (bottom panel), and other predictors. Bold text indicates a statistically significant coefficient at the $p < 0.05$ level. Marginal $R^2$ represents the model fit for fixed effects only, whereas conditional $R^2$ includes fixed effects and site as random effect.

| Variable | log(cyano. cell count) | log(total cell count) | log(cyano. biovol.) | log(total biovol.) |
|---|---|---|---|---|
| Intercept | **840.23** | **411.47** | 233.99 | **357.87** |
| log(TP) | **1.39** | **1.37** | **2.01** | **1.32** |
| log(Turbidity) | **-0.31** | **-0.17** | -0.33 | -0.08 |
| Lake elevation | **-0.18** | **-0.09** | -0.05 | **-0.08** |
| Month 5 | **-1.75** | -0.39 | **-2.53** | 0.00 |
| Month 6 | 0.03 | 0.48 | 0.04 | 0.66 |
| Month 7 | **1.59** | **1.53** | **2.50** | **2.08** |
| Month 8 | 0.22 | 0.47 | 0.36 | 0.80 |
| Month 9 | 0.44 | 0.73 | 1.16 | **1.43** |
| Month 10 | -0.20 | **0.77** | -0.15 | **1.07** |
| Month 11 | -1.25 | 0.43 | -1.62 | 0.53 |
| 1\|Site | random | random | random | random |
| Marginal $R^2$ | 0.30 | 0.36 | 0.29 | 0.40 |
| Conditional $R^2$ | 0.44 | 0.48 | 0.42 | 0.46 |

| Variable | log(cyano. cell count) | log(total cell count) | log(cyano. biovol.) | log(total biovol.) |
|---|---|---|---|---|
| Intercept | **1209.35** | **993.19** | **856.16** | **902.19** |
| log(TN) | **-1.19** | **-0.76** | **-1.57** | **-0.63** |
| log(Turbidity) | -0.20 | -0.04 | -0.20 | 0.04 |
| Lake elevation | **-0.27** | **-0.22** | **-0.19** | **-0.20** |
| Month 5 | **-1.54** | -0.08 | -2.22 | 0.29 |
| Month 6 | -0.05 | 0.55 | -0.06 | 0.72 |
| Month 7 | **1.62** | **1.70** | **2.57** | **2.25** |
| Month 8 | 0.50 | **0.80** | 0.72 | **1.14** |
| Month 9 | 0.41 | 0.75 | 1.10 | **1.45** |
| Month 10 | -0.13 | **0.89** | -0.07 | **1.18** |
| Month 11 | -1.19 | 0.61 | -1.58 | 0.67 |
| 1\|Site | random | random | random | random |
| Marginal $R^2$ | 0.29 | 0.15 | 0.29 | 0.27 |
| Conditional $R^2$ | 0.44 | 0.53 | 0.40 | 0.53 |

### Ongoing Questions

Do we need to generate statistical models of specific HAB taxa vs. nutrient concentrations?

## Dynamics in Cyanobacteria and toxins

The Utah Lake Water Quality Study Steering Committee prepared a Management Goals table as part of the Framework document. They have tasked the Science Panel with providing important scientific feedback on defensible assessment endpoints, measures, targets and target development to evaluate progress towards management goals.

Question: What is the relationship between cyanobacteria density and toxin concentration?

***Data and Methods***

UDWQ HAB monitoring data, comprising phytoplankton abundance data and cyanotoxin data, were provided by UDWQ (https://deq.utah.gov/division-water-quality). Two primary laboratories analyzed toxin samples contained in the dataset, the Utah Public Health Laboratory (UPHL) and the Utah Department of Agriculture and Food (UDAF). A small amount of samples from the Environmental Protection Agency (EPA) and Greenwater were available as well. In most cases, UPHL and UDAF samples were available simultaneously, so the paired samples were analyzed to assess agreement between labs. Anatoxin concentrations were always below 1 µg/L and had similar distributions for both labs (Figure 2.4.16). Subsequent analyses were not conducted for anatoxin given the low concentrations. Microcystin concentrations ranged from below detection to over 10,000 µg/L. The relationship between labs fell along the 1:1 line ($R^2 = 0.80$, df = 157, $p < 0.0001$; Figure 2.4.17). Given the strong correlation and the lack of bias in concentrations between labs, subsequent analyses combined all microcystin measurements and used the average microcystin concentration when multiple lab measurements were available.

Cell counts were computed by Rushforth in 2016 and by Phycotech in 2017-2020. Further, cells were hand counted in 2017 and counted a FlowCytobot instrument in 2018-2020. The dataset was examined for any potential sources of bias arising from the analytical methodology among years. There did not appear to be a systematic over- or underestimation of cell count in certain years, so all years were retained in the analysis as provided in the original dataset.

To determine how representative the HAB monitoring program samples are of the conditions across Utah Lake, cyanobacterial cell counts for the HAB monitoring program and the routine monitoring program were compared (for the same subset of months, April-November; Figure 2.4.18). Median cell count was higher in the HAB monitoring program dataset than in the routine monitoring program dataset, but the overall ranges of cyanobacterial cell count for each dataset were similar.

The relationships between microcystin and cyanobacterial cell count were analyzed by linear regression and logistic regression. Several covariates of interest were identified as potential modifying factors for the relationship between cell count and toxins. The first was the depth at which samples were collected. The HAB sampling program collects both surface and composite (integrated photic zone) samples, noted as such in the sample logs. Additional covariates included seasonality and location.

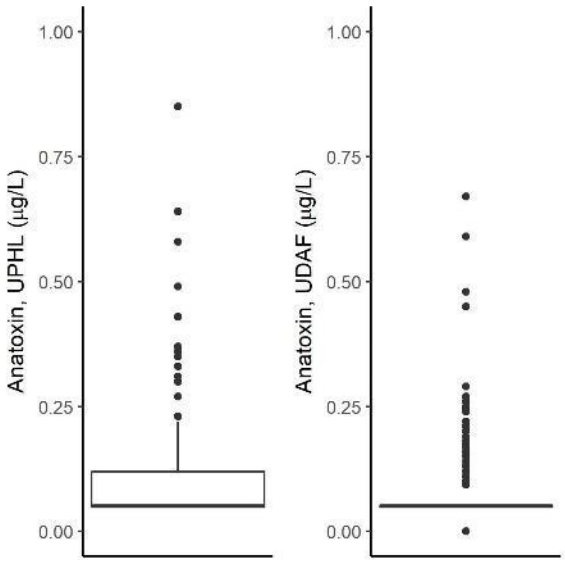


**Figure 2.4.16.** Anatoxin concentrations measured by UDAF and UPHL.

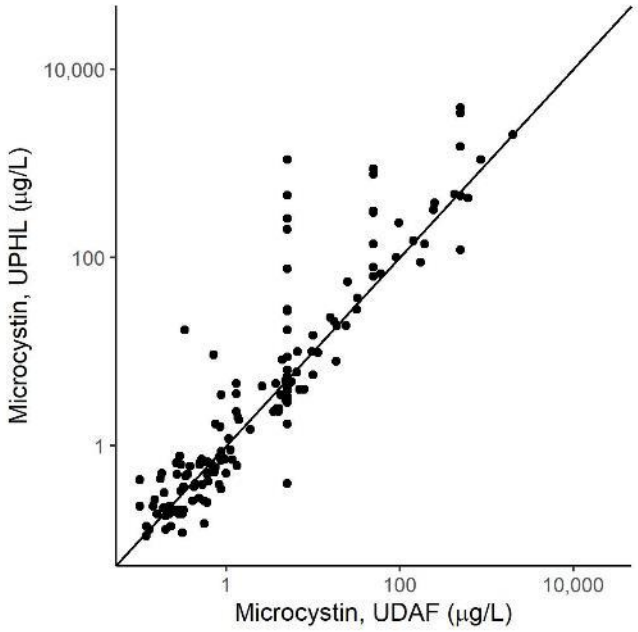


**Figure 2.4.17.** Microcystin concentrations measured by UDAF and UPHL. Solid line = 1:1 relationship.

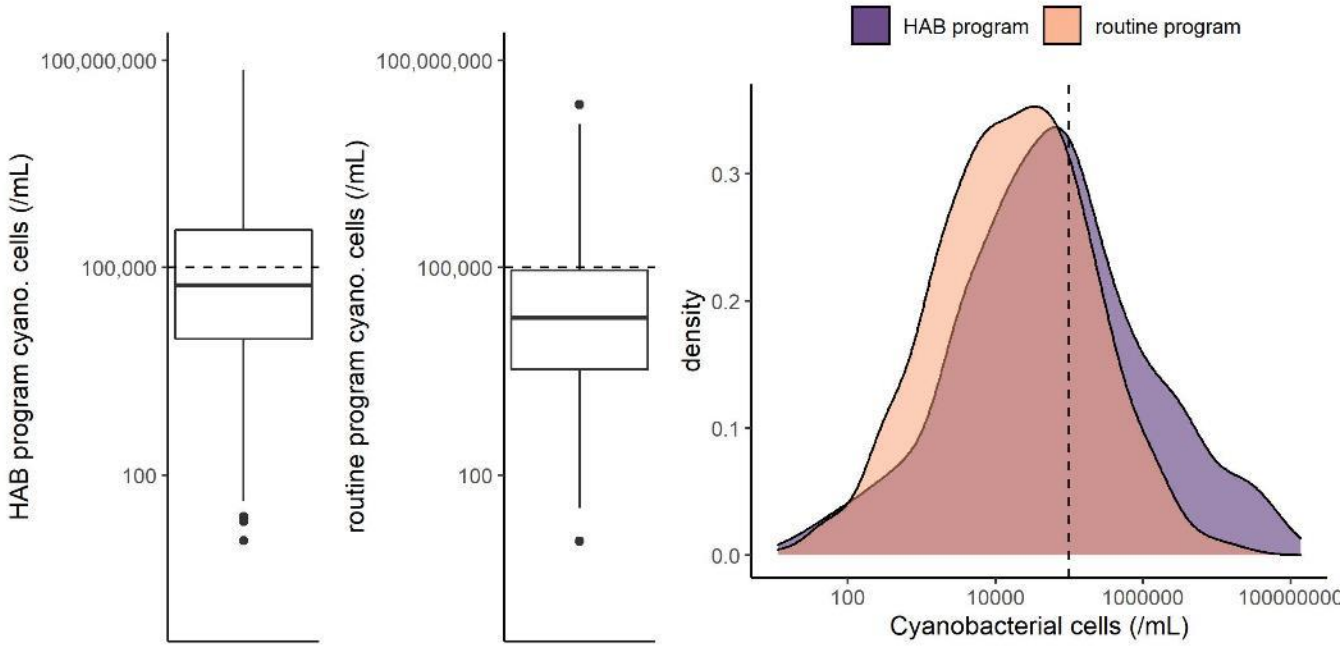


**Figure 2.4.18.** Cyanobacterial cell count comparisons between the HAB monitoring program and the routine monitoring program, as shown by boxplots (left) and density plots (right). A cyanobacterial cell count of 100,000 is shown as a dotted line.

***Results***

Microcystin concentrations were positively correlated with total phytoplankton cell count ($R^2$ = 0.42, df = 211, p < 0.0001), total cyanobacterial cell count ($R^2$ = 0.54, df = 237, p < 0.0001), and toxigenic cyanobacterial concentration ($R^2$ = 0.44, df = 216, p < 0.0001; Figure 2.4.19). Specific toxigenic genera of microcystin-producing

cyanobacteria (*Dolichospermum, Microcystis*, and *Planktothrix*) were also positively correlated with microcystin. Cyanobacterial cell count was used in subsequent analyses since it had the strongest correlation with microcystin. The probability of microcystin concentrations exceeding 8 µg/L increased as total cyanobacterial cell count increased (Figure 2.4.20).

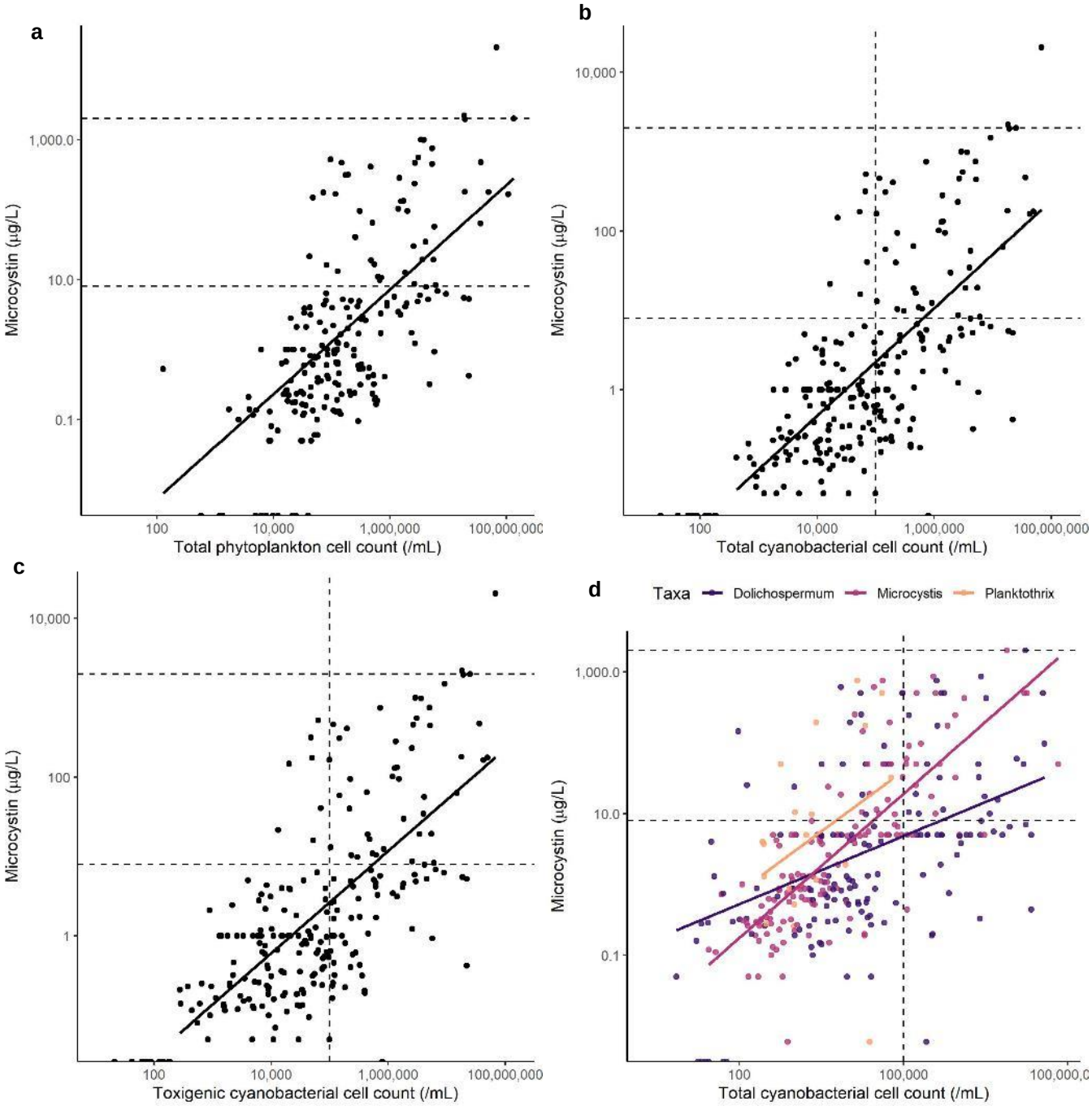


**Figure 2.4.19.** Relationship of (a) total phytoplankton cell count, (b) total cyanobacterial cell count, (c) toxigenic cyanobacterial cell count, and (d) specific toxigenic cyanobacterial cell count with microcystin. Microcystin concentrations of 8 and 2,000 µg/L are shown as a horizontal line, and a cyanobacterial cell count of 100,000 cells/mL is shown as a vertical line (relevant thresholds for Utah Lake advisories).

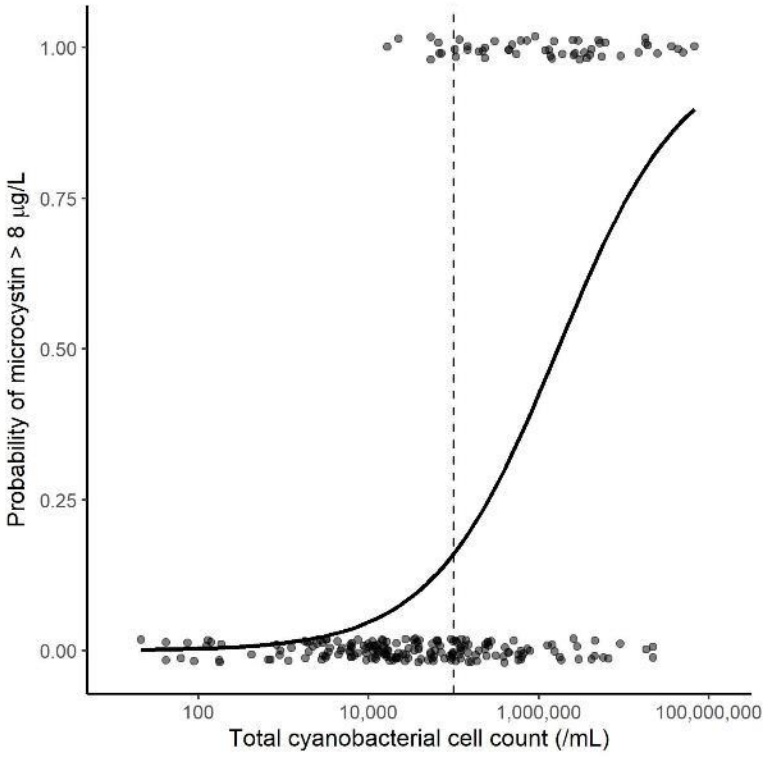


**Figure 2.4.20.** Logistic regression of total cyanobacterial cell count and the probability of microcystin exceeding 8 ug/L. Points represent samples taken as part of the HAB monitoring program, with microcystin noted as either above or below 8 ug/L, coded as 1 or 0, respectively (points jittered for visualization purposes).

There was a significant interaction between sampling depth and cyanobacterial cell count, where the slope and intercept of surface samples was higher and steeper than that of composite samples ($R^2 = 0.34$, df = 157, $p < 0.0001$; Figure 2.4.21). These data show that surface samples are generally associated with higher cell count and microcystin concentrations than composite samples, and the relationship between cell count and microcystin concentration is dependent on whether the sample is taken as a surface or composite sample. In terms of predicting the probability of exceeding a microcystin concentration of 8 µg/L, composite samples are predicted to rarely exceed that threshold whereas the probability increases at higher cell counts for surface samples. Seasonality appears to have a strong effect on the relationship between cell count and microcystin concentration (Figure 2.4.22). In the relationships for both composite and surface samples, samples falling below the regression line tend to occur in the early part of the season (microcystin over-predicted for a given cell count), whereas samples falling above the regression line tend to occur in the late part of the season (microcystin under-predicted for a given cell count).

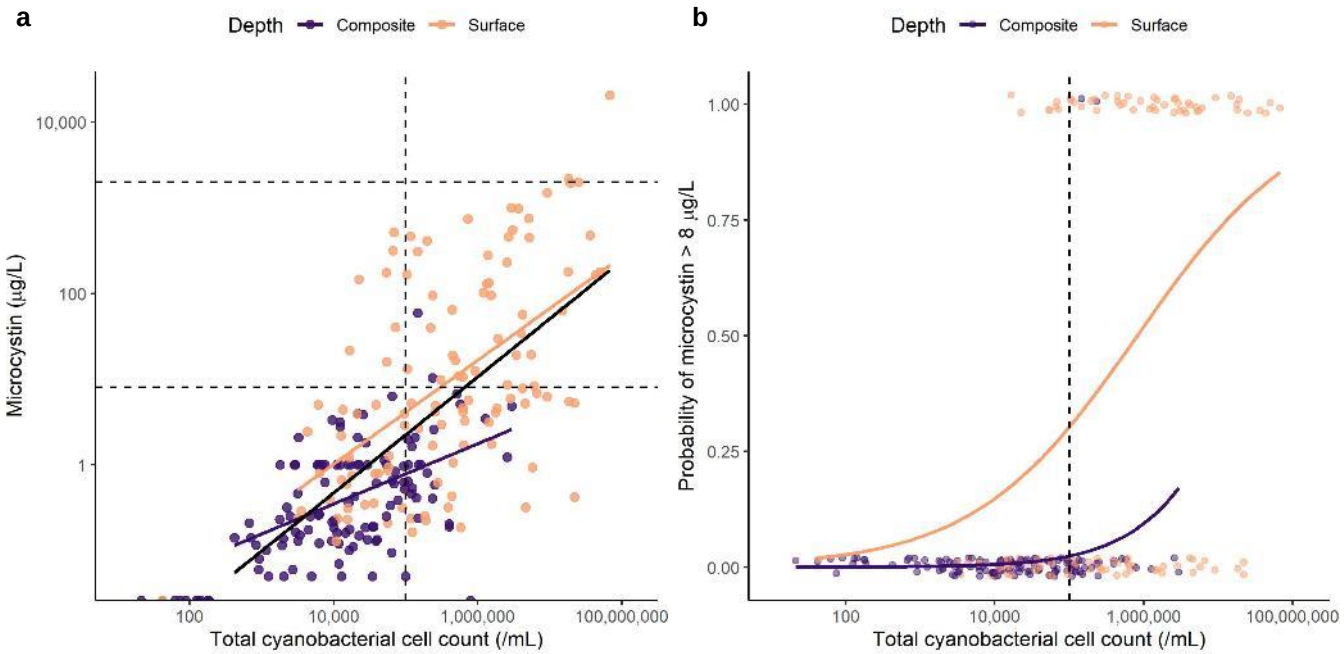


**Figure 2.4.21.** (a) Linear regression and (b) logistic regression of total cyanobacterial cell count and microcystin. In (b), microcystin noted as either above or below 8 ug/L, coded as 1 or 0, respectively (points jittered for visualization purposes). Microcystin concentrations of 8 and 2,000 µg/L are shown as horizontal lines, and a cyanobacterial cell count of 100,000 cells/mL is shown as a vertical line (relevant thresholds for Utah Lake advisories). The black line in (a) represents the overall regression with no depth term, and the colored lines represent the regression with depth as an interaction term.

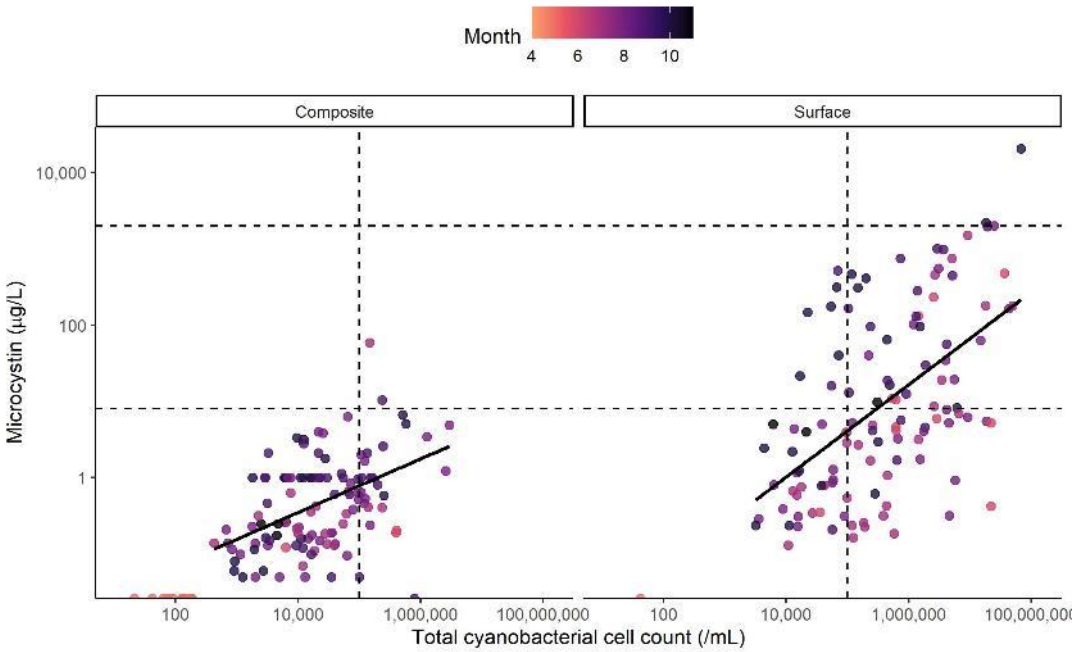


**Figure 2.4.22.** Linear regression of cyanobacterial cell count and microcystin, divided by surface and composite samples and colored by month. Microcystin concentrations of 8 and 2,000 µg/L are shown as horizontal lines, and a cyanobacterial cell count of 100,000 cells/mL is shown as a vertical line (relevant thresholds for Utah Lake advisories).

Samples were also compared by site type (Figure 2.4.23). Beach samples (n = 107) tended to fall on the high end of cyanobacterial cell count and microcystin concentrations, whereas Provo Bay (n = 66) and Goshen Bay (n = 9) tended to have low microcystin concentrations regardless of cyanobacterial cell count. Marina (n = 59) and open water (OW; n = 199) samples tended to be distributed across cell count and microcystin concentrations and on both sides of the line of best fit.

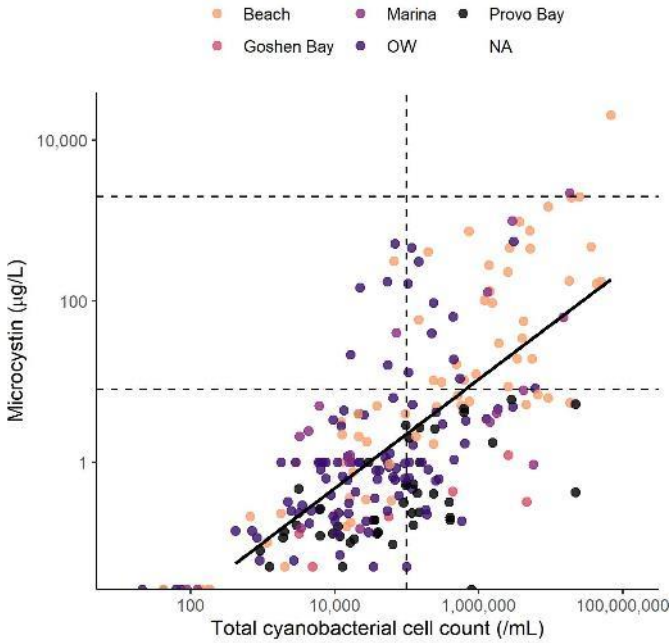


**Figure 2.4.23.** Linear regression of cyanobacterial cell count and microcystin, colored by sample location. Microcystin concentrations of 8 and 2,000 µg/L are shown as horizontal lines, and a cyanobacterial cell count of 100,000 cells/mL is shown as a vertical line (relevant thresholds for Utah Lake advisories).

***Conclusions***

There was a significant positive relationship between cyanobacterial cell counts and microcystin concentration in Utah Lake. Cyanobacterial cell counts explained 54 % of the variance in microcystin concentration. The relationship between cell counts and toxins in Utah Lake was weaker than systems that experience near monocultures of Microcystis (e.g., Lake Taihu, Lake Erie; Wilhelm et al. 2011, Otten et al. 2012) but stronger than systems that have a more diverse phytoplankton assemblage (e.g., Lake Okeechobee, Klamath River; Kramer et al. 2018, Watercourse Engineering 2020). The risk of microcystin concentrations exceeding 8 µg/L is uniformly low below 10,000 cyanobacterial cells/mL, rises to equal likelihood at 1,000,000 cells/mL, and is more likely than not at cell counts exceeding 1,000,000 cells/mL. Concentrations of other toxins were either too low to establish a relationship (anatoxin) or were not sampled (cylindrospermopsin). Meaningful covariates of interest to improve prediction of toxins include sampling depth (surface vs. composite), location of sample, and time of year. Scenario analysis could proceed from these predictive relationships.

## Dynamics in plankton pattern related to climate

**Proposed**

Question: If there are linkages between changes in nutrient regime and HABs, what role if any does precipitation play? (Attachment A ULWQS Science Panel Ideas for Studies, Experiments, and Literature Reviews question).

Objective: Test for a relationship between antecedent precipitation and HAB abundances.

Approach: Using the spatial analyses conducted in previous sub-analyses, test for relationships between antecedent precipitation and HAB abundance. Using Phase I and II data, Cyan data (as allowed by availability), and downloaded climate data, estimate the relationship between temporal differences in precipitation and plankton (including HAB) abundance. This extends the plankton spatial analysis to add antecedent precipitation as a predictor in multivariate models of plankton structure. We will also extend the ANCOVA like models of the previous sub-analysis of dynamics in plankton pattern related to nutrients to add antecedent precipitation as a predictor and test for an effect on nutrient-plankton response relationships. Different temporal ranges of antecedent conditions will be explored (day, week, month).

**Actual**

***Data and Methods***

Weather data were acquired from NOAA's climate data online search (https://www.ncdc.noaa.gov/cdo-web/search) Daily data for precipitation, evaporation, and air temperature were acquired for the Jordan Basin (HUC 160202). If multiple sites had measured data for a given date, the average among sites was calculated. For each date, antecedent precipitation and evaporation were calculated as the rolling sum for the previous 7, 14, and 28 days. Similarly, the rolling mean of air temperature for the previous 7, 14, and 28 days was calculated to capture antecedent temperature conditions. The average air temperature and the sum of precipitation for each water year (October-September) were also calculated, representing annual conditions.

A linear regression was run to assess which period of precipitation, evaporation, and air temperature (7 days, 14 days, 28 days, or annual) most effectively predicted cyanobacteria and total phytoplankton cell count and biovolume. Overall across the phytoplankton metrics, 28-day antecedent precipitation and air temperature yielded the best model fits, whereas evaporation tended to be a non-significant predictor in the univariate models. 28-day antecedent conditions were therefore chosen to incorporate into hierarchical models that predicted phytoplankton metrics from TP, precipitation, evaporation, and air temperature as fixed effects and site as a random effect. The proportion variance explained by fixed effects (marginal $R^2$) was compared to the proportion of variance explained when the random site effect was added (conditional $R^2$).

Additional information may be generated by the paleolimnological study.

***Results***

TP, precipitation, evaporation, and air temperature were all significant predictors of phytoplankton metrics, except in the case of total phytoplankton cell count and biovolume, where air temperature was not a significant predictor. Variance inflation factors for each predictor variable did not exceed 3, indicating there was not a high degree of covariance among variables. All phytoplankton parameters were negatively correlated with antecedent precipitation and evaporation, and cyanobacterial parameters were positively correlated with antecedent air temperature (figure 2.4.23). Note that while evaporation alone was not a significant predictor of phytoplankton metrics, it was a significant predictor in all hierarchical models (table 2.4.3). In context, periods of higher phytoplankton abundance are likely to occur when TP and temperature are high and when precipitation and evaporation are low. The conditional $R^2$ was higher than the marginal $R^2$ for all phytoplankton metrics, indicating that incorporating spatial variability as a random effect explained more variability in the dataset than with fixed effects alone.

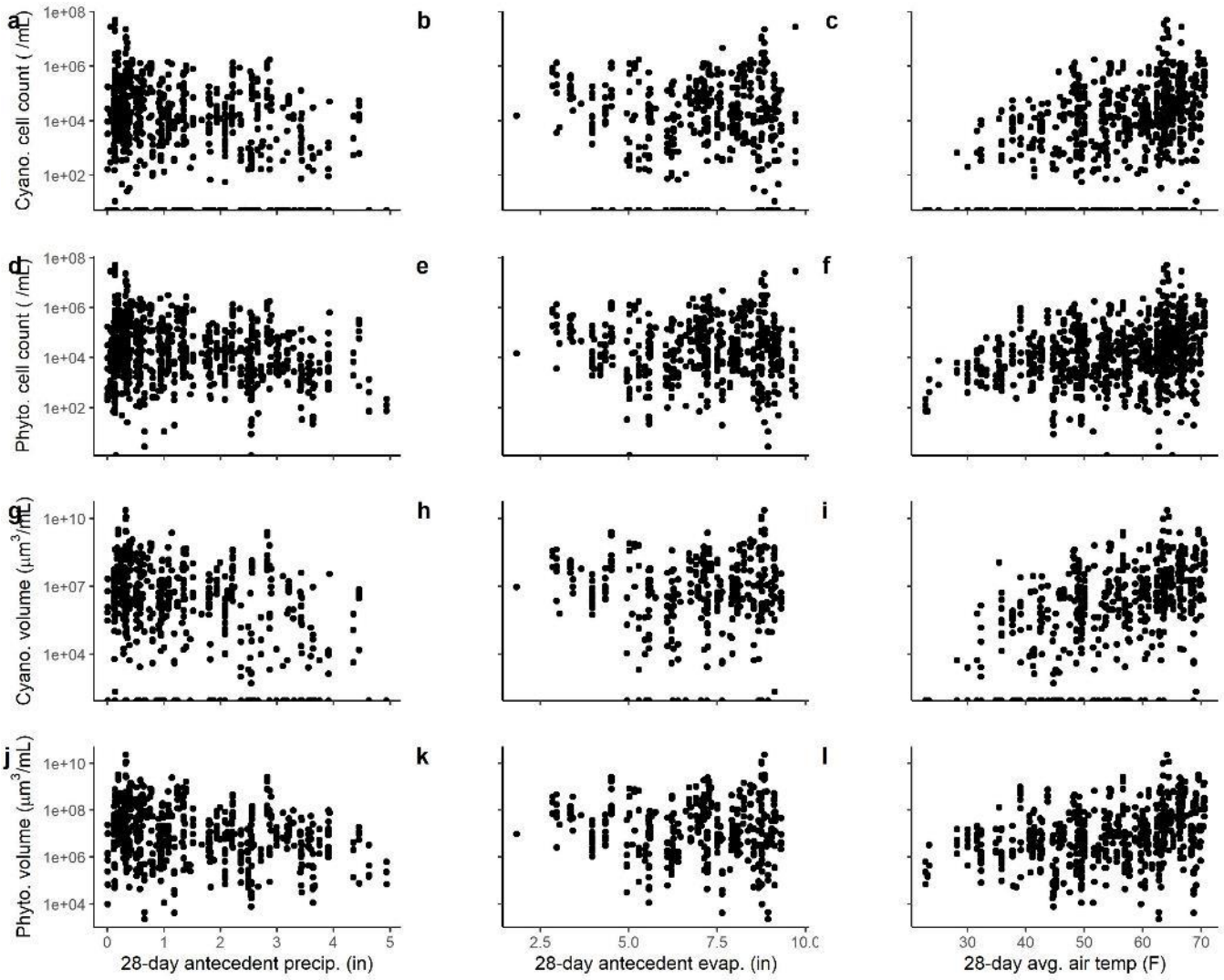


**Figure 2.4.23.** Relationships of (a, b, c) cyanobacterial cell count, (d, e, f) total phytoplankton cell count, (g, h, i) cyanobacterial biovolume, and (j, k, l) total phytoplankton biovolume to 28-day antecedent conditions of cumulative precipitation, cumulative precipitation, and average air temperature. Note the logged y axis for all panels.

**Table 2.4.3.** Coefficients and model fit of hierarchical models to predict phytoplankton metrics (top row). Bold text indicates a statistically significant coefficient at the $p < 0.05$ level. Marginal $R^2$ represents the model fit for fixed effects only, whereas conditional $R^2$ includes fixed effects and site as random effect.

| Variable | log(cyano. cell count) | log(total cell count) | log(cyano. biovol.) | log(total biovol.) |
|---|---|---|---|---|
| Intercept | **4.98** | **6.91** | **7.99** | **10.57** |
| log(TP) | **1.60** | **1.62** | **1.83** | **1.70** |
| 28-day precip. | **-0.42** | **-0.34** | **-0.62** | **-0.41** |
| 28-day evap. | **-0.33** | **-0.22** | **-0.56** | **-0.33** |
| 28-day air temp. | **0.05** | 0.01 | **0.07** | 0.01 |
| 1\|Site | random | random | random | random |
| Marginal $R^2$ | 0.21 | 0.28 | 0.17 | 0.30 |
| Conditional $R^2$ | 0.41 | 0.47 | 0.30 | 0.39 |

## 2.5 ENVIRONMENTAL REQUIREMENTS OF DIATOMS AND MACROPHYTES

**Proposed**

Question: What are the environmental requirements for submerged macrophytes currently present at Utah Lake? Are certain species more resilient to drawdowns and nutrient related impacts? Can some species establish/adapt more quickly? (Charge question 2.2/2.2.i)

Objective: Identify the autecology of Utah Lake diatom and macrophyte species.

Approach: To the extent provided by available diatom and macrophyte autecological databases, summarize the environmental requirements of common diatom species and target macrophyte taxa; for the former, especially nutrient optima and for the latter, especially optima for nutrients, light and inundation.

**Actual**

***Data and Methods***

We determined diatom autoecology from an index derived from the River Invertebrate Prediction and Classification Model as described in Tyree et al. (2020). Diatom taxa present in the phytoplankton dataset for Utah Lake were matched with taxa in the index, and the index characteristics were collected for each taxon. The 29 taxa in the Utah Lake database were reduced to 10 indexed taxa due to naming redundancy (n = 13), lack of genus-level information (n = 5), and absence in the index (n = 1). We gathered paleolimnological diatom abundance from Bolland 1974, which divided sediment core data into 7 zones, zone 1 being the most recent (1965) and zones 4-7 occurring during pre-industrial times. Sediment dating before 1880 was not available. Diatom taxa lists were indexed, as above, and the metric that was available for the most taxa (biological condition) was incorporated into final analyses.

Submerged macrophyte taxa documented as being present in Utah Lake (Brotherson 1981, Miller and Crowl 2006, Landom et al. 2019) were queried in the freshwaterecology.info database (WISER consortium). The database included Lake Macrophyte Intercalibration Metric (LMICM) and Ellenberg scores for specific macrophyte taxa. LMICM scores range from 0-10, 0 representing oligotrophic conditions and 10 for highly eutrophic conditions. Ellenberg scores, an earlier version of LMICM scores, range from 1-8, 1 representing low nutrient environments and 8 representing nutrient-rich environments.

***Results***

The greatest number of contemporary diatom taxa were categorized as eutraphentic taxa (trophic = 5, associated with nutrient-rich environments; figure 2.5.1a). Oxygen tolerance ranged from O1 (oxygen saturation nearly 100%) to O3 (oxygen saturation > 50% saturation; Figure 2.5.1b). Taxa were most often associated with a biological condition rating of 4 (tolerant of moderate human impact), but ratings ranged from 2 (moderately sensitive) to 5 (highly tolerant; Figure 2.5.1c). Eight of 10 diatom taxa were sestonic (Figure 2.5.1d) and ranged in size, with small being the most common size (Figure 2.5.1e). Of the 10 diatom taxa present in the index, each individual taxon did not always appear for every metric.

For paleolimnological data, diatoms from ubiquitous taxa groups (biological condition = 3) and highly tolerant taxa groups (biological condition = 5) were present across all zones, with some variability in counts and additional biological condition groups (Figure 2.5.2). It should be noted that Figure 2.5.2 displays only counts of taxa that were present, not their relative or absolute abundance. Bolland (1974) notes that diatoms are dominated by taxa from alkaline, warm, and eutrophic lakes for more modern samples, whereas diatoms from older samples were dominated by taxa from alkaline, cool, and oligotrophic-mesotrophic lakes.

Nutrient metrics for submerged macrophytes ranged from 2.96-8.02 (LMICM) and 4-8 (Ellenberg; Table 2.5.1). Taxa from the most recent reports (Miller and Crowl 2006, Landom et al. 2019) have exclusively high scores, representing eutrophic conditions.

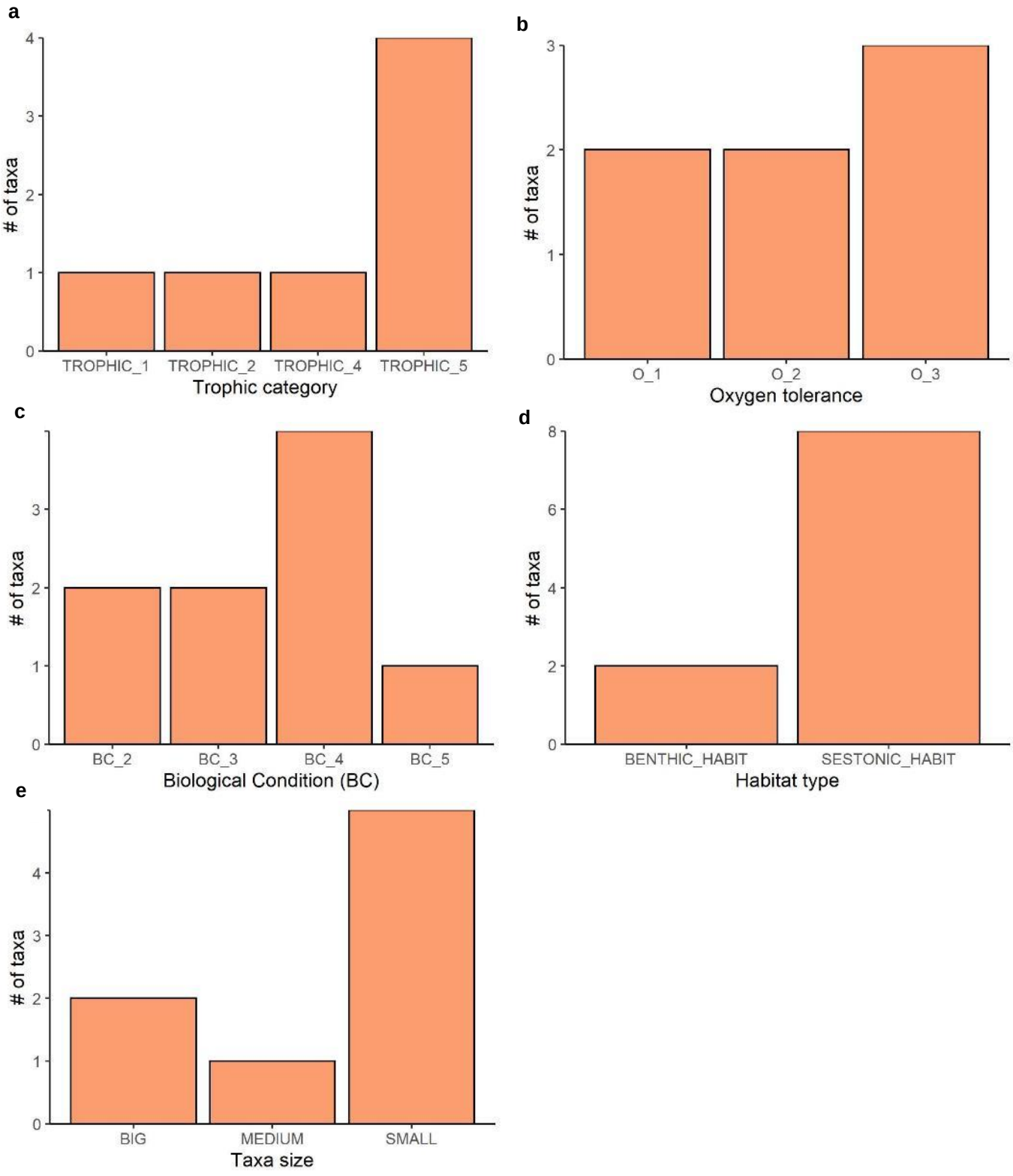


**Figure 2.5.1.** Index metrics for diatom taxa present in the Utah Lake phytoplankton dataset (contemporary taxa). Metrics were not available for every taxa; total counts for each metric vary.

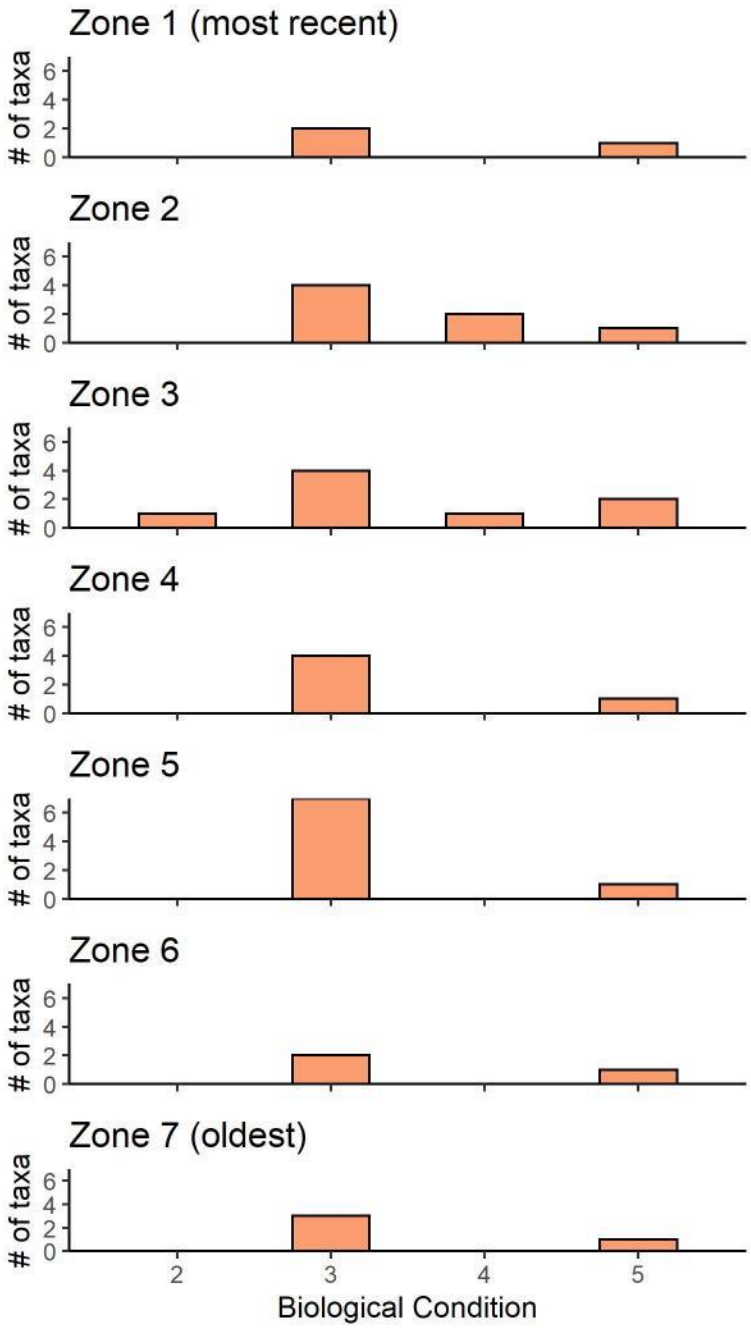


**Figure 2.5.2.** Biological condition metrics for paleolimnological diatom taxa documented in Bolland (1974).

**Table 2.5.1.** Nutrient metric scores for submerged macrophyte taxa found in Utah Lake. Dashes represent scores that were not available from the database (WISER Consortium). LMICM = Lake Macrophyte Intercalibration Metric.

| Taxa | LMICM | Ellenberg | Citation (for Utah Lake) |
|---|---|---|---|
| *Ceratophyllum demersum* | 7.82 | 8 | Brotherson 1981<br>Landom et al. 2019 |
| *Elodea canadensis* | 7.42 | 7 | Brotherson 1981 |
| *Myriophyllum spicatum* | 7.30 | 7 | Brotherson 1981 |
| *Potamogeton crispus* | 8.02 | 5 | Brotherson 1981 |
| *Potamogeton filiformis* | 2.96 | 5 | Brotherson 1981 |
| *Potamogeton foliosus* | - | - | Brotherson 1981 |
| *Potamogeton latifolius* | - | - | Brotherson 1981 |
| *Potamogeton nodosus* | - | - | Brotherson 1981 |
| *Potamogeton pectinatus* | 8.64 | 8 | Brotherson 1981<br>Miller and Crowl 2006 |
| *Potamogeton praelongus* | 4.08 | 4 | Brotherson 1981 |
| *Stuckenia pectinata* | - | - | Landom et al. 2019 |

## 2.6 WIND AND TURBIDITY

**Proposed**

Question: What is the relationship between carp, wind, and macrophytes on non-algal turbidity and nutrient cycling in the lake? What impact could macrophyte reestablishment have? (Charge question 2.2.ii)

Objective: Identify wind condition necessary to entrain bottom sediments in Utah Lake.

Approach: Using physical limnological/hydrodynamic theory, calculate forces necessary to mix and entrain bottom sediments. Using mixing potential indices, like Wedderburn numbers, and calculations for bottom shear stress like the Darcy-Weisbach expression, calculate wind speeds necessary to entrain bottom sediments in Utah Lake. Using existing climate data on wind speeds and directions, calculate how frequently such wind speeds occur, where, and any pattern in their seasonality. Using existing turbidity data from synoptic and continuous samplers, develop empirical regression models relating wind speed or mixing force (e.g., Wedderburn number) to observed turbidities.

**Actual**

***Data and Methods***

Wind speeds and directions were gathered from the Provo Airport and from the Lindon and Spanish Fork meteorological stations. The additional two stations are located north and southeast of the Provo Airport, respectively. The Provo Airport data were used for wind and shear stress calculations due to this station's proximity to the lake, but the comparisons among weather sampling stations may be useful to characterize the variability of wind conditions in the region. Wind speeds and directions were converted from hourly to average daily. Fetch at buoy locations was calculated for each day wind data was available from the Provo Airport. Daily wind direction was matched to the buoy location, and a daily fetch was calculated based on the dimensions of the lake. Note: fetch calculations include distances that cross land. We can back-calculate shorter fetch distances for these data points if more precision is desired.

Historical data for lake depths and buoy data for turbidity and temperature were incorporated into analyses (figure 2.6.1). Depth measurements were not available for all buoy sites. The nearest sites at which depth was measured were selected as follows (from northernmost to southernmost site):

- North buoy site (4917365): located between sites 4917310 and 4917530; a mean of all samples at both locations was computed.
- State Park buoy site (4917390): concurrent depth location
- Provo Bay buoy site (4917446): depth at site 4917770
- South buoy site (4917715): depth at site 4917700

Depth was averaged across all monitored dates to obtain a mean depth measurement. An ongoing question is whether a mean depth across all sampled dates is representative.

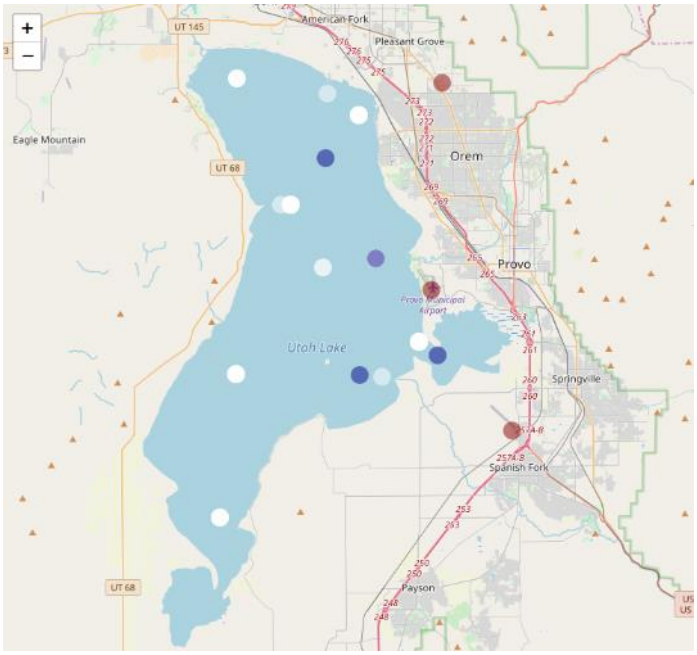


**Figure 2.6.1.** Monitored sites in Utah Lake. Red symbols are wind monitoring stations, blue symbols are buoy sites, and white symbols are depth sites. Note there is one site where a buoy and depth site coincide, producing a lighter blue dot.

Theoretical analysis was conducted to calculate the shear necessary to entrain particle from the lake bottom. The equation for wave-induced shear in shallow lakes was calculated as:

$$\tau_{WAVE} = 0.5 \times \rho \times f_W \times U_w^2$$

where $\tau$ is shear stress, $\rho$ is water density, $f_w$ is bottom friction factor, and $U_w$ is amplitude of the orbital wave velocity (Chao et al. 2008; equations 20-26). The theoretical impact of depth, fetch, and wind speed on shear stress was explored. The average wind speed at Provo Airport (2.63 m/s) and the dominant wind direction (SE/SSE) were entered into the theoretical equations. Based on the dominant wind direction, the maximum fetch was 24 km. Fetch values of 9.6 and 16 km were also considered, representing the probable fetch from the northwest side of Utah Lake at Saratoga Springs. Observations from specific dates and buoy sites were also used to generate empirical calculations of wave shear. The observational data included water temperature (which dictates $\rho$ and viscosity), fetch, depth, and wind speed. Relationships among wave shear and wind speed were analyzed, and critical shear (the shear value needed to entrain sediments) was calculated. Additionally, the shear created by wind-driven waves vs. water currents was compared.

***Results***

There was a positive relationship between wind speed at Lindon and Spanish Fork (R = 0.26), but there was a high degree of variability in this relationship (Figure 2.6.2a). If wind directions were consistent across stations, we would expect all points to fall near the 1:1 line. Points seemed to cluster near the 1:1 line, but there was considerable variability in wind direction from station to station (Figure 2.6.2b). There did not seem to be a strong seasonal effect on the relationships of wind speed or direction between stations.

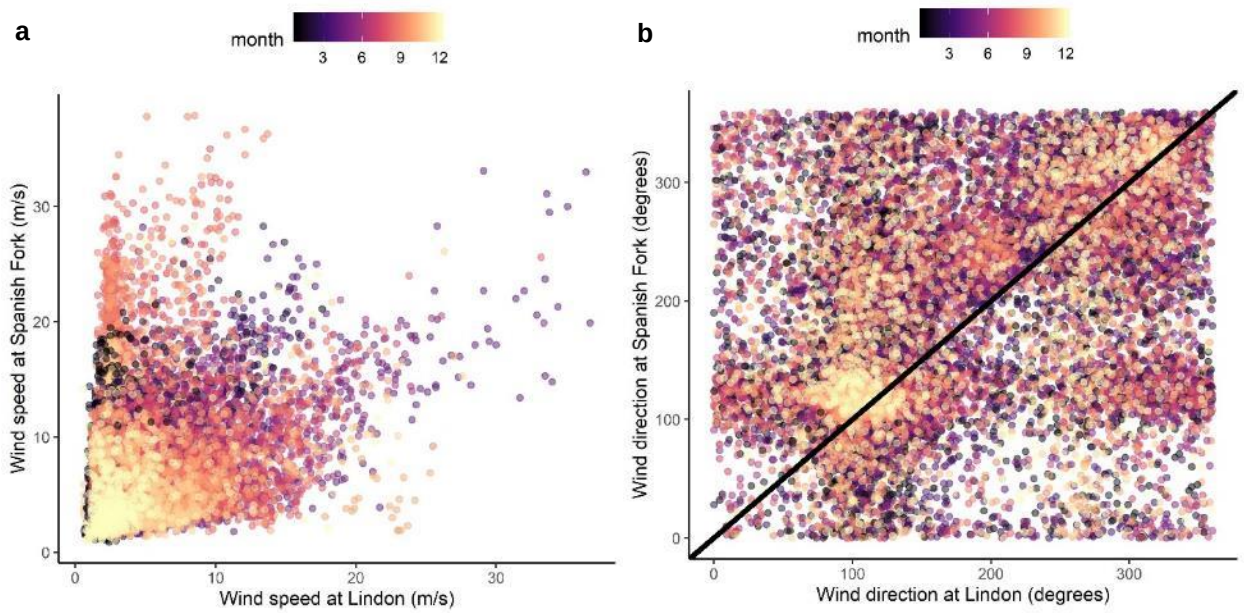


**Figure 2.6.2.** (a) wind speed and (b) wind direction at Lindon and Spanish Fork stations.

High turbidity was common across buoy sites, with no noticeable seasonal patterns (Figure 2.6.3). For the most part, high turbidity at a given site coincided with high turbidity at other sites. Turbidity and wind speed were positively correlated. When departures from the turbidity-wind speed relationship occurred, they appeared to be associated with temperature, with high turbidity at relatively low wind speed occurring at low temperature and low turbidity at relatively high wind speed occurring at high temperature (Figure 2.6.4). A multiple linear regression with an interaction between wind speed, temperature, and site indicated these variables explained 46% of variance in turbidity across sites (Figure 2.6.4; df = 1322, $R^2 = 0.46$, $p < 0.0001$).

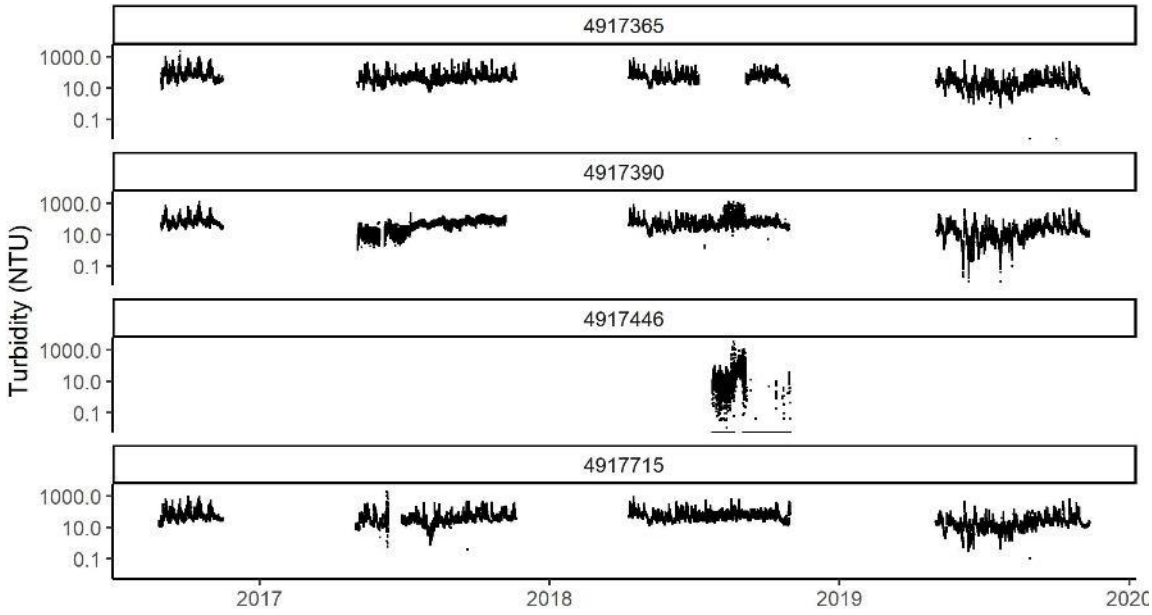


**Figure 2.6.3.** Time series of turbidity at buoy sites. Site codes are as follows: North = 4917365, State Park = 4917390, Provo Bay = 4917446, South = 4917715. NTU = nephelometric turbidity units. Note logged y axis.

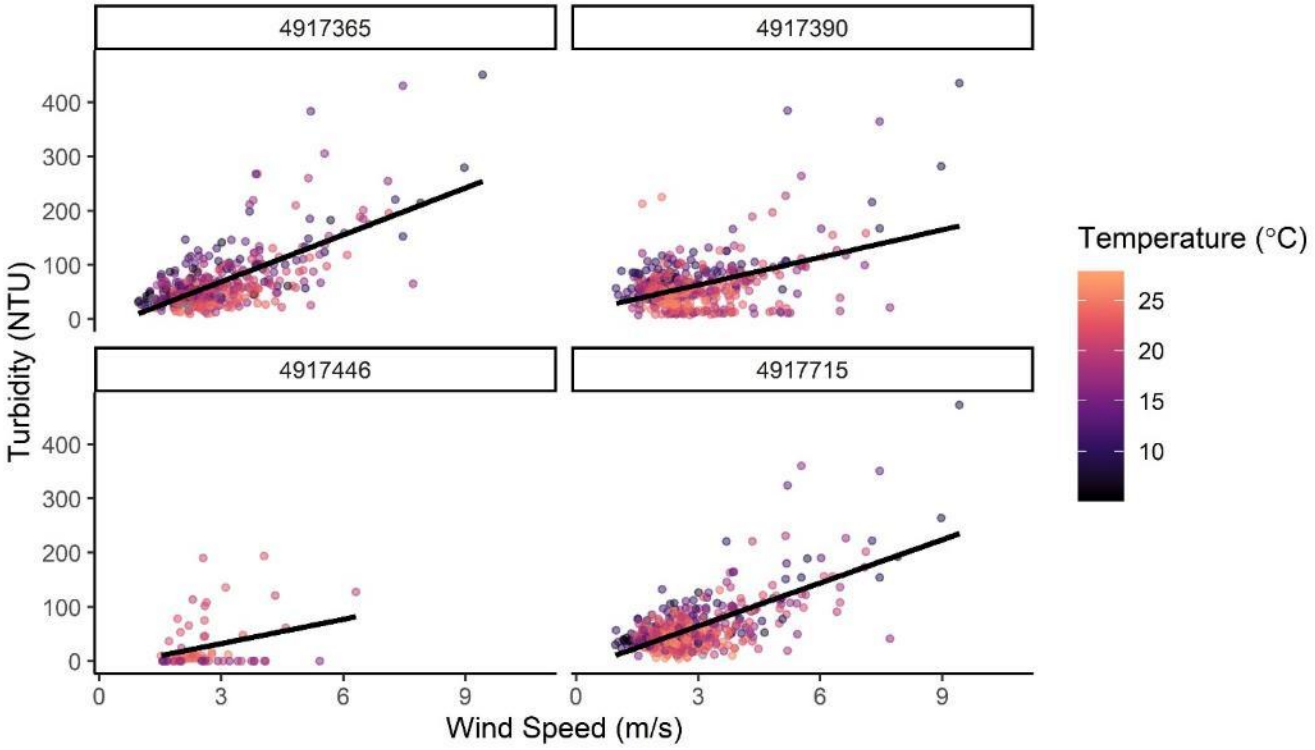


**Figure 2.6.4.** Relationships between wind speed and turbidity at buoy sites. Site codes are as follows: North = 4917365, State Park = 4917390, Provo Bay = 4917446, South = 4917715. NTU = nephelometric turbidity units.

From theoretical calculations, it is evident that water depth and wind speed have a large effect on shear, whereas fetch has a relatively small effect on shear (Table 2.6.1). While the measured fetch at each buoy site, based on the average daily wind direction, varied substantially (Figure 2.6.5), it is likely based on the theoretical calculations and the relationship of wind speed and turbidity that variation in fetch is not a major driver of turbidity in Utah Lake.

**Table 2.6.1.** Theoretical calculations of shear stress ($\tau_w$) as a function of depth, wind speed, and fetch. Lakewide averages are represented in the first row, and theoretical variations are highlighted in bold italic.

| depth (m) | Wind speed (m/s) | Fetch (km) | $\tau_w$ (N/m$^2$) |
|---|---|---|---|
| 3 | 2.63 | 24 | 0.027 |
| ***1.5*** | 2.63 | 24 | 0.106 |
| ***6*** | 2.63 | 24 | 0.002 |
| 3 | ***0.986*** | 24 | < 0.001 |
| 3 | ***4.67*** | 24 | 0.188 |
| 3 | 2.63 | ***12*** | 0.023 |
| 3 | 2.63 | ***6*** | 0.018 |

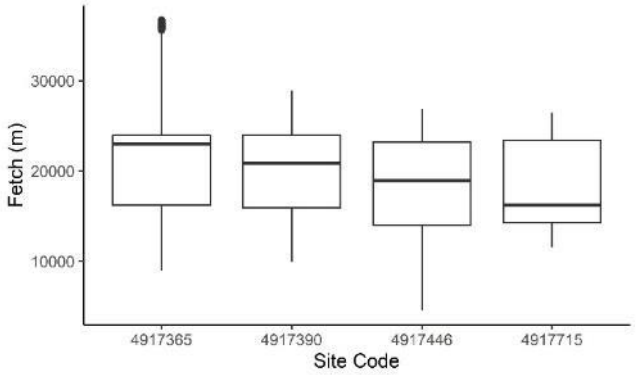


**Figure 2.6.5.** Distribution of fetch at buoy sites. Site codes are as follows: North = 4917365, State Park = 4917390, Provo Bay = 4917446, South = 4917715.

Wave shear exhibited a positive correlation with turbidity, but the model fit was worse than it was for the wind speed and temperature model for turbidity (Figure 2.6.6). Wave shear explained 5-42 % of variance in turbidity across sites, but it is clear there are sources of unexplained variance. A potential explanation for the poor model fit is the presence of an inflection point. At high wave shear, sediments are entrained into the water column, resulting in a positive correlation between wave shear and turbidity. At low wave shear, however, the shear is not high enough to entrain sediments but there may be residual sediment in the water column that has not settled to the bottom, resulting in a flat relationship between wave shear and turbidity. The inflection point of this relationship is referred to as critical shear (Wang et al. 2010). Inflection points were found for each of the four buoy sites, where slope is assumed to be zero at lower values of $\tau_{wave}$ (turbidity unrelated to wave shear) and slope is positive at lower values of $\tau_{wave}$ (turbidity is a function of wave shear). Critical shear values were detected as 0.160, 0.169, not detected, and 0.162 N/m$^2$ for the North, State Park, Provo Bay, and South buoy sites, respectively. Given how close these inflection points are to one another, it might be reasonable to assume that critical shear values across the lake are consistent.

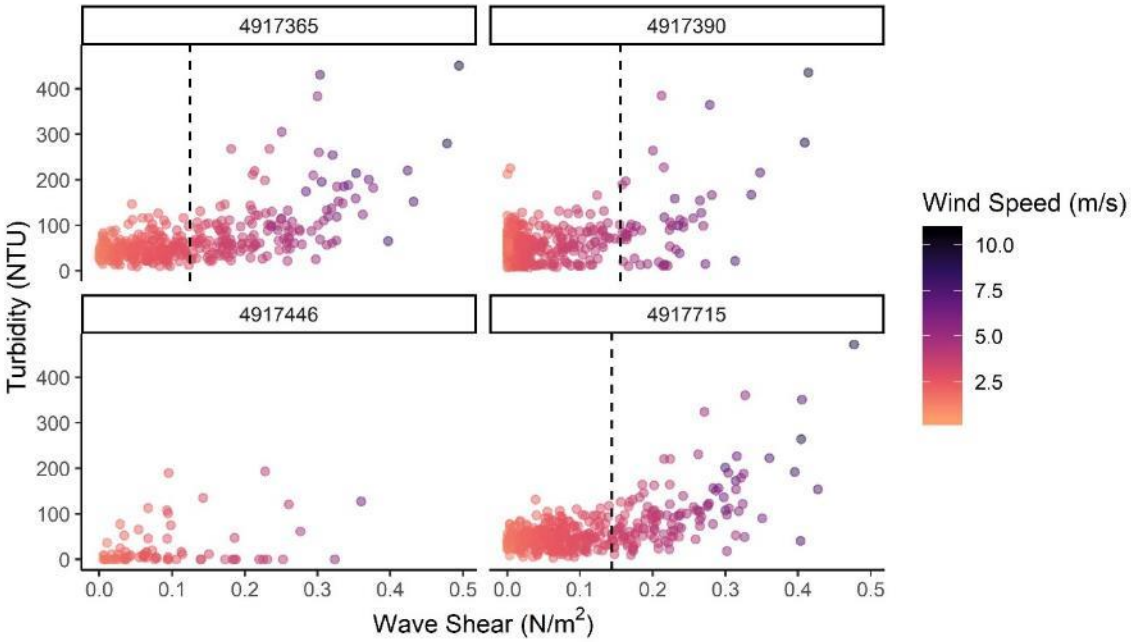


**Figure 2.6.6.** Wave shear and turbidity relationships in Utah Lake as they relate to wind speed. Site codes are as follows: North = 4917365, State Park = 4917390, Provo Bay = 4917446, South = 4917715. The dashed vertical line on each panel represents the statistically determined inflection point of the regression, representing the critical shear value.

The computed critical shear values from the inflection point analysis were compared with theoretical critical shear based on particle size:

$$\tau_{crit} = 0.06 \times g \times (\rho_s - \rho) \times D$$

where g is gravitational acceleration, $\rho_s$ is sediment density, and D is median particle size. In Utah Lake, the median particle size is < 0.005 mm, similar to clay (0.002 mm), with an average bulk density of 600 kg/m$^3$ (Goel, Pers. Comm.). These values yield a critical shear of -0.47 N/m$^2$, a functional impossibility. If 2,000 kg/m$^3$ is used as the bulk density, the critical shear value rises to 1.17 N/m$^2$. Chao et al. (2008) report a range of critical shear from 0.009 to 0.25 N/m$^2$ for cohesive lake sediments. The critical shear values calculated from inflection point analysis fall within this reported range, suggesting that the inflection point approach may be a more reliable estimate of critical shear in the absence of detailed sediment data to calculate theoretical critical shear. Critical shear values fall above the median observed wave shear at the North and South sites and fall above the 3rd quartile of observed wave shear at the State Park site (Figure 2.6.7). More than 75 % of observed wave shear in Utah Lake fall within the published range of critical shear values.

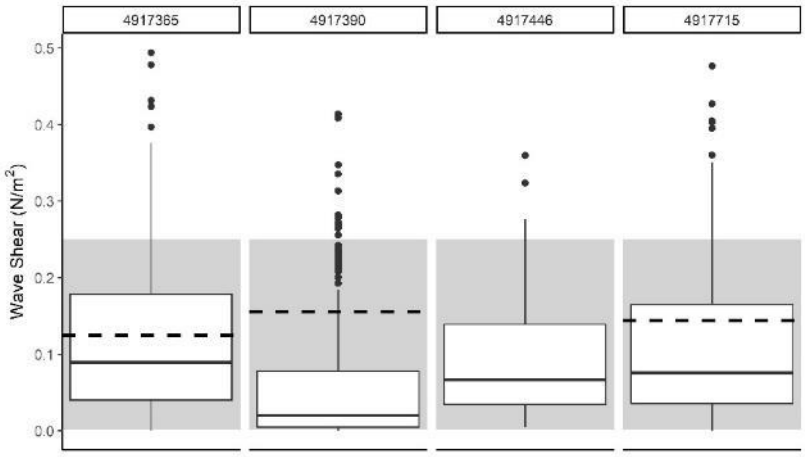


**Figure 2.6.7.** Observed wave shear in Utah Lake (boxplots) as compared to calculated critical shear values (dotted lines) and literature critical shear values from other systems (Chao et al. 2008). Site codes are as follows: North = 4917365, State Park = 4917390, Provo Bay = 4917446, South = 4917715.

Together, these data suggest that wind conditions in the lake are sometimes, but not usually, sufficient to entrain sediments into the water column (typically wind speeds above 3-4.5 m/s depending on site; Figure 2.6.8). Critical shear was exceeded for 24% of samples at the North site, 7 % of samples at the State Park site, and 15% of samples at the South site. On days when wave shear does not exceed critical shear, turbidity is typically lower but may still exceed 100 NTU (Figure 2.6.6). Given the small particle size of sediments, the observation of high turbidity on days when wave shear is low may be a function of slow particle sinking rates, the effects of carp bioturbation, and phytoplankton. These findings suggest that while average conditions in the lake are not sufficient to retrain sediments into the water column, high wind events drive sediment resuspension events that are maintained after windy conditions subside.

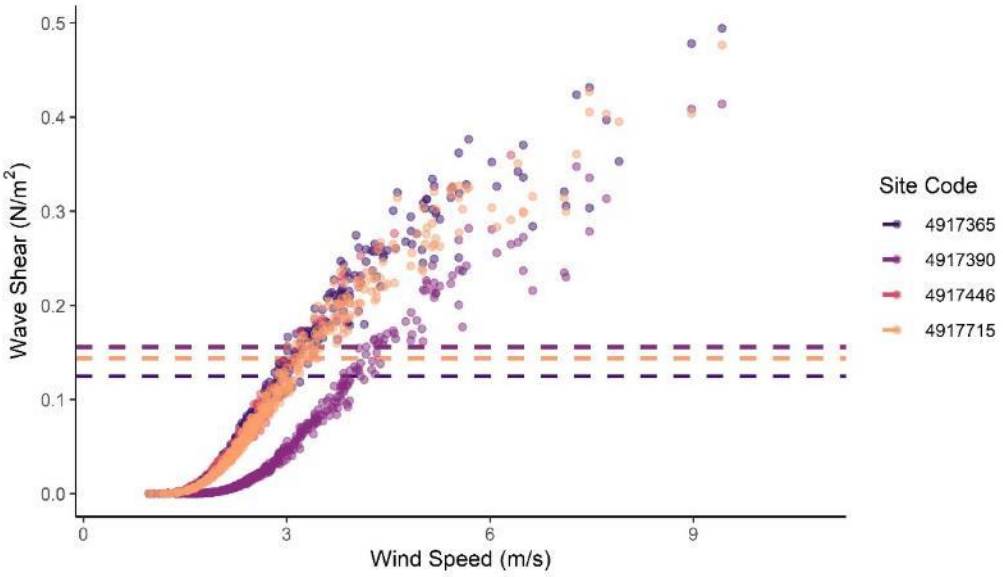


**Figure 2.6.8**. Relationship between wind speed and observed wave shear. Dotted lines represent the calculated critical shear value for each site. Site codes are as follows: North = 4917365, State Park = 4917390, Provo Bay = 4917446, South = 4917715.

The shallow lake literature largely ignores current shear because they are usually dealing with very small, shallow lakes. According to recent analysis by Nick Von Stackelberg, this assumption is likely invalid for Utah Lake. The lake has a seiche and there is evidence of wind induced currents. Preliminary EFDC current data at buoy sites suggests that current shear rarely exceeds the critical shear for sediment resuspension (Figure 2.6.9). While wind shear is evidently a stronger source of shear stress in Utah Lake than current shear, it is worth noting that wind and current forces are additive. Ignoring current shear, therefore, may result in an underestimation of anticipated sediment resuspension in Utah Lake.

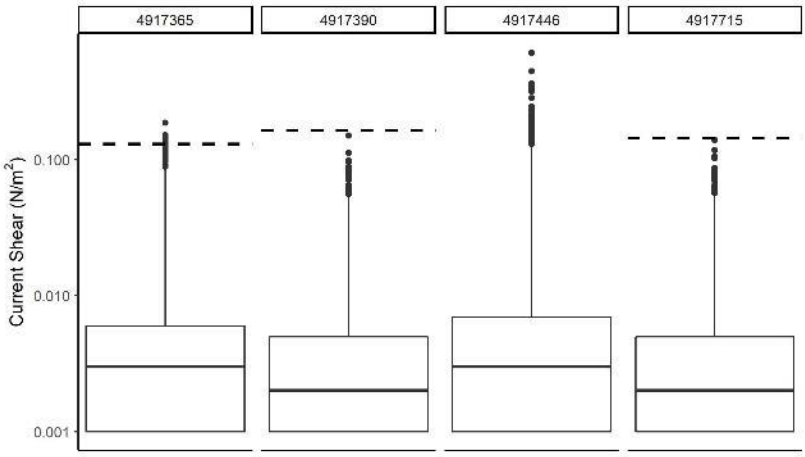


**Figure 2.6.9.** Modeled current shear in Utah Lake (boxplots) as compared to calculated critical shear values (dotted lines). Site codes are as follows: North = 4917365, State Park = 4917390, Provo Bay = 4917446, South = 4917715.

### Ongoing Questions

Using wave shear and turbidity relationships, we were able to avoid the need for detailed sediment data (particle diameter, density, cohesiveness, sinking rates). Do we want to pursue any empirical sediment data?

## 2.7 TURBIDITY AND MACROPHYTES

**Proposed**

Question: What is the relationship between carp, wind, and macrophytes on non-algal turbidity and nutrient cycling in the lake? What impact could macrophyte reestablishment have? (Charge question 2.2.ii)

Objective: Identify the potential contribution of macrophytes to reducing turbidity.

Approach: Again, using the data from the previous sub-analyses and using physical limnological/hydrodynamic theory, calculate the effect of bottom roughness represented by macrophyte densities (using observed or literature data) and its effect on reducing bottom velocities using Manning's roughness or equivalent, and calculate the change in the effective windspeed then needed to entrain bottom sediments in the presence of macrophytes.

**Actual**

***Data and Methods***

Previous studies document decreased bed shear stress when macrophytes are present, leading to less sediment resuspension because bed shear decreases to below critical shear. Actual predictions for how much macrophytes could reduce turbidity depend on macrophyte percent bottom cover, canopy cover, biomass density, sediment characteristics. This topic is well-studied in the coastal marine literature but less so in lakes and streams. In two freshwater studies, James et al. (2004) demonstrated a 46 and 63% reduction in bed shear for two different species of macrophytes at low biomass (<20 $g/m^2$), and Wang et al. (2010) demonstrated a 20-80% reduction in bed shear when macrophytes were present.

A critical shear value of 0.16 $N/m^2$ was assumed for Utah Lake, a conservative value from the observed range of 0.1604-0.1690 across sites. This critical shear threshold was applied to the range of wave shear values observed across the lake, and scenarios of reduced wave shear were applied to each measurement.

***Results***

Assuming that sampled dates and locations are representative of the lake, resuspension events would be nearly eliminated if macrophyte cover reduced bed shear by 60% or more (Table 2.7.1). It appears that macrophytes would reduce sediment resuspension events, but the question remains how slow particle sinking rates will impact macrophyte establishment. Madsen et al. (2001) indicated that alternating suspension-deposition cycles can be beneficial to macrophyte growth, as resuspension events can avoid burial and provide nutrient subsidies to macrophytes. However, high levels of turbidity can shade macrophytes beyond photosynthetically active radiation (PAR) levels needed for photosynthesis, which is addressed in the next section of the report.

**Table 2.7.1.** Percent of observed wave shear measurements in Utah Lake that exceed critical shear under scenarios of reduced wave shear.

| Macrophyte reduction in wave shear (%) | Samples exceeding critical shear (%) |
|---|---|
| 0 (current) | 22 |
| 20 | 15 |
| 40 | 6 |
| 60 | 1 |
| 80 | 0 |

### *Ongoing Questions*

These calculations extrapolate from wide ranges in the literature. Any data available on anticipated macrophyte percent ground cover, canopy cover, biomass density, and (actual) sediment characteristics would help to constrain these estimates. Does more information exist on the goals for macrophyte reestablishment?

## 2.8 LIGHT EXTINCTION

**Proposed**

Question: What is the relationship between light extinction and other factors (e.g., algae, TSS, turbidity)? (Charge question 2.3.vi)

Objective: Identify the potential contribution of turbidity/TSS and algal biomass to turbidity.

Approach: Using empirical models of light attenuation ($k_d$) for lakes as well as empirical data from Utah Lake, we will attempt to identify the contributions of non-algal turbidity and chlorophyll to light attenuation. Decomposing attenuation into these effects will require calculating $k_d$ from Secchi depth, from which there are established equations which will be validated using existing measured light attenuation and Secchi depth data for Utah Lake. Then, correlation and regression models of TSS, turbidity, and chlorophyll and $k_d$ will be constructed and compared to published models.

**Actual**

### *Data and Methods*

Light profiles, Secchi depth, turbidity, and concentrations of chlorophyll, total suspended solids (TSS), volatile suspended solids (VSS), and dissolved organic carbon (DOC) were analyzed from the monitoring dataset. Light profiles were compared to literature values for macrophyte colonization depth and light compensation depth to predict sites where macrophyte establishment may be successful. A logistic regression was performed to predict the likelihood of crossing the light compensation point at various depths. The PAR light attenuation coefficient (k) was calculated from light profiles according to the exponential decay of PAR with depth. Note: k is made up of several components, including light attenuation from water, dissolved constituents ($k_d$), inorganic particles, and phytoplankton ($k_c$). The relationship between k and Secchi depth was modeled on a log-log basis (Idso and Gilbert 1974). k values for occurrences when Secchi depth but not light profiles were measured were then calculated based on this relationship.

The contributions of non-algal turbidity to light attenuation were analyzed by several means. First, trophic state index (TSI) was calculated based on chlorophyll and secchi depth (Carlson 1977). The observed and expected secchi depth from equation 5 in Carlson (1977) were computed. Next, we compute attenuation due to nonalgal turbidity and compare it to total attenuation. From equation 2 in Smith (1990), a linear regression of secchi depth and chlorophyll was performed and the relationship from the regression used to compute the contribution of non-algal turbidity to light attenuation. Non-algal light attenuation was then compared to total light attenuation (k) to determine the proportion of light attenuation attributed to non-algal turbidity. The comparison of k with non-algal light attenuation was made using both measured k values and Secchi depth-derived k values (“estimated k”), which had sample sizes of 44 and 2,555, respectively.

Model selection was performed to determine which components of light attenuation (TSS, chlorophyll, DOC) and spatial factors (latitude, longitude) predict k and Secchi depth in Utah Lake. The most parsimonius fit of predictor variables and the relative importance of each variable included in the model were determined by stepwise AIC.

Measured values of k were incorporated into the model rather than estimated k values, as there was a considerable amount of error around k values estimated from Secchi depth.

Comparisons of VSS and TSS were made as an additional line of evidence for organic vs. inorganic components of water clarity reductions. The ratio of VSS to TSS was analyzed to determine the proportion of suspended solids that were organic in nature (i.e., volatile).

***Results***

Across sites in Utah Lake, PAR attenuated rapidly with depth. Light attenuation was strongest in the late summer and fall and weakest in the spring and early summer (Figure 2.8.1).

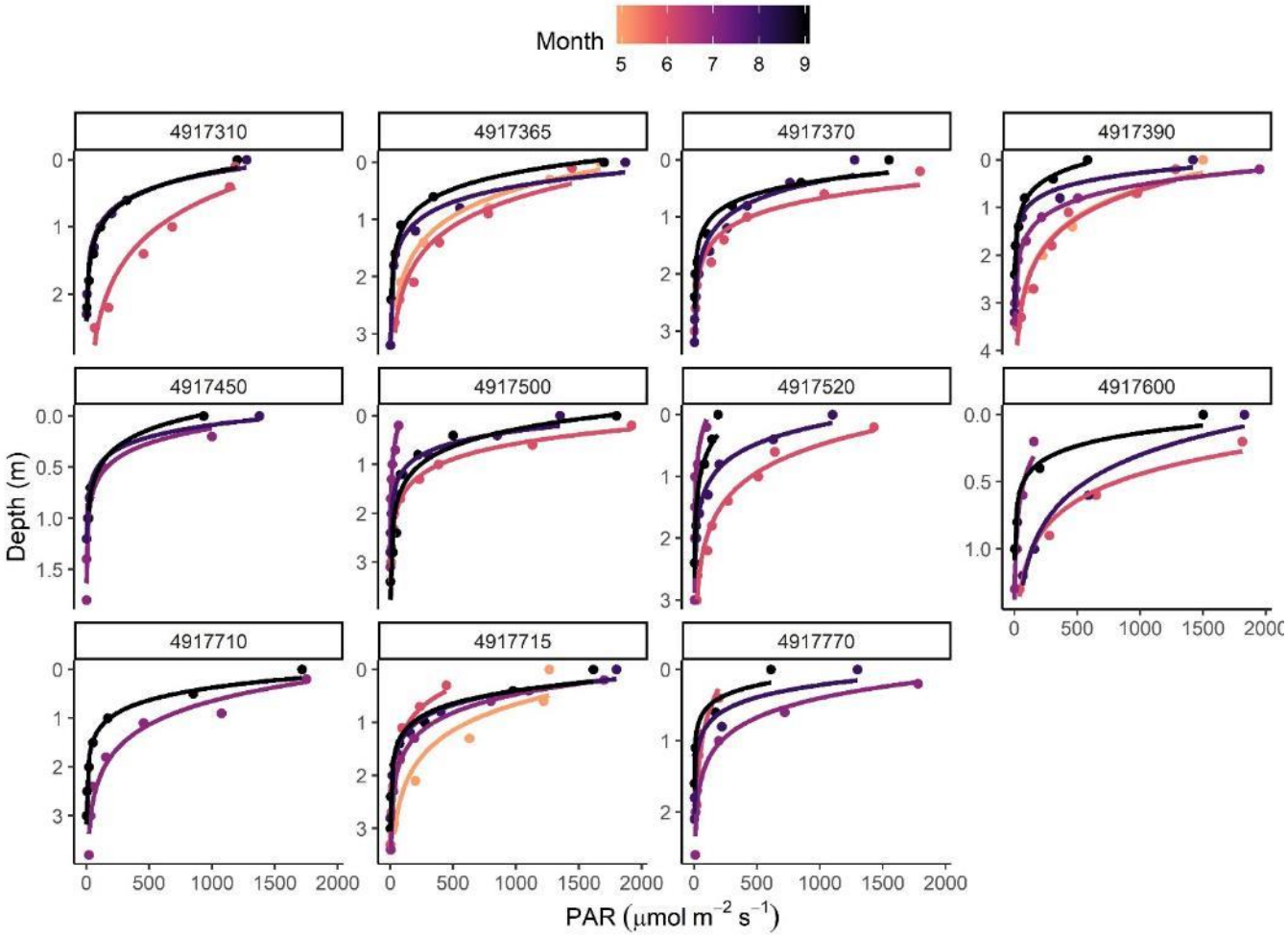


**Figure 2.8.1.** Attenuation of photosynthetically active radiation (PAR) with depth in Utah Lake. Panels represent sampling sites, with named sites as follows: North = 4917365, State Park = 4917390, South = 4917715.

The amount of benthic primary production is negatively correlated with k (Ask et al. 2009), consistent with the lack of macrophyte presence in Utah Lake. The question remains: in the current light environment, is it possible for macrophytes to establish? For submerged macrophytes, the light compensation point (PAR level at which photosynthesis matches respiration and net growth is zero) can help predict potential limitations on colonization depth. Light compensation points for species documented in Utah Lake (*Ceratophyllum demersum*, *Elodea canadensis*, *Myriophyllum spicatum*, *Potamogeton pectinatus*, *Potamogeton praelongus*; Brotherson 1981, Miller

and Crowl 2006, Landom et al. 2019) range from 3.5-45 µmol $m^{-2}$ $s^{-1}$ (Madsen et al. 1991, Sand-Jensen and Madsen 1991, Spencer and Rejmanek 2010). *C. demersum*, a submerged macrophyte documented in the most recent report (Landom et al. 2019), was found to have a light compensation point of 7.2 µmol $m^{-2}$ $s^{-1}$, within the range of compensation points for seven species (6.9 ± 1.9 µmol $m^{-2}$ $s^{-1}$; Sand-Jensen and Madsen 1991). Assuming a light compensation point of 10 µmol $m^{-2}$ $s^{-1}$, 22% of sampled light conditions in Utah Lake are below the compensation point, compared to 26% at a compensation point of 20 µmol $m^{-2}$ $s^{-1}$ and 18 % at a compensation point of 7 µmol $m^{-2}$ $s^{-1}$. A light compensation point of 10 µmol $m^{-2}$ $s^{-1}$ was entered into the logistic regression, which showed increased probability of a sample being below the light compensation point with increasing depth (Figure 2.8.2). Time of year had a significant effect as well. The probability of being below the light compensation point was 5% at 1 m depth, 23% at 2 m depth, and 61% at 3 m depth. The depth at which there were equal odds of being above and below the compensation point was 2.73 m. These results suggest that shallow zones may be the best option for macrophyte restoration. However, colonization depth may be somewhat independent of transparency, as macrophytes may grow taller to harvest light near the surface (Middelboe and Markager 1997), and similarly may overcome late-season decreases in water transparency through early season growth. As detailed in the previous section, macrophyte establishment is predicted to decrease sediment

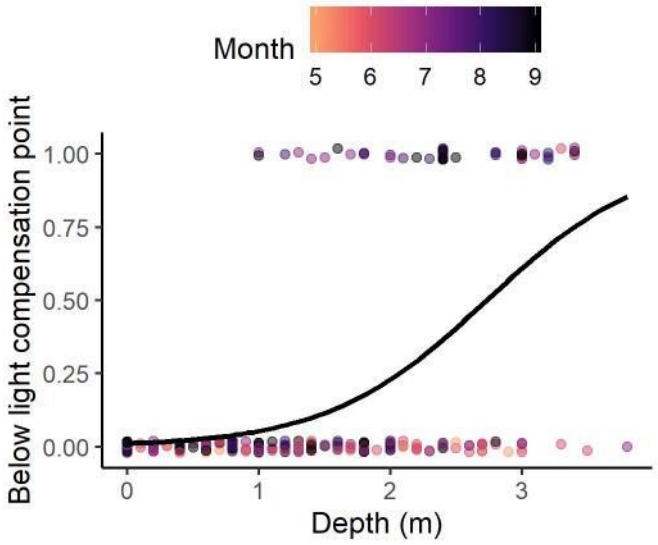


resuspension events, potentially resulting in clearer waters and activating a positive feedback loop for macrophyte restoration.

**Figure 2.8.2.** Logistic regression of water depth and samples above and below the light compensation point (0 and 1, respectively). The light compensation point was set at 10 µmol $m^{-2}$ $s^{-1}$. The solid line represents the probability of a sample being below the light compensation point. Note: y axis values are either 0 or 1, but points are jittered to enable visualization of overlapping points.

k values in Utah Lake ranged from 1.12-6.90 $m^{-1}$ (mean ± SD: 2.60 ± 1.26 $m^{-1}$). Secchi depth rarely exceeded 1 m. For observations when light profiles and Secchi depth were measured concurrently, k was negatively correlated with Secchi depth on a log-log scale (Figure 2.8.3; $R^2 = 0.52$, df = 42, $p < 0.0001$). The lowest k values and highest Secchi depth measurements occurred early in the year. Based on the established relationship of k and Secchi depth, k values were calculated for observations when Secchi depth was measured. Secchi depths measured on days and locations concurrently with light profiles were representative of all Secchi depths, and estimated k values approximated a similar distribution as measured k values.

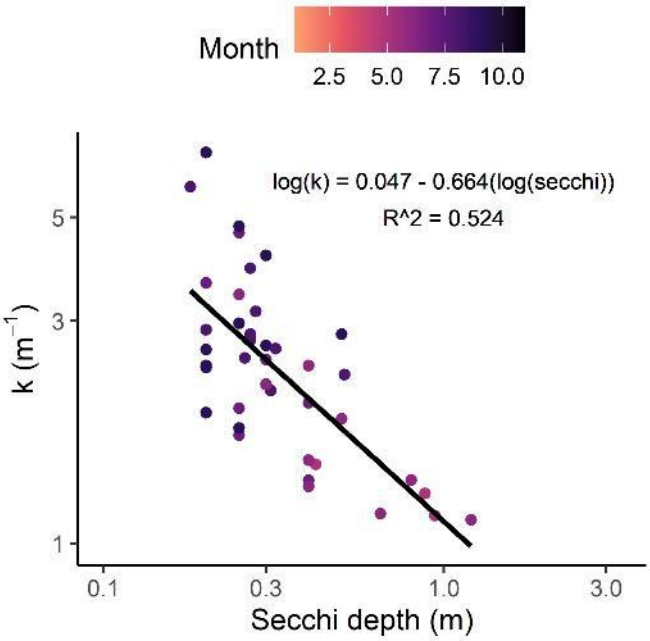


**Figure 2.8.3.** Relationship between Secchi depth and light attenuation coefficient (k) in Utah Lake.

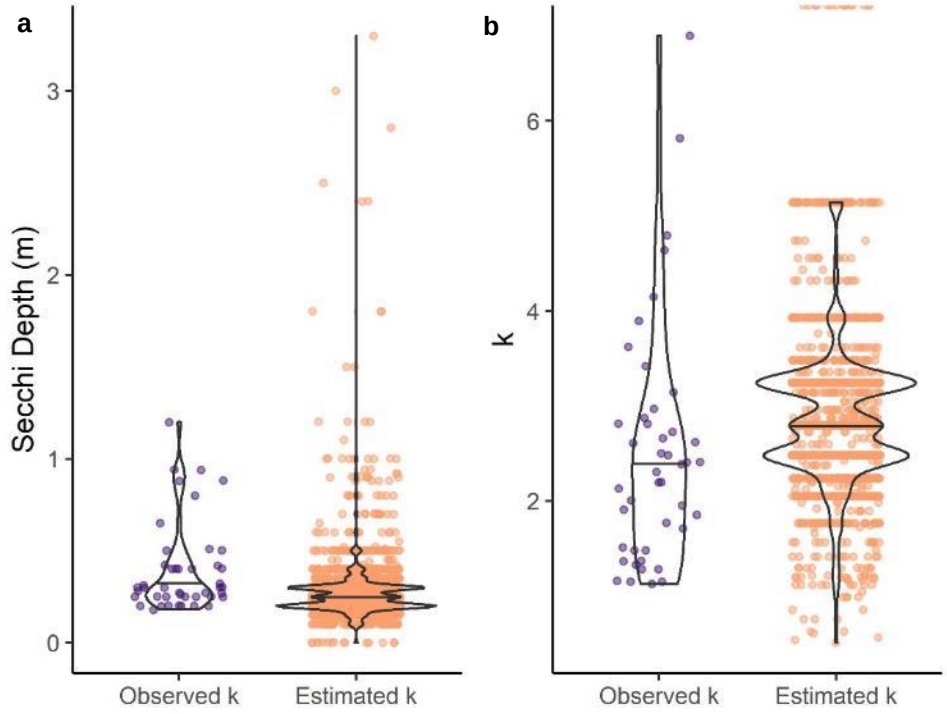


**Figure 2.8.4**. Comparisons of distributions of (a) secchi depth and (b) light attenuation coefficient (k) for samples with a light profile (and thus observed k) available and those for which k was estimated.

TSI values as computed from secchi depth were significantly higher than those computed from chlorophyll (Figure 2.8.5; t-test, df = 1865, t = 62.15, p < 0.0001), indicating non-algal turbidity contributes to reductions in clarity. The ratio of observed to expected (i.e., based on chlorophyll) secchi depth was 0.33 ± 0.23 (mean ± standard deviation), supporting the same conclusion. Light attenuation from non-algal turbidity made up 74 ± 8% (mean ± standard deviation) of total light attenuation (k; Figure 2.8.6). Note a small number of samples have a proportion greater than 100%, a practical impossibility that was a function of the variability in the dataset.

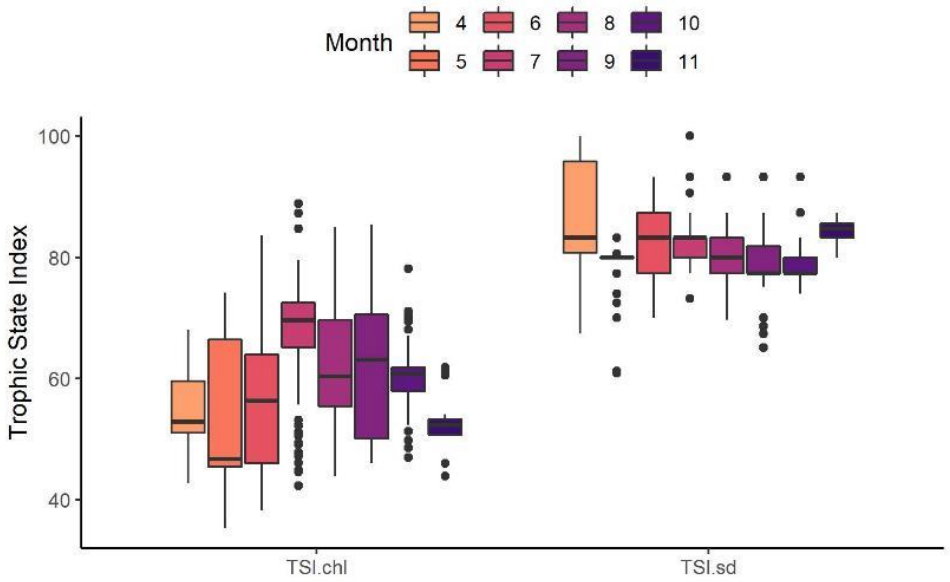


**Figure 2.8.5.** Comparisons of trophic state index as computed from chlorophyll (TSI.chl) and Secchi depth (TSI.sd).

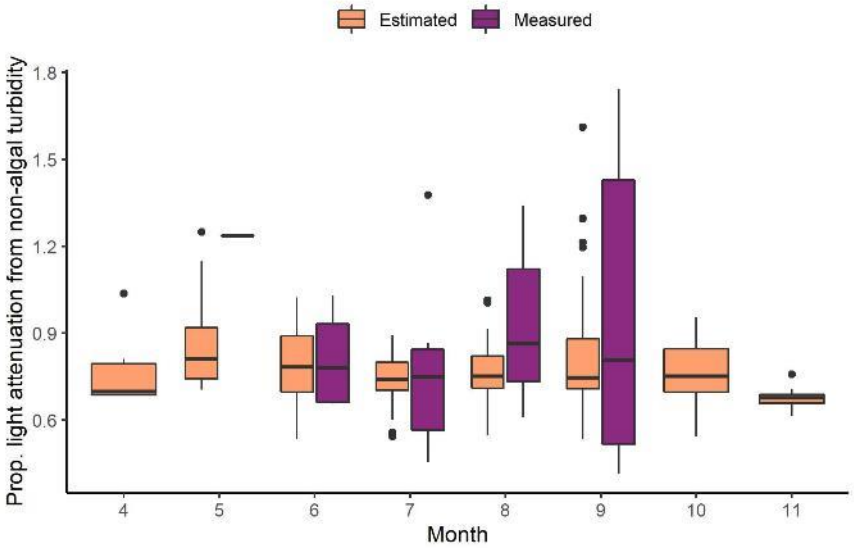


**Figure 2.8.6.** Proportion of total light attenuation contributed from non-algal turbidity. Measured values are derived from k values from PAR profiles, and estimated values are derived from estimated k values converted from secchi depths according to the regression in Figure 2.8.3.

As anticipated (Brown 1984), there was a positive correlation between turbidity and TSS (Figure 2.8.7; $R^2 = 0.73$, df = 253, $p < 0.0001$). Turbidity and TSS values in Provo Bay were distributed across the range of values in the main basin, but three out of the four highest TSS measurements were measured in Provo Bay. TSS was included in models rather than turbidity, as it was a more direct measure of particulates.

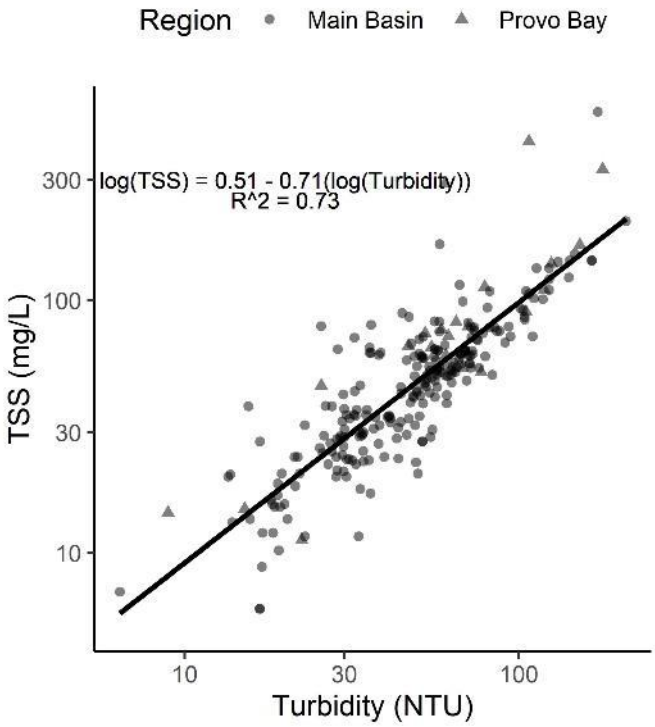


**Figure 2.8.7.** Relationship of turbidity and total suspended solids (TSS) in Utah Lake. NTU = nephelometric turbidity units.

k was positively linearly correlated with turbidity, suspended solids, chlorophyll, and DOC, consistent with the relationship observed in the literature (Figure 2.8.8; Brown 1984, Armengol et al. 2003, Zhang et al. 2007, Devlin et al. 2008). Measurements in Provo Bay (n = 3) were on the upper end of k values and corresponding concentrations of explanatory variables. Model selection indicated that chlorophyll was not a significant predictor of k. Stepwise AIC revealed that the best set of predictor variables for k, in order of importance, were DOC, latitude, TSS, and longitude ($R^2 = 0.61$, df = 37, $p < 0.0001$). k decreased with increasing latitude; the water column tends to have higher clarity on the north side of the lake. Longitude, although included in the multiple regression by stepwise AIC, was not a significant predictor of k.

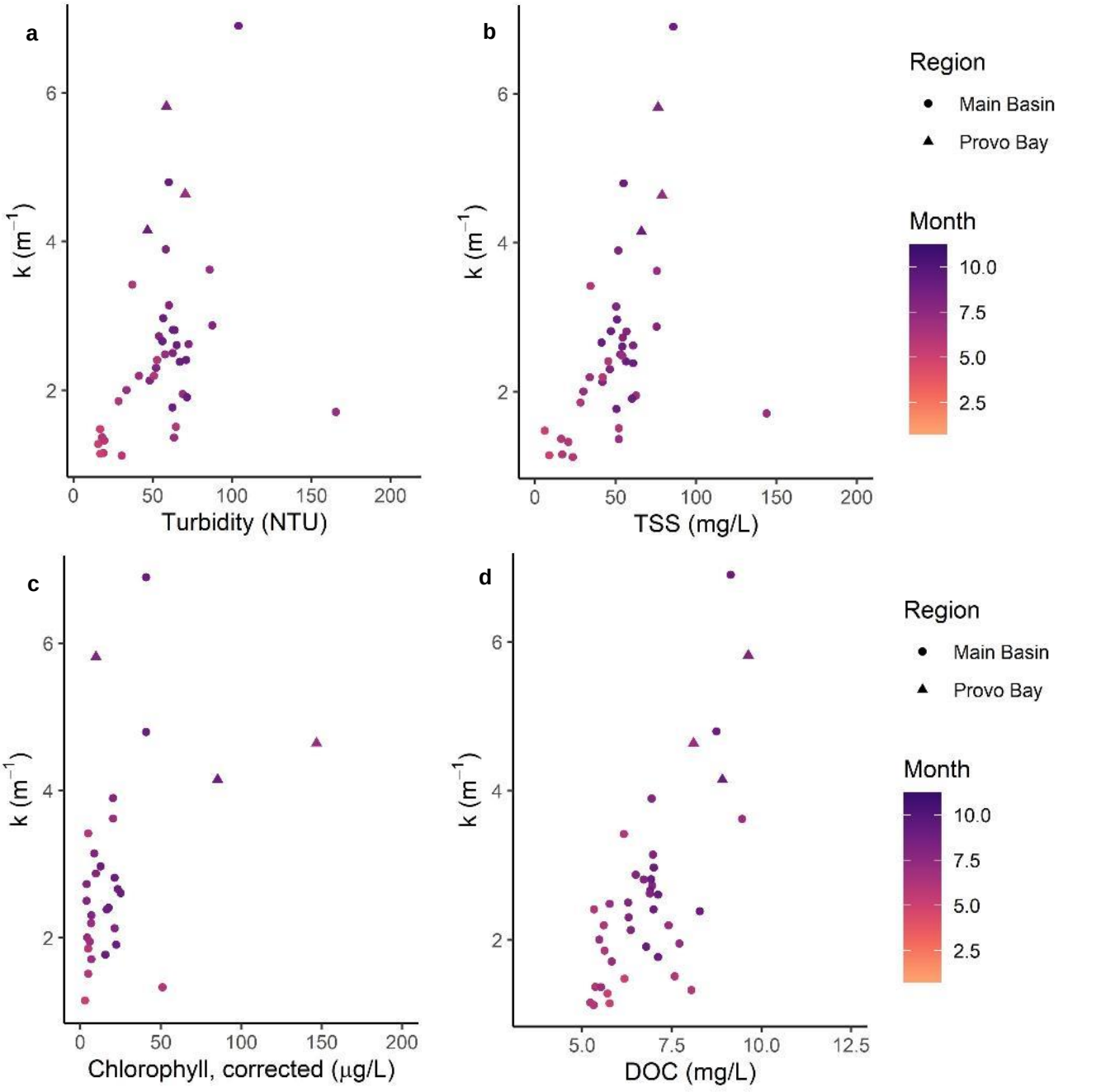


**Figure 2.8.8.** Relationship between light attenuation coefficient (k) with (a) turbidity, (b) total suspended solids (TSS), (c) chlorophyll corrected for pheophytin, and (d) dissolved organic carbon (DOC). NTU = nephelometric turbidity units.

Secchi depth was negatively correlated with logged turbidity, suspended solids, chlorophyll, and DOC, consistent with the relationship observed in the literature (Figure 2.8.9; Brown 1984, Armengol et al. 2003). High outliers for turbidity are noted with site IDs. Many of the lowest values for Secchi depth and highest values for explanatory variables were located in Provo Bay, although Provo Bay samples were not exclusively distributed on that end of the relationship. Model selection indicated that DOC was not a significant predictor of Secchi depth. Stepwise AIC revealed that the best set of predictor variables for Secchi depth, in order of importance, were logged TSS, logged chlorophyll, latitude, and longitude ($R^2 = 0.19$, df = 1253, $p < 0.0001$). k decreased with increasing latitude and longitude; the water column tends to have higher clarity on the north and east sides of the lake.

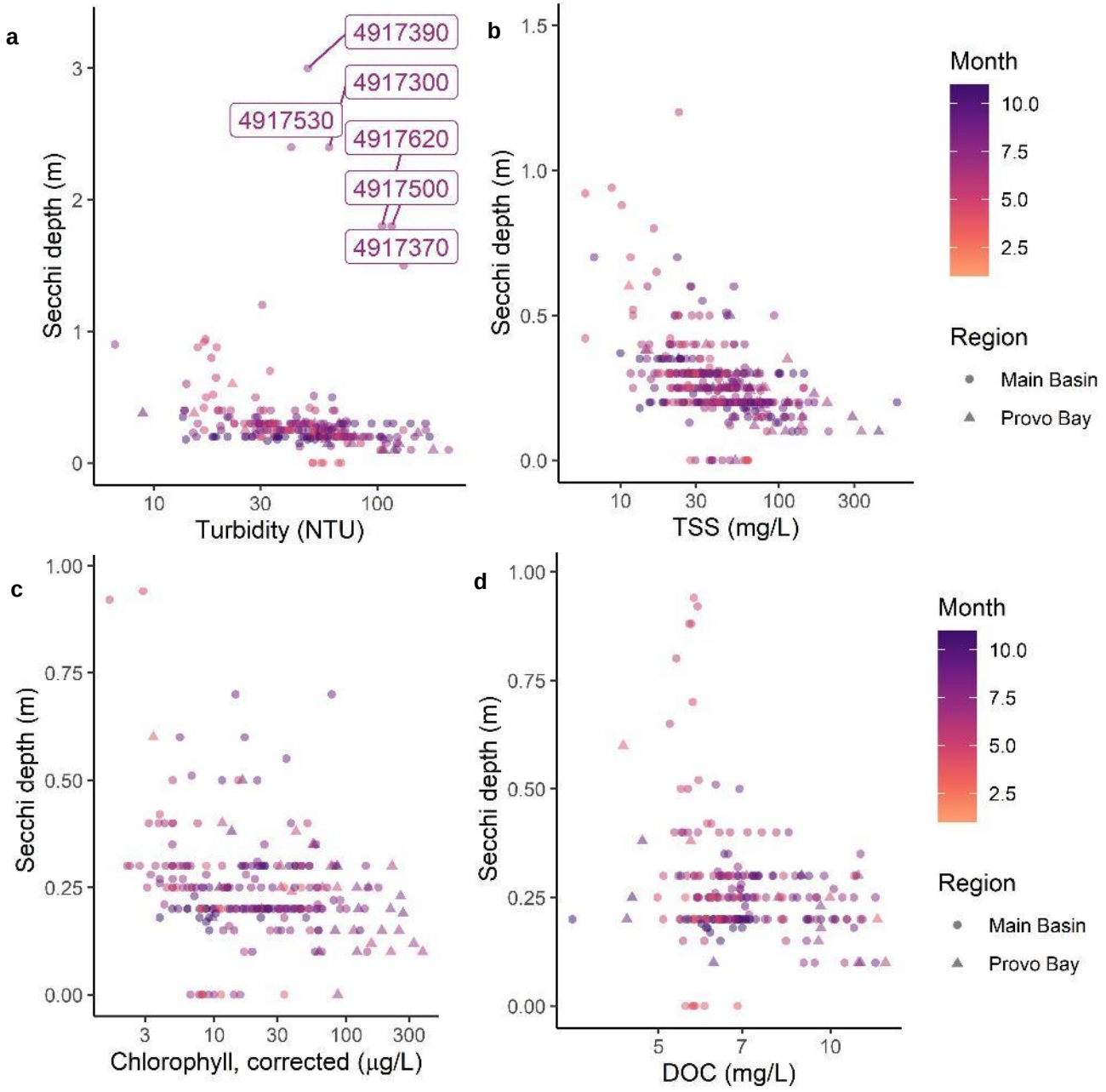


**Figure 2.8.9.** Relationship between Secchi depth with (a) turbidity, (b) total suspended solids (TSS), (c) chlorophyll corrected for pheophytin, and (d) dissolved organic carbon (DOC). NTU = nephelometric turbidity units.

Overall, the models suggest that TSS is a greater determinant of water clarity than chlorophyll and DOC. This finding is consistent with the literature for productive systems with high suspended sediment loads (Armengol et al. 2003). Another shallow eutrophic lake, Lake Taihu (China) exhibits similar drivers of water clarity, with suspended material, chlorophyll, and dissolved organic matter contributing in order of importance to k (Zhang et al. 2007).

VSS concentrations were positively related to TSS concentrations, with VSS making up a variablel proportion of TSS (Figure 2.8.10). Higher chlorophyll concentrations were associated with higher VSS concentrations, and samples from Provo Bay tended to have highest concentrations of VSS and TSS. The VSS/TSS ratio was higher at lower TSS values, indicating a higher proportion of inorganic particulates when TSS was high and a higher proportion of organic particulates when TSS was low (Figure 2.8.11). High chlorophyll concentrations were associated with high VSS/TSS as well as high TSS concentrations. VSS/TSS ratios were variable across months with no clear seasonal trend, and VSS/TSS ratios were higher in Provo Bay than they were in the main basin of Utah Lake (Figure 2.8.12).

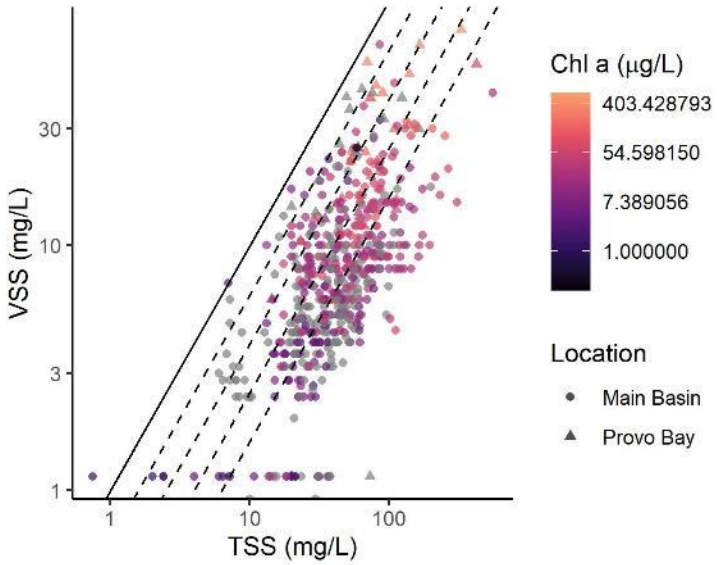


**Figure 2.8.10.** Comparison of TSS and VSS concentrations in Utah Lake across chloropohyll concentrations and sampling locations. The solid line indicates a 1:1 relationship between TSS and VSS, and dotted lines indicate relationships of VSS/TSS ratios of 0.8, 0.6, 0.4, and 0.2 proceeding down and right in order. Gray points indicate an absence of paired chlorophyll data.

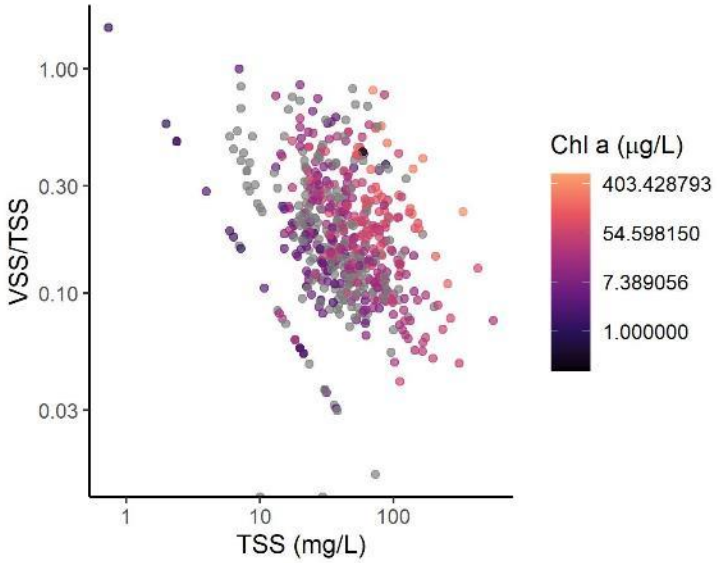


**Figure 2.8.11.** Comparison of TSS concentrations and VSS/TSS ratios in Utah Lake across chloropohyll concentrations. Gray points indicate an absence of paired chlorophyll data.

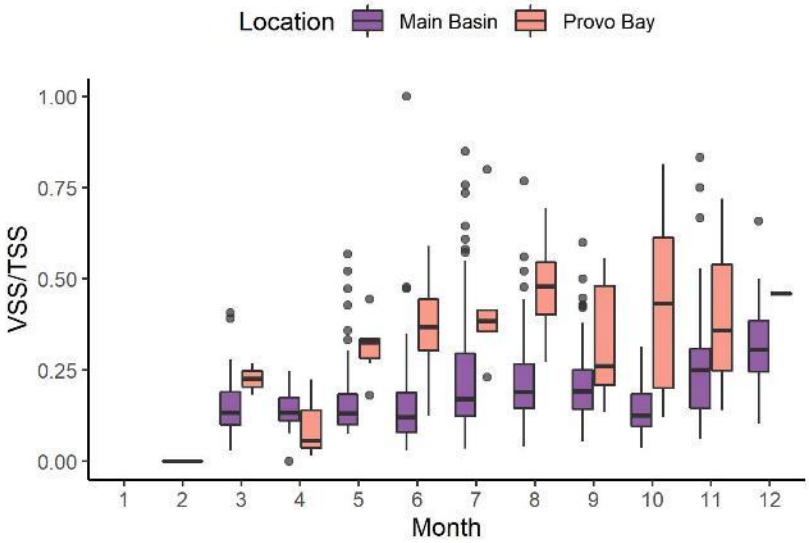


**Figure 2.8.12.** VSS/TSS ratios across months between Provo Bay and the main basin of Utah Lake.

.

# 3. REFERENCES

Armengol J, Caputo L, Comerma M, Feijoo C, Garcia JC, Marce R, Navarro E, and Ordonez J. 2003. Sau reservoir's light climate: relationships between Secchi depth and light extinction coefficient. Limnetica 22(1-2): 195-210.

Ask J, Karlson J, Persson L, Ask P, Bystrom P, and Jansson M. 2009. Terrestrial organic matter and light penetration: Effects on bacterial and primary production in lakes. Limnology and Oceanography 54(6): 2034-2040.

Bolland RF. 1974. Paleoecological interpretation of the diatom succession in the recent seciments of Utah Lake, Utah. University of Utah PhD Dissertation.

Brotherson JD. 1981. Aquatic and semiaquatic vegetation of Utah Lake and its bays. Great Basin Naturalist Memoirs 5: article 5.

Brown R. 1984. Relationships between suspended solids, turbidity, light attenuation, and algal productivity. Lake and Reservoir Management 1(1): 198-205. doi: 10.1080/07438148409354510

Carlson RE. 1977. A trophic state index for lakes. Limnology and Oceanography 22(2): 361-369. doi: 10.4319/lo.1977.22.2.0361

Chao X, Jia Y, Shields Jr FD, Wang SSY, and Cooper CM. 2008. Three-dimensional numerical modeling of cohesive sediment transport and wind wave impact in a shallow oxbow lake. Advances in Water Resources 31: 1004-1014.

Cresson, Travers-Trolet, Rouquette, Timmerman, Giraldo, Lefebre, and Ernande. 2017. Underestimation of chemical contamination in marine fish muscle tissue can be reduced by considering variable wet:dry weight ratios. Marine Pollution Bulletin 123(1-2):279-285. doi: 10.1016/j.marpolbul.2017.08.046

Devlin MJ, Barry J, Mills DK, Gowen, RJ, Foden J, Sivyer D, and Tett P. 2008. Relationships between suspended particulate material, light attenuation and Secchi depth in UK marine waters.

Gaeta and Landom. 2016. A whole-ecosystem response of a shallow lake to drought and an invasive carp removal, with an emphasis on endangered fish conservation. Utah Lake Ecosystem Monitoring 2015 Report.

Gaeta, Waldworth, and Landom. 2019. An age-structured common carp population model and standardized seining to support common carp removal in Utah Lake, UT. Draft report submitted to the June Sucker Recovery Implementation Program.

Idso SB and Gilbert RG. 1974. On the universality of the Poole and Atkins Secchi disk-light extinction equation. Journal of Applied Ecology 11(1): 399-401.

James, Barko, and Butler. 2004. Shear stress and sediment resuspension in relation to submersed macrophyte biomass. Hydrobiologia 515: 181-191.

Kramer BJ, Davis TW, Meyer KA, Rosen BH, Goleski JA, Dick GJ, Oh G, Gobler CJ. 2018. Nitrogen limitation, toxin synthesis potential, and toxicity of cyanobacterial populations in Lake Okeechobee and the St. Lucie River Estuary, Florida, during the 2016 state of emergency event. PLoS ONE 13(5): e0196278.

Landom K, Dillingham R, and Gaeta JW. 2019a. Utah Lake Ecosystem Metadata.

Landom K, Dillingham R, and Gaeta JW. 2019b. Seasonal and annual changes in the near-shore Utah Lake macrophyte community. Draft report submitted to the June Sucker Recovery Implementation Program.

Landom K and Walsworth TE. 2020. Biotic community response to Common Carp removal and lake level fluctuations in Utah Lake, UT. Draft report submitted to the June Sucker Recovery Implementation Program.

Madsen JD, Hartleb CF, and Boylen CW. 1991. Photosynthetic characteristics of *Myriophyllum spicatum* and six submerged aquatic macrophyte species native to Lake George, New York. Freshwater Biology 26: 233-240.

Madsen JD, Chambers PA, James WF, Koch EW, and Westlake DF. 2001. The interaction between water movement, sediment dynamics and submersed macrophytes. Hydrobiologia 444: 71-84.

Merritt and Miller. 2016. Interim Report on Nutrient Loadings to Utah Lake. Prepared for the Jordan River, Farmington Bay and Utah Lake Water Quality Council.

Middelboe and Markager. 1997. Depth limits and minimum light requirements of freshwater macrophytes. Freshwater Biology 37: 553-568.

Miller SA and Crowl TA. 2006. Effects of common carp (*Cyprinus carpio*) on macrophytes and invertebreate communities in a shallow lake. Freshwater Biology 51: 85-94.

Otten TG, Hu H, Qin B, Zhu G, and Paerl HW. 2012. Spatiotemporal patterns and ecophysiology of toxigenic Microcystis blooms in Lake Taihu, China: Implications for water quality management. Environmental Science & Technology 46: 3480-3488.

Psomas and SWCA. 2007. Utah Lake TMDL: Pollutant Loading Assessment and Designated Use Beneficial Use Impairment Assessment. Prepared for the State of Utah Division of Water Quality.

Sand-Jensen K and Madsen TV. 1991. Minimum light requirements of submerged freshwater macrophytes in laboratory growth experiments. Journal of Ecology 79(3): 749-764.

Smith VH. 1990. Effects of nutrients and non-algal turbidity on blue-green algal biomass in four North Carolina reservoirs. Lake and Reservoir Management 6(2): 125-131. doi: 10.1080/07438149009354702

Tallberg P, Horppila J, Vaisanen A, and Nurminen L. 1999. Seasonal succession of phytoplankton and zooplankton along a trophic gradient in a eutrophic lake – implications for food web management. Hydrobiologia 412: 81-94.

Tyree MA, Carlisle DM, and Spaulding SA. 2020. Diatom enumeration method influences biological assessments of southeastern USA streams. Freshwater Science 39(1): 183-195.

ULWQS Steering Committee. 2020. Utah Lake Management Goals, Assessment Endpoints, Measures, and Targets – Approved November 30, 2020

USFWS. 2010. Final Environmental Assessment for Removal and Control of NonNative Carp in Utah Lake to Support June Sucker Recovery. USFWS.

Wang C, Wang C, and Wang Z. 2010. Effects of submerged macrophytes on sediment suspension and $NH_4$-N release under hydrodynamic conditions. Journal of Hydrodynamics 22(6): 810-815.

Watercourse Engineering. 2020. Klamath River water quality sampling final 2019 annual report. Prepared for the KHSA Water Quality Monitoring Group.

Wilhelm SW, Farnsley SE, LeCleir GR, Layton AC, Satchwell MF, DeBruyn JM, Boyer GL, Zhu G, and Paerl HW. 2011. The relationships between nutrients, cyanobacterial toxins and the microbial community in Taihu (Lake Tai), China. Harmful Algae 10: 207-215.

WISER Consortium: Dataset "Macrophytes" (according to European intercalibration groups and the EU-projects REBECCA/WISER). www.freshwaterecology.info - the taxa and autecology database for freshwater organisms, version 7.0 (accessed 2020-08-11).

Zhang Y, Zhang B, Ma R, Feng S, and Le C. 2007. Optically active substances and their contributions to the underwater light climate in Lake Taihu, a large shallow lake in China. Fundamental and Applied Limnology 170(1): 11-19. doi: 10.1127/1863-9135/2007/0170-0011